Gut

Genetic editing of colonic organoids provides a molecularly distinct and orthotopic preclinical model of serrated carcinogenesis.

Journal:	*Gut*
Manuscript ID	gutjnl-2017-315920.R1
Article Type:	Original Article
Date Submitted by the Author:	n/a
Complete List of Authors:	Lannagan, Tamsin; The University of Adelaide, School of Medicine; South Australian Health and Medical Research Institute, Department of Medicine Lee, Young; The University of Adelaide, School of Medicine; South Australian Health and Medical Research Institute, Department of Medicine Wang, Tongtong; The University of Adelaide, School of Medicine; South Australian Health and Medical Research Institute, Department of Medicine Roper, Jatin; Massachusetts Institute of Technology, The David H. Koch Institute for Integrative Cancer Research ; Tufts Medical Center, Division of Gastroenterology Bettington, Mark; Envoi Specialist Pathologists, Anatomical Pathology; QIMR Berghofer Medical Research Institute, The Conjoint Gastroenterology Laboratory Fennell, Lochlan; QIMR Berghofer Medical Research Institute, The Conjoint Gastroenterology Laboratory Vrbanac, Laura; The University of Adelaide, School of Medicine; South Australian Health and Medical Research Institute, Department of Medicine Jonavicius, Lisa; Flinders Medical Centre, Department of Anatomical Pathology Somashekar, Roshini; The University of Adelaide, School of Medicine; South Australian Health and Medical Research Institute, Department of Medicine Gieniec, Krystyna; The University of Adelaide, School of Medicine; South Australian Health and Medical Research Institute, Department of Medicine Yang, Miao; The University of Adelaide, School of Medicine; South Australian Health and Medical Research Institute, Department of Medicine Ng, Jia; The University of Adelaide, School of Medicine; South Australian Health and Medical Research Institute, Department of Medicine Suzuki, Nobumi; South Australian Health and Medical Research Institute, Cancer Theme Ichinose Suzuki, Mari; South Australian Health and Medical Research Institute, Cancer Theme Wright, Josephine; The University of Adelaide, School of Medicine; South Australian Health and Medical Research Institute, Department of Medicine Kobayashi, Hiroki; The University of Adelaide, School of Medicine; Nagoya University Graduate School of Medicine, Department of Pathology Putoczki, Tracey; Walter and Eliza Hall Institute of Medical Research;

	university of melbourne, Department of Medical Biology Mukherjee, Siddhartha; Columbia University Medical Center, Medicine Hayakawa, Yoku; Graduate School of Medicine, The University of Tokyo, Department of Gastroenterology Leedham, Simon; Wellcome Trust Centre for Human Genetics; John Radcliffe Hospital, Nuffield Department of Clinical Medicine Abud, Helen; Monash University, Monash Biomedicine Discovery Institute ; Monash University, Department of Anatomy and Developmental Biology Yilmaz, Omer; Massachusetts Institute of Technology, The David H. Koch Institute for Integrative Cancer Research ; Massachusetts General Hospital, Department of Pathology Marker, Julie; Cancer Voices SA Klebe, Sonja; Flinders Medical Centre, Department of Anatomical Pathology Wirapati, Pratyaksha; Swiss Institute of Bioinformatics, Bioinformatics Core Facility Tejpar, Sabine; University Ospital Gasthuisberg, Digestive Oncology Unit Leggett, Barbara; The Royal Brisbane and Women's Hospital, Department of Gastroenterology and Hepatology & School of Medicine, University of Queensland; QIMR Berghofer Medical Research Institute, The Conjoint Gastroenterology Laboratory Whitehall, Vicki; QIMR Berghofer Medical Research Institute, The Conjoint Gastroenterology Laboratory; Queensland Pathology, & School of Medicine, University of Queensland Daniel, Worthley; The University of Adelaide, School of Medicine; South Australian Health and Medical Research Institute, Department of Medicine Woods, Susan; The University of Adelaide, School of Medicine; South Australian Health and Medical Research Institute, Cancer Theme
Keywords:	COLORECTAL CANCER, GENE MUTATION, CANCER GENETICS, ONCOGENES, METHYLATION

Title: Genetic editing of colonic organoids provides a molecularly distinct and orthotopic preclinical model of serrated carcinogenesis.

Dual corresponding author details:
Dr. Susan Woods, PhD.
Postal address- GICB Lab, Level 5 South
South Australian Health & Medical Research Institute (SAHMRI)
North Terrace
Adelaide SA 5000
AUSTRALIA
p: (08) 8128 4386 m: 0488 737408 e: susan.woods@adelaide.edu.au

Dr. Daniel Worthley, MBBS(Hons), PhD, MPH, FRACP.
Postal address- GICB Lab, Level 5 South
South Australian Health & Medical Research Institute (SAHMRI)
North Terrace
Adelaide SA 5000
AUSTRALIA
p: (08) 8128 4386 m: 0400 363208 e: Dan.worthley@sahmri.com

Co-author details:
Tamsin RM Lannagan[1], Young K Lee[1], Tongtong Wang[1], Jatin Roper[2,3], Mark L Bettington[4,5], Lochlan Fennell[5], Laura Vrbanac[1], Lisa Jonavicius[6], Roshini Somashekar[1], Krystyna Gieniec[1], Miao Yang[1], Jia Q Ng[1], Nobumi Suzuki[1], Mari Ichinose[1], Josephine A Wright[1], Hiroki Kobayashi[1], Tracy L Putoczki[7], Siddhartha Mukherjee[8], Yoku Hayakawa[9],Simon Leedham[10], Helen E Abud[11], Ömer H. Yilmaz[2,12], Julie Marker[13], Sonja Klebe[6], Pratyaksha Wirapati[14], Sabine Tejpar[15], Barbara A Leggett[5,16,17], Vicki LJ Whitehall[5,16,18], Daniel L Worthley[1]*, Susan L Woods[1]*.

Affiliations as listed page 2 of manuscript.

Word count: (excluding title page, affiliations, abstract, references, figures and tables.)
3883

Abbreviations: colorectal cancer (CRC), mitogen activated kinase (MAPK), CpG Island Methylator Phenotype (CIMP), chromosomal instability (CIN), *Adenomatous polyposis coli* (*APC),* Epidermal growth factor (EGF), bone morphogenic protein (BMP), The Cancer Genome Atlas (TCGA), microsatellite instability (MSI), transforming growth factor-β (TGFβ), *MutL homolog 1* (*MLH1),* 4-hydroxytamoxifen (4-OHT), epidermal growth factor receptor (EGFR), clustered regularly interspaced short palindromic repeats (CRISPR), wild type (WT), Quantitative real-time PCR (qRT-PCR), guideRNAs (gRNAs), MSI-High (MSI-H), NOD.Cg-*Prkdc*^{scid}*Il2rg*$^{tm1Wjl/Szj}$ (NSG), multidimensional scaling (MDS), gene set enrichment analysis (GSEA), sphingolipid (SP), sphingosine kinase 1 (SPHK1), sphingosine-1-phosphate phosphatase 1 (SGPP1), sphingosine 1-phosphate (S1P), *Braf*^{V600E}*Tgfbr2*$^{Δ/Δ}$ *(Braf*^{V600E}*ΔT)*, *Braf*^{V600E} *Tgfbr2*$^{Δ/Δ}$ *Rnf43*$^{Δ/Δ}$*/Znrf3*$^{Δ/Δ}$ *p16Ink4a*$^{Δ/Δ}$ *(Braf*^{V600E}*ΔTRZI)*, *Braf*^{V600E} *Tgfbr2*$^{Δ/Δ}$*Rnf43*$^{Δ/Δ}$*/Znrf3*$^{Δ/Δ}$ *p16Ink4a*$^{Δ/Δ}$*Mlh1*$^{Δ/Δ}$ *(Braf*^{V600E}*ΔTRZIM),* Wnt-3a (W), Rspo-2 (R), Noggin (N), TGFβ1 (T), 5-Fluorouracil (5FU), Enrichment score (ES), normalised enrichment score (NES), false discovery rate (FDR).

Title: Genetic editing of colonic organoids provides a molecularly distinct and orthotopic preclinical model of serrated carcinogenesis.

Tamsin RM Lannagan[1], Young K Lee[1], Tongtong Wang[1], Jatin Roper[2,3], Mark L Bettington[4,5], Lochlan Fennell[5], Laura Vrbanac[1], Lisa Jonavicius[6], Roshini Somashekar[1], Krystyna Gieniec[1], Miao Yang[1], Jia Q Ng[1], Nobumi Suzuki[1], Mari Ichinose[1], Josephine A Wright[1], Hiroki Kobayashi[1], Tracy L Putoczki[7], Siddhartha Mukherjee[8], Yoku Hayakawa[9],Simon Leedham[10], Helen E Abud[11], Ömer H. Yilmaz[2,12], Julie Marker[13], Sonja Klebe[6], Pratyaksha Wirapati[14], Sabine Tejpar[15], Barbara A Leggett[5,16,17], Vicki LJ Whitehall[5,16,18], Daniel L Worthley[1]*, Susan L Woods[1]*.

[1]School of Medicine, University of Adelaide and South Australian Health and Medical Research Institute, Adelaide, SA Australia
[2] The David H. Koch Institute for Integrative Cancer Research at MIT, Cambridge, MA
[3]Division of Gastroenterology, Tufts Medical Center, Boston, MA, United States
[4]Envoi Specialist Pathologists, Brisbane, QLD Australia
[5]QIMR Berghofer Medical Research Institute, Brisbane, QLD Australia
[6]Department of Anatomical Pathology, Flinders Medical Centre, Bedford Park, SA Australia
[7]Department of Medical Biology, University of Melbourne and the Walter and Eliza Hall Institute of Medical Research, Melbourne, VIC Australia
[8]Department of Medicine, Columbia University Medical Center, New York, NY, USA.
[9]Dept of Gastroenterology, University of Tokyo, Japan
[10]Gastrointestinal Stem Cell Biology Laboratory, Wellcome Trust Centre for Human Genetics University of Oxford, Oxford, & Translational Gastroenterology Unit, Experimental Medicine Division, Nuffield Department of Clinical Medicine, John Radcliffe Hospital, Oxford, Headington, UK
[11]Cancer Program, Monash Biomedicine Discovery Institute and the Department of Anatomy and Developmental Biology, Monash University, Clayton, VIC Australia
[12]Department of Pathology, Massachusetts General Hospital, Boston, MA United States
[13]Cancer Voices SA, SA Australia
[14]Swiss Institute of Bioinformatics, Bioinformatics Core Facility, Lausanne, Switzerland.
[15]Digestive Oncology Unit, Department of Oncology, University Hospitals Leuven, Leuven, Belgium.
[16]School of Medicine, University of Queensland, QLD Australia
[17]Royal Brisbane and Womens Hospital, Brisbane, QLD Australia
[18]Pathology Queensland, Brisbane, QLD

*=correspondence to either:
Dr. Daniel Worthley, South Australian Health & Medical Research Institute, Adelaide SA Australia. Dan.Worthley@sahmri.com
Dr. Susan Woods, South Australian Health & Medical Research Institute, Adelaide SA Australia. Susan.Woods@adelaide.edu.au

ABSTRACT:

Objective: Serrated colorectal cancer (CRC) accounts for approximately 25% of cases, and includes tumours that are amongst the most treatment resistant and with worst outcomes. This CRC subtype is associated with activating mutations in the mitogen activated kinase (MAPK) pathway gene, *BRAF*, and epigenetic modifications termed the CpG Island Methylator Phenotype (CIMP), leading to epigenetic silencing of key tumour suppressor genes. It is still

not clear which (epi-)genetic changes are most important in neoplastic progression and we begin to address this knowledge gap herein.

Design: We utilise organoid culture combined with CRISPR/Cas9 genome engineering, to sequentially introduce genetic alterations associated with serrated CRC and which regulate the stem cell niche, senescence and DNA mismatch repair.

Results: Targeted biallelic gene alterations were verified by DNA sequencing. Organoid growth in the absence of niche factors was assessed, as well as analysis of downstream molecular pathway activity. Orthotopic engraftment of complex organoid lines, but not $Braf^{V600E}$ alone, quickly generated adenocarcinoma *in vivo* with serrated features consistent with human disease. Loss of the essential DNA mismatch repair enzyme, Mlh1, led to microsatellite instability. Sphingolipid metabolism genes are differentially regulated in both our mouse models of serrated CRC and human CRC, with key members of this pathway having prognostic significance in the human setting.

Conclusion: We generate rapid, complex models of serrated CRC to determine the contribution of specific genetic alterations to carcinogenesis. Analysis of our models alongside patient data has led to the identification of a potential susceptibility for this tumour type.

SUMMARY BOX:

What is already known about this subject:

- 25% of colorectal cancers (CRC) form via an alternate molecular pathway typified by activating mutation in the BRAF kinase and accrual of epigenetic modifications at specific promoter locations.
- The molecular evolution of these serrated CRCs and how this relates to natural history is poorly understood and may hold the key to better treatment and prevention options for this form of CRC.

What are the new findings:

- Here we use next generation sequence information from human serrated CRC, combined with organoid culture, gene editing and orthotopic transplantation techniques to rapidly generate complex, preclinical models of serrated CRC.

How might it impact on clinical practice in the foreseeable future?

- These preclinical models will allow therapeutic evaluation in known, previously untested genetic landscapes.
- Transcriptomic analysis of our models, combined with patient data, have suggested potential vulnerabilities for this tumour type that we will test in the future.

INTRO:

Sporadic colorectal cancer (CRC) develops via two main genetic pathways. The conventional pathway described by Fearon & Vogelstein [1] has characteristic chromosomal instability (CIN) with stepwise loss of key tumour suppressors (eg. *Adenomatous polyposis coli*, *APC*)

and activation of oncogenes (eg. *KRASG12D* mutation). In the last two decades, an alternate molecular pathway has been identified that accounts for 25% of CRC [2]. This subtype of CRC is named for the serrated, or saw-toothed, morphology of the precursor lesion, including sessile serrated polyps, and comprises a molecularly distinct, somewhat heterogeneous tumour type that forms without CIN. It can be best differentiated from conventional CRC by two characteristic molecular markers; the presence of the $BRAF^{V600E}$ mutation that activates the mitogen-activated protein kinase (MAPK) pathway and the coincident, coordinated epigenetic modification of specific target promoters termed the CpG Island Methylator Phenotype (CIMP) [3]. $BRAF^{V600E}$/$CIMP^{+}$ tumours account for 8-20% of all CRC [2, 4]. These are preferentially located in the proximal colon, frequently present with higher grade and contain a group of cancers with the worst prognosis of all CRC [2, 5]. Furthermore, of relevance to the gastrointestinal cancer preventionist, these serrated lesions are less well detected by current CRC screening programs and are overrepresented in colonoscopic interval cancers [6, 7]. The molecular basis for these subtype characteristics are not well understood, but may hold the key to preventing and treating serrated CRC.

The culture of normal and tumour derived organoids pioneered by Hans Clevers and his group [8, 9] allows the indefinite, *in vitro* propagation of primary gut epithelia and neoplastic specimens. Cells are grown in self-organising aggregates with representative epithelial architecture, suspended within a basement membrane-gel matrix and supported by stem cell niche signalling factors. For the colon these factors, Wnt/R-spondin, Epidermal growth factor (EGF), and Noggin activate the Wnt and MAPK pathways and inhibit the bone morphogenic protein (BMP) pathway, respectively. This culture system supports the stem cell population, as well as more differentiated cell types, allowing long-term primary culture containing many of the representative epithelial cell types of the original tissue.

The next-generation sequencing revolution has armed us with more information than ever before about the (epi-)genetic changes associated with serrated CRC. Mining this static data is relatively simple, yet understanding the contribution of genetic events to carcinogenesis is a real challenge. To this end, we have combined recent advances in stem cell biology [10] with genome editing techniques [11], to produce a system in which multiple genetic alterations can be assessed for their contribution to serrated CRC. This is analogous to the approach taken to model the conventional pathway to CRC [12, 13] and is inspired by the observation that many recurrent CRC mutations lie within genes involved in key signalling pathways that are essential for maintenance of the intestinal stem cell niche [14]. Our work provides new insights into the importance of common (epi-)genetic alterations found in human serrated CRC and highlights a potential vulnerability of this cancer type.

RESULTS:

To identify recurrent serrated CRC associated alterations in stem cell niche signalling and senescence pathways, we analysed The Cancer Genome Atlas (TCGA) (epi-)genomic data for 633 CRC cases [15]. $BRAF^{V600E}$ mutation is estimated to mark 50-67% of serrated CRCs [2] and, in the absence of microsatellite instability (MSI), is associated with poor outcome for late stage disease [2, 16]. As only 30% of serrated CRCs retain serrated crypt morphology [2], we use the $BRAF^{V600E}$ molecular marker rather than histological appearance to extract serrated CRC cases from the TCGA set. In the 50 TCGA CRC cases that contain $BRAF^{V600E}$ (depicted in **Figure 1**), we then used a candidate gene approach to look for frequently co-

altered genes that play important roles in regulating the stem cell niche or senescence. *p16 INK4A* encodes a tumour suppressor protein critical for oncogene induced senescence. Loss of *p16 INK4a* expression is associated with the conversion of serrated polyps to high-grade dysplasia/CRC and cooperates with $Braf^{V600E}$ in a mouse model of serrated CRC [17, 18, 19]. Consistent with previous reports, we detected *p16 INK4A* hypermethylation or mutation in 46% of TCGA CRC cases overall and in 84% of $BRAF^{V600E}$ CRC (**Figure 1**) [20, 21, 22]. The Wnt pathway intricately regulates intestinal stem cell proliferation and differentiation. The classic Wnt-pathway regulator, *APC*, is the most commonly mutated gene in CRC [15]. However for $BRAF^{V600E}$ CRC, we identified two negative regulators, *ZNRF3* and *RNF43*, as the most commonly altered Wnt pathway genes (**Figure 1**) [23]. Interestingly, in mice, cooperative inactivation of both *Rnf43* and *Znrf3* are required for polyp formation [24] and we detect alteration of both genes in 32% of $BRAF^{V600E}$ CRC. This is consistent with reports of differential Wnt pathway disruption in precursor lesions of the serrated pathway to CRC compared to the conventional pathway [25, 26]. The mutation rate of *RNF43* is likely under-represented in the TCGA dataset due to incomplete calling of frame-shift mutations because of their similarity to technical DNA polymerase slippage errors [27]. The transforming growth factor-β (TGFβ) pathway is frequently aberrantly regulated in CRC, often through mutation of *TGFβ receptor 2* (*TGFβR2*) [15]. *TGFβR2* mutation occurred in 10% of the $BRAF^{V600E}$ CRC cases we examined (**Figure 1**), again reflecting under calling of the polyadenine repeat tract mutations in the TCGA dataset as use of older sequencing modalities identified *TGFBR2* as mutated in 90% of MSI CRC [28]. Lastly, we wanted to model MSI CRC and so examined the key mismatch repair gene, *MutL homolog 1* (*MLH1)*. In line with a meta-analysis of *MLH1* methylation frequency in CRC, we detected *MLH1* hypermethylation in 20% of TCGA CRC cases [29]. This increased to 74% alteration in $BRAF^{V600E}$ CRC (**Figure 1**).

Carcinogenesis is a story of liberation and, as we genetically engineer successive stages of serrated CRC, we select organoids through their unique biology, microenvironmental requirements and treatment sensitivities. Firstly, the $BRAF^{V600E}$ mutation is an early genetic change in serrated polyps [30]. To first incorporate this mutation, we established colon organoid cultures from $BRAF^{CA}/Villin^{CreERT}$mice (**Figure 2**). *In vitro* treatment with 4-hydroxytamoxifen (4-OHT) induced highly efficient recombination to $Braf^{V600E}$ (**Supplementary Figure 1**) and activation of ERK1/2 phosphorylation (**Figure 2A**). This *in vitro* system mimics the chemoresistance to epidermal growth factor receptor (EGFR) inhibitors observed for MAPK mutant CRC in the clinic [31]. Treatment with EGFR inhibitor results in a significant growth inhibition of wild-type organoids in culture but not $Braf^{V600E}$ organoids (**Figure 2B**, **Supplementary Figure 2**).

Genome editing using microbial Cas9 nucleases from the clustered regularly interspaced short palindromic repeats (CRISPR) adaptive immune system has revolutionised the field of genome editing [11]. We have modelled serrated CRC using this genome editing technique. Thus, following mutation of *Braf* we sequentially incorporated 4 further genetic alterations using CRISPR/Cas9 [11] (**Figure 2**). Similar to previous work [12, 13], the addition of Tgfβ to culture medium selected for organoids with functional loss of the Tgfβ pathway, in this case Tgfβr2 ($Braf^{V600E}$*;* $Tgfbr2^{\Delta/\Delta}$, abbreviated to $Braf^{V600E}\Delta T$) (**Figure 2B**). Indeed, wild type (WT), $Braf^{V600E}$ and control transfected cultures do not survive in the presence of Tgfβ [32] (**Figure 2B**). Quantitative real-time PCR (qRT-PCR) analysis of the Tgfβ response gene,

Serpin1, showed that Tgfβ can activate this pathway in *Braf*^{V600E} organoids as shown by an increase in *Serpin1* mRNA levels. However, organoids containing loss of function of *Tgfβr2* have low basal expression of *Serpin1* and are not Tgfβ responsive (**Supplementary Figure 3**). Next, removal of Wnt-ligands, Wnt3a and Rspo2, kills WT, *Braf*^{V600E}, *Braf*^{V600E}Δ*T* and control transfected cultures (**Figure 2B)**. However, transfection of plasmids encoding Cas9 and guideRNAs (gRNAs) targeting the negative Wnt regulators, *Rnf43* and *Znrf3*, allowed outgrowth of organoids with cystic morphology (**Figure 2B,** growth of organoids in Wnt-ligand deficient NT medium). Loss of the p16Ink4a tumour suppressor was not directly selected for using changed media conditions, but this gene was targeted simultaneously with *Rnf43* and *Znrf3* and its loss likely provided a growth advantage to *Braf*^{V600E} mutant cells [17]. This resulted in *Braf*^{V600E}*;Tgfbr2*$^{\Delta/\Delta}$*;Rnf43*$^{\Delta/\Delta}$*/Znrf3*$^{\Delta/\Delta}$*;p16 Ink4a*$^{\Delta/\Delta}$ (*Braf*^{V600E}Δ*TRZI)* organoids. qRT-PCR analysis of the Wnt-pathway response genes, *Axin2* and *Lgr5*, showed that activation of this pathway in the *Braf*^{V600E}Δ*TRZI* organoids in the absence of Wnt ligands is similar to the level in control *Braf*^{V600E} organoids cultured in the presence of Wnt ligands, i.e. the pathway is super-activated by targeting *Rnf43* and *Znrf3* (**Supplementary Figure 3**). qRT-PCR analysis also indicates a reduction in p16Ink4a mRNA levels in *Braf*^{V600E}Δ*TRZI* compared to *Braf*^{V600E} organoids (**Supplementary Figure 3**).

Lastly, to select for loss of *Mlh1* we exploited the clinical finding that MSI-High (MSI-H) cancers are reported to show relative resistance to backbone chemotherapeutic 5-fluorouracil (5-FU) [33]. We used media containing 5-FU to promote DNA mismatches [34]. Mlh1 is an essential component of the DNA mismatch machinery [35] and so we hypothesised that inactivation of *Mlh1* would lead to increased survival of cells despite DNA damage-arrest signals, consistent with the poor response of MSI CRC to 5-FU based adjuvant chemotherapy [33]. Organoids that had been transfected with a plasmid encoding Cas9 and a gRNA targeting *Mlh1* (*Braf*^{V600E}Δ*TRZIM)* were better able to withstand a pulse of 5FU treatment than control transfected *Braf*^{V600E}Δ*TRZI* (**Figure 2B**). The activity of previously unpublished gRNAs (*Tgfβr2* and *Mlh1* gRNAs) was evaluated in polyclonal organoids before proceeding to handpicking single clones and expansion of lines (**Supplementary Figure 4**). We also used bioinformatic prediction of the possible off-target sites for each of these gRNAs and verified that they were not changed in our organoid lines by Sanger sequencing (**Supplementary Table 1**). Bi-allelic, loss of function insertions and deletions (indels) in target genes were verified using DNA sequencing (**Figure 2C, Supplementary Table 2**).

To assess the effect of this series of genetic alterations on colorectal tumourigenesis, we transplanted organoids into NOD.Cg-*Prkdc*^{scid}*Il2rg*$^{tm1Wjl/Szj}$ (NSG) mice and used *in vivo* murine colonoscopy to directly visualize and score pathologic changes (**Figure 3A, Supplementary Videos**). Using a modified needle attachment, we injected organoids into the orthotopic site, the mucosal layer of the colon wall (**Figure 3A, Supplementary Figure 5A, 5B**) [36]. Injection of *Braf*^{V600E} mutant organoids failed to induce tumour formation over a 3 month time course as assessed by colonoscopic surveillance, at necropsy and by pathological evaluation (**Figure 3B, 4B, Supplementary Figure 6**). Introduction of Tgfβ pathway perturbation in *Braf*^{V600E}Δ*T* organoids results in 57% of organoid injections forming tumours within 3 months (**Figure 3B**). However, significantly more *Braf*^{V600E}Δ*TRZI* and *Braf*^{V600E}Δ*TRZIM* injected organoids formed tumours, 98% and 100% respectively (**Figure 3B**, $p<0.05$). Similar to human sessile serrated polyps, 94% (n=11 mice) of *Braf*^{V600E}Δ*TRZI*

and 100% (n=8 mice) of *Braf*^{V600E}Δ*TRZIM* tumours developed a noticeable mucus cap visible from two weeks post-injection via colonoscopic surveillance [37] (**Supplementary Figure 5C**). This is in contrast to only 9% (n=12 mice) of the *Braf*^{V600E}Δ*T* tumours with a mucus cap. The more genetically complex organoids (*Braf*^{V600E}Δ*TRZI* and *Braf*^{V600E}Δ*TRZIM*) grew significantly more quickly than *Braf*^{V600E}Δ*T* tumours (**Figure 3C, Supplementary Figure 6,** p<0.001) and overall survival was also significantly decreased, with mean time from injection to humane endpoint of the experiment at 6 weeks for *Braf*^{V600E}Δ*TRZI* and 4 weeks for *Braf*^{V600E}Δ*TRZIM* (**Figure 3D**, p<0.001).

Histologically, tumours generated using *Braf*^{V600E}Δ*T*, *Braf*^{V600E}Δ*TRZI* and *Braf*^{V600E}Δ*TRZIM* organoids are invasive, adenocarcinomas with features of human serrated CRC (**Figure 4, Supplementary Table 3**) [2, 38]. We observed infrequent liver metastasis (9% or 1 out of 11) mice), with no macro-metastasis to other sites (lung, peritoneum) after injection with *Braf*^{V600E}Δ*TRZI* (**Supplementary Figure 5D**). Organoid-derived cells were readily visualised by morphology and using immunohistochemical detection of Braf^{V600E} (**Figure 4D, Supplementary Figure 5E**). The tumours display a substantial desmoplastic stromal reaction (**Figure 4E**), particularly with *Braf*^{V600E}Δ*TRZI* compared to the less genetically complex *Braf*^{V600E}Δ*T* (85% vs. 33% p<0.05, **Supplementary Table 3**). Thus the genetics of the tumour in this model was important in the co-evolution of the stroma. This stromal reaction is composed of smooth muscle actin expressing cancer activated fibroblasts amongst other cell types (**Figure 4G**). The more complex *Braf*^{V600E}Δ*TRZI* and *Braf*^{V600E}Δ*TRZIM,* but not *Braf*^{V600E}Δ*T* tumours, featured tumour budding (**Figure 4F, Supplementary Figure 5F**) and approximately half were categorised as mucinous adenocarcinoma [38], indicating a change to the amount of mucin produced by tumours with more complex genetic alterations, (42-50% vs. 0% p<0.01, **Supplementary Table 3**). This could also be visualised using Alcian Blue mucin staining (**Figure 4G**). *Muc2* mRNA, encoding a core component of mucus, was increased in the *Braf*^{V600E}Δ*TRZI* but not the *Braf*^{V600E} or *Braf*^{V600E}Δ*T* organoids (p<0.05, **Supplementary Figure 7**).

To investigate the consequences of mutating the essential DNA damage response gene, *Mlh1*, we analysed microsatellite marker length in our organoid series. *Braf*^{V600E}Δ*TRZIM,* but not *Braf*^{V600E}Δ*TRZI* organoids have altered microsatellite length (MSI) when compared to the donor mouse from which organoids were derived, in 4 mononucleotide markers previously validated for use in mouse [39, 40]. These cells accrued further MSI *in vivo*, with *Braf*^{V600E}Δ*TRZIM*, but not *Braf*^{V600E}Δ*TRZI* tumours containing additional microsatellite tract length variability (**Supplementary Figure 8**).

Discrete transcript profiles of serrated and conventional pathway tumours

In addition to our series of serrated pathway tumours, we also generated tumours driven by alteration of commonly mutated conventional CRC pathway genes, *Apc* and *Kras*^{G12D}. Similar to previous reports [36], colonic organoids expressing adeno-virally delivered Cre, derived from *Kras*$^{LSL\text{-}G12D/+}$;*Apc*$^{fl/fl}$ mice survived culture in the absence of Wnt3a or Rspo2 (**Supplementary Figure 9**). Adenocarcinomas arising from orthotopic injection of *Kras*$^{G12D/+}$;*Apc*$^{fl/fl}$ organoids, were verified as *Kras*$^{G12D/+}$;*Apc*$^{\Delta 580l/\Delta 580}$ (*Kras*^{G12D};*Apc*$^{\Delta/\Delta}$) genotype and displayed nuclear β-catenin localisation (**Supplementary Figure 9**). We isolated RNA from our series of serrated and conventional pathway tumours and compared

mRNAseq expression profiles between these different tumours and normal colonic mucosa from tumour bearing animals (n=4 biological replicates per group). The multidimensional scaling (MDS) plot generated from our RNAseq data showed that, as expected, the normal colon samples had quite different transcript profiles to the tumour samples (**Figure 5A**). In comparison, the *Braf*^{V600E}, serrated subtype tumours all clustered closely together and separated from the *Kras*^{G12D}*;Apc*$^{\Delta/\Delta}$ tumours (**Figure 5A**). Consistent with alterations to the MAPK pathway in our *Braf*^{V600E} organoid series, gene set enrichment analysis (GSEA) identified differential expression of MAPK-pathway transcripts as enriched in the *Braf*^{V600E} tumours compared to normal colon (**Supplementary Figure 10A**). Validating our attempt to model MSI CRC, the tumours derived from *Braf*^{V600E}Δ*TRZIM* organoids were also significantly enriched for differential expression of a human MSI CRC-associated gene set (**Supplementary Figure 10B**) [41].

The top enriched gene set based on normalised enrichment score in our analyses across all *Braf*^{V600E}, but not *Kras*^{G12D}*;Apc*$^{\Delta/\Delta}$, tumours when compared to normal colon was the sphingolipid (SP) *de novo* biosynthesis pathway (**Figure 5B, Supplementary Table 4**). We validated the differential expression of SP pathway transcripts from the leading edge of the GSEA by real-time qPCR in *Braf*^{V600E} and conventional pathway tumours (**Figure 5C, Supplementary Figure 11)**. Two key enzymes regulating S1P levels in this pathway are sphingosine kinase 1 (SPHK1) and the counter-acting sphingosine-1-phosphate phosphatase 1 (SGPP1) [42]. Consistent with previous reports in human CRC [43, 44], we observed increased expression of *Sphk1* transcripts in our series of *Braf*^{V600E} tumours compared to normal mouse colon and a converse decrease in *Sgpp1* transcripts (**Figure 5C)**. This suggested at the transcriptomic level that the pathway may be primed for increased production of the pro-survival molecule sphingosine 1-phosphate (S1P) in our model of serrated CRC [42]. We next wished to determine if this shift at the transcript level was also observed in human CRC samples. *SPHK1* was significantly upregulated in 622 TCGA CRC samples compared to matched normal controls, with greatest expression levels in *BRAF*^{V600E} tumours (**Figure 5D**). Conversely, *SGPP1* expression was significantly decreased in all CRC samples compared to matched normal controls. Increased expression of *SPHK1* and decreased expression of *SGPP1* were both separately associated with poor survival in the TCGA cohort (**Figure 5E**).

DISCUSSION:

Here we have focused on the serrated pathway to CRC that accounts for up to 25% of all CRC, and for microsatellite stable cases has very poor outcome [2]. We have developed a panel of CRISPR/Cas9 genome engineered organoids that model DNA alterations found in *BRAF* mutant serrated CRC. In this way we are producing novel, preclinical models of colorectal adenocarcinoma with features of serrated CRC, and most notably desmoplastic stromal responses, infiltrative growth, tumour budding and mucinous differentiation [2, 45, 46] (**see Figure 4, Supplementary Table 3 & Figure 5**). Mucous caps characterise human serrated polyps at colonoscopy. When we look at an early time point in tumour development in our serrated CRC mouse models with complex genetics (*Braf*^{V600E}Δ*TRZI* and *Braf*^{V600E}Δ*TRZIM*) we also observe mucous caps. Previous studies using CRISPR/Cas9 to model the conventional molecular pathway to CRC using human intestinal organoids were

either unable to generate invasive CRC [12], or required 4 gene alterations for invasive tumour growth [13]. We find here that alterations to just two genes, *Braf* and *Tgfbr2*, results in transmurally invasive adenocarcinoma. Further altering the oncogene-induced senescence factor, *p16 Ink4a*, and the Wnt pathway leads to increased tumour initiation and decreased survival time (**Figure 3 & 4**). These more genetically complex tumours had increased stromal response, tumour budding and mucinous differentiation. We also model MSI "hypermutator" CRC by inducing loss-of-function mutations in the DNA mismatch repair gene, *Mlh1*. Similar to recent work describing a 6-fold higher DNA mutation rate in CRISPR/Cas9 engineered $MLH1^{\Delta/\Delta}$ human colon organoid lines [47], we have successfully generated the MSI phenotype as judged by instability in microsatellite repeat tract length (**Supplementary Figure 8**).

We utilise the recently adapted small animal colonoscopy technique [36, 48] to enable rapid, orthotopic injection of engineered organoids to the mucosal layer of the colon wall and tumour monitoring thereafter (**Supplementary Figure 5 & videos**). This is especially salient given the observed differences in metastatic potential for engineered conventional pathway CRC organoids delivered either subcutaneously or using a rectal prolapse model, where only tumours growing at the orthotopic colon site produced liver metastases [49]. A second report using similar conventional pathway mutant organoids injected using a colonoscope resulted in metastasis in 30% of mice [36]. We observe liver metastasis in the serrated CRC models presented here, albeit infrequently, and no lung or peritoneal spread of the disease. This may be due to the model not containing strong metastasis promoting alterations or alternately, in the future, luminal preservation through colonoscopic biopsy may allow a more complete evaluation of disease progression.

These models will advance this field by providing a rapid, inexpensive and pathologically faithful approach to studying the biology of serrated CRC. Other models, whilst valuable in their own right, are slow, require complicated *in vivo* breeding and have a prescribed number and sequence of genetic alterations [18, 19, 50, 51, 52, 53]. Our models can be readily adapted to investigate the many leads generated by next generation sequencing of human serrated CRC and will be particularly valuable for testing potential therapeutics in the setting of complex, but known, genetic landscapes. Transcriptome analysis of our genome engineered models of serrated and conventional CRC have identified putative changes to sphingolipid metabolism in these tumours. The differential expression of transcripts encoding two key enzymes in this pathway are mirrored in human CRC and are associated with worse prognosis. Future work will investigate the therapeutic efficacy of targeting the sphingolipid biosynthesis pathway for $BRAF^{V600E}$ CRC.

METHODS

Mouse experiments. This study was approved by the MIT Institutional Animal Care and Use Committee, QIMR Berghofer and SAHMRI Animal Ethics committees (P1208, SAM174, SAM205). Mice heterozygous for both the conditionally active $Braf^{CA}$ and $Villin\text{-}Cre^{ERT2}$ alleles to induce the mutation analogous to human $BRAF^{V600E}$ specifically in the intestine were generated as described [52]. Similarly, mice containing the $Kras^{LSL\text{-}G12D/+}$ [54] and $Apc^{CKO/CKO}$ [55] alleles were interbred to produce double transgenic offspring that were used to generate $Kras^{G12D/+}$; $Apc^{\Delta 580l/\Delta 580}$ colonic organoids [36].

Orthotopic Injection. NOD.Cg-*Prkdc*^{scid}*Il2rg*^{tm1Wjl}/SzJ (NSG) mice (male and female, 6-12 weeks old) were obtained from the SAHMRI Bioresources facility and housed under pathogen-free conditions. Organoids were isolated from matrigel and dissociated to single cells and small clusters using TrypLE. The cell clusters (equivalent to ~150 organoids) were washed three times with cold PBS containing 10uM Y-27632 and then resuspended in 20ul 10% GFR matrigel 1:1000 india ink, 10uM Y-27632 in PBS and injected into the mucosa of the distal colon of anaesthetised NSG mice. Colonoscopy-guided orthotopic injection into the colon wall was undertaken as previously described [36] with modifications described in Supplementary methods.

Genome engineering. gRNAs specific for each target gene were either published sequences targeting *Rnf43, Znrf3* or *p16 Ink4a* [56, 57] or designed *de novo* using the CRISPR design Tool to target the first exon immediately downstream of the translation start codon [11] (see Supplementary Methods table 2). gRNA oligos were cloned into px-459, which expresses both the Cas9 nuclease and single gRNAs [11]. Organoid transfection and culture details are included in the Supplementary methods section.

Nucleic acid analyses, bioinformatics, western blotting and immunohistochemistry. Please see the Supplementary Methods section.

ACKNOWLEDGMENTS:

The Rspo-2 expression plasmid was a kind gift from Prof. Anthony Burgess (Walter & Eliza Hall Institute of Medical Research, Australia), L-Wnt3a cells were a kind gift of Prof. Hans Clevers (Hubrecht Institute, The Netherlands). Dr. Mark Van der Hoek and staff at the David R. Gunn Genomics Facility at SAHMRI, John Toubia, Andreas Schreiber, Joel Geoghegan and staff at the Adelaide Australian Cancer Research Foundation Genomics Facility for useful discussions.

This work was supported by Cure Cancer Australia/Cancer Australia (APP1102534), the Cancer Council SA Beat Cancer Project on behalf of its donors and the State Government of South Australia through the Department of Health SA, by Pathology Queensland, by the Australian National Health and Medical Research Council (NHMRC) through (APP1081852, APP1140236), by the National Institutes of Health (NIH) (K08 CA198002, R00 AG045144, R01 CA211184), the Department of Defense (CA120198), the V Foundation V Scholar Award, the Sidney Kimmel Scholar Award, the Pew-Stewart Trust Scholar Award, the Koch Institute Frontier Research Program through the Kathy and Curt Marble Cancer Research Fund, the American Federation of Aging Research, as well as by the Koch Institute Support Grant P30-CA14051 from the National Cancer Institute. DLW is supported by a NHMRC Career Development Fellowship, VLW by a Gastroenterological Society of Australia Senior Research Fellowship.

REFERENCES

1 Fearon ER, Vogelstein B. A genetic model for colorectal tumorigenesis. Cell 1990;**61**:759-67.

2 Bettington M, Walker N, Clouston A, Brown I, Leggett B, Whitehall V. The serrated pathway to colorectal carcinoma: current concepts and challenges. Histopathology 2013;**62**:367-86.
3 Weisenberger DJ, Siegmund KD, Campan M, Young J, Long TI, Faasse MA*, et al.* CpG island methylator phenotype underlies sporadic microsatellite instability and is tightly associated with BRAF mutation in colorectal cancer. Nature genetics 2006;**38**:787-93.
4 Tejpar S, Bertagnolli M, Bosman F, Lenz HJ, Garraway L, Waldman F*, et al.* Prognostic and predictive biomarkers in resected colon cancer: current status and future perspectives for integrating genomics into biomarker discovery. Oncologist 2010;**15**:390-404.
5 Pai RK, Jayachandran P, Koong AC, Chang DT, Kwok S, Ma L*, et al.* BRAF-mutated, microsatellite-stable adenocarcinoma of the proximal colon: an aggressive adenocarcinoma with poor survival, mucinous differentiation, and adverse morphologic features. Am J Surg Pathol 2012;**36**:744-52.
6 Rex DK, Ahnen DJ, Baron JA, Batts KP, Burke CA, Burt RW*, et al.* Serrated lesions of the colorectum: review and recommendations from an expert panel. Am J Gastroenterol 2012;**107**:1315-29.
7 Anderson JC, Robertson DJ. Serrated Polyp Detection by the Fecal Immunochemical Test: An Imperfect FIT. Clinical gastroenterology and hepatology : the official clinical practice journal of the American Gastroenterological Association 2017;**15**:880-2.
8 Sato T, Stange DE, Ferrante M, Vries RG, Van Es JH, Van den Brink S*, et al.* Long-term expansion of epithelial organoids from human colon, adenoma, adenocarcinoma, and Barrett's epithelium. Gastroenterology 2011;**141**:1762-72.
9 Barker N. Adult intestinal stem cells: critical drivers of epithelial homeostasis and regeneration. Nature reviews Molecular cell biology 2014;**15**:19-33.
10 Clevers H. Modeling Development and Disease with Organoids. Cell 2016;**165**:1586-97.
11 Ran FA, Hsu PD, Wright J, Agarwala V, Scott DA, Zhang F. Genome engineering using the CRISPR-Cas9 system. Nat Protoc 2013;**8**:2281-308.
12 Matano M, Date S, Shimokawa M, Takano A, Fujii M, Ohta Y*, et al.* Modeling colorectal cancer using CRISPR-Cas9-mediated engineering of human intestinal organoids. Nat Med 2015;**21**:256-62.
13 Drost J, van Jaarsveld RH, Ponsioen B, Zimberlin C, van Boxtel R, Buijs A*, et al.* Sequential cancer mutations in cultured human intestinal stem cells. Nature 2015;**521**:43-7.
14 Fujii M, Shimokawa M, Date S, Takano A, Matano M, Nanki K*, et al.* A Colorectal Tumor Organoid Library Demonstrates Progressive Loss of Niche Factor Requirements during Tumorigenesis. Cell Stem Cell 2016;**18**:827-38.
15 Cancer Genome Atlas N. Comprehensive molecular characterization of human colon and rectal cancer. Nature 2012;**487**:330-7.
16 Cohen R, Cervera P, Svrcek M, Pellat A, Dreyer C, de Gramont A*, et al.* BRAF-Mutated Colorectal Cancer: What Is the Optimal Strategy for Treatment? Curr Treat Options Oncol 2017;**18**:9.
17 Kriegl L, Neumann J, Vieth M, Greten FR, Reu S, Jung A*, et al.* Up and downregulation of p16(Ink4a) expression in BRAF-mutated polyps/adenomas indicates a senescence barrier in the serrated route to colon cancer. Modern pathology : an official journal of the United States and Canadian Academy of Pathology, Inc 2011;**24**:1015-22.
18 Bennecke M, Kriegl L, Bajbouj M, Retzlaff K, Robine S, Jung A*, et al.* Ink4a/Arf and oncogene-induced senescence prevent tumor progression during alternative colorectal tumorigenesis. Cancer Cell 2010;**18**:135-46.
19 Rad R, Cadinanos J, Rad L, Varela I, Strong A, Kriegl L*, et al.* A genetic progression model of Braf(V600E)-induced intestinal tumorigenesis reveals targets for therapeutic intervention. Cancer Cell 2013;**24**:15-29.
20 Krtolica K, Krajnovic M, Usaj-Knezevic S, Babic D, Jovanovic D, Dimitrijevic B. Comethylation of p16 and MGMT genes in colorectal carcinoma: correlation with clinicopathological features and prognostic value. World J Gastroenterol 2007;**13**:1187-94.

21 Ma X, Wang YW, Zhang MQ, Gazdar AF. DNA methylation data analysis and its application to cancer research. Epigenomics 2013;**5**:301-16.
22 Herman JG, Merlo A, Mao L, Lapidus RG, Issa JP, Davidson NE*, et al.* Inactivation of the CDKN2/p16/MTS1 gene is frequently associated with aberrant DNA methylation in all common human cancers. Cancer Res 1995;**55**:4525-30.
23 Bond CE, McKeone DM, Kalimutho M, Bettington ML, Pearson SA, Dumenil TD*, et al.* RNF43 and ZNRF3 are commonly altered in serrated pathway colorectal tumorigenesis. Oncotarget 2016;**7**:70589-600.
24 Koo BK, Spit M, Jordens I, Low TY, Stange DE, van de Wetering M*, et al.* Tumour suppressor RNF43 is a stem-cell E3 ligase that induces endocytosis of Wnt receptors. Nature 2012;**488**:665-9.
25 Murakami T, Mitomi H, Saito T, Takahashi M, Sakamoto N, Fukui N*, et al.* Distinct WNT/beta-catenin signaling activation in the serrated neoplasia pathway and the adenoma-carcinoma sequence of the colorectum. Modern pathology : an official journal of the United States and Canadian Academy of Pathology, Inc 2015;**28**:146-58.
26 Borowsky J, Dumenil T, Bettington M, Pearson SA, Bond C, Fennell L*, et al.* The role of APC in WNT pathway activation in serrated neoplasia. Modern pathology : an official journal of the United States and Canadian Academy of Pathology, Inc 2017.
27 Giannakis M, Hodis E, Jasmine Mu X, Yamauchi M, Rosenbluh J, Cibulskis K*, et al.* RNF43 is frequently mutated in colorectal and endometrial cancers. Nature genetics 2014;**46**:1264-6.
28 Parsons R, Myeroff LL, Liu B, Willson JK, Markowitz SD, Kinzler KW*, et al.* Microsatellite instability and mutations of the transforming growth factor beta type II receptor gene in colorectal cancer. Cancer research 1995;**55**:5548.
29 Li X, Yao X, Wang Y, Hu F, Wang F, Jiang L*, et al.* MLH1 promoter methylation frequency in colorectal cancer patients and related clinicopathological and molecular features. PLoS One 2013;**8**:e59064.
30 IJspeert J, Vermeulen L, Meijer GA, Dekker E. Serrated neoplasia-role in colorectal carcinogenesis and clinical implications. Nat Rev Gastroenterol Hepatol 2015;**12**:401-9.
31 Di Nicolantonio F, Martini M, Molinari F, Sartore-Bianchi A, Arena S, Saletti P*, et al.* Wild-type BRAF is required for response to panitumumab or cetuximab in metastatic colorectal cancer. Journal of clinical oncology : official journal of the American Society of Clinical Oncology 2008;**26**:5705-12.
32 Fessler E, Drost J, van Hooff SR, Linnekamp JF, Wang X, Jansen M*, et al.* TGFbeta signaling directs serrated adenomas to the mesenchymal colorectal cancer subtype. EMBO Mol Med 2016;**8**:745-60.
33 Ribic CM, Sargent DJ, Moore MJ, Thibodeau SN, French AJ, Goldberg RM*, et al.* Tumor Microsatellite-Instability Status as a Predictor of Benefit from Fluorouracil-Based Adjuvant Chemotherapy for Colon Cancer. New England Journal of Medicine 2003;**349**:247-57.
34 Longley DB, Harkin DP, Johnston PG. 5-fluorouracil: mechanisms of action and clinical strategies. Nat Rev Cancer 2003;**3**:330-8.
35 Li GM. Mechanisms and functions of DNA mismatch repair. Cell Res 2008;**18**:85-98.
36 Roper J, Tammela T, Cetinbas NM, Akkad A, Roghanian A, Rickelt S*, et al.* In vivo genome editing and organoid transplantation models of colorectal cancer and metastasis. Nat Biotechnol 2017;**35**:569-76.
37 Saito S, Tajiri H, Ikegami M. Serrated polyps of the colon and rectum: Endoscopic features including image enhanced endoscopy. World J Gastrointest Endosc 2015;**7**:860-71.
38 Bosman FT, Carneiro, F., Hruban, R.H., Theise, N.D. WHO Classification of Tumours of the Digestive System, 2010.
39 Bacher JW, Abdel Megid WM, Kent-First MG, Halberg RB. Use of mononucleotide repeat markers for detection of microsatellite instability in mouse tumors. Mol Carcinog 2005;**44**:285-92.
40 Kabbarah O, Mallon MA, Pfeifer JD, Edelmann W, Kucherlapati R, Goodfellow PJ. A panel of repeat markers for detection of microsatellite instability in murine tumors. Mol Carcinog 2003;**38**:155-9.

41 Watanabe T, Kobunai T, Toda E, Yamamoto Y, Kanazawa T, Kazama Y*, et al.* Distal colorectal cancers with microsatellite instability (MSI) display distinct gene expression profiles that are different from proximal MSI cancers. Cancer Res 2006;**66**:9804-8.
42 Pitson SM. Regulation of sphingosine kinase and sphingolipid signaling. Trends Biochem Sci 2011;**36**:97-107.
43 Kawamori T, Osta W, Johnson KR, Pettus BJ, Bielawski J, Tanaka T*, et al.* Sphingosine kinase 1 is up-regulated in colon carcinogenesis. FASEB J 2006;**20**:386-8.
44 Oskouian B, Saba J. Sphingosine-1-phosphate metabolism and intestinal tumorigenesis: lipid signaling strikes again. Cell Cycle 2007;**6**:522-7.
45 Chen D, Huang JF, Liu K, Zhang LQ, Yang Z, Chuai ZR*, et al.* BRAFV600E mutation and its association with clinicopathological features of colorectal cancer: a systematic review and meta-analysis. PLoS One 2014;**9**:e90607.
46 Garcia-Solano J, Conesa-Zamora P, Trujillo-Santos J, Makinen MJ, Perez-Guillermo M. Tumour budding and other prognostic pathological features at invasive margins in serrated colorectal adenocarcinoma: a comparative study with conventional carcinoma. Histopathology 2011;**59**:1046-56.
47 Drost J, van Boxtel R, Blokzijl F, Mizutani T, Sasaki N, Sasselli V*, et al.* Use of CRISPR-modified human stem cell organoids to study the origin of mutational signatures in cancer. Science 2017;**358**:234-8.
48 Zigmond E, Halpern Z, Elinav E, Brazowski E, Jung S, Varol C. Utilization of murine colonoscopy for orthotopic implantation of colorectal cancer. PLoS One 2011;**6**:e28858.
49 de Sousa e Melo F, Kurtova AV, Harnoss JM, Kljavin N, Hoeck JD, Hung J*, et al.* A distinct role for Lgr5(+) stem cells in primary and metastatic colon cancer. Nature 2017;**543**:676-80.
50 Carragher LA, Snell KR, Giblett SM, Aldridge VS, Patel B, Cook SJ*, et al.* V600EBraf induces gastrointestinal crypt senescence and promotes tumour progression through enhanced CpG methylation of p16INK4a. EMBO molecular medicine 2010;**2**:458-71.
51 Davies EJ, Marsh Durban V, Meniel V, Williams GT, Clarke AR. PTEN loss and KRAS activation leads to the formation of serrated adenomas and metastatic carcinoma in the mouse intestine. The Journal of pathology 2014;**233**:27-38.
52 Bond CE, Liu C, Kawamata F, McKeone DM, Fernando W, Jamieson S*, et al.* Oncogenic BRAF mutation induces DNA methylation changes in a murine model for human serrated colorectal neoplasia. Epigenetics 2017:01-20.
53 Coffee EM, Faber AC, Roper J, Sinnamon MJ, Goel G, Keung L*, et al.* Concomitant BRAF and PI3K/mTOR blockade is required for effective treatment of BRAF(V600E) colorectal cancer. Clinical cancer research : an official journal of the American Association for Cancer Research 2013;**19**:2688-98.
54 Jackson EL, Willis N, Mercer K, Bronson RT, Crowley D, Montoya R*, et al.* Analysis of lung tumor initiation and progression using conditional expression of oncogenic K-ras. Genes Dev 2001;**15**:3243-8.
55 Kuraguchi M, Wang XP, Bronson RT, Rothenberg R, Ohene-Baah NY, Lund JJ*, et al.* Adenomatous polyposis coli (APC) is required for normal development of skin and thymus. PLoS Genet 2006;**2**:e146.
56 Schwank G, Koo BK, Sasselli V, Dekkers JF, Heo I, Demircan T*, et al.* Functional repair of CFTR by CRISPR/Cas9 in intestinal stem cell organoids of cystic fibrosis patients. Cell Stem Cell 2013;**13**:653-8.
57 Chen S, Sanjana NE, Zheng K, Shalem O, Lee K, Shi X*, et al.* Genome-wide CRISPR screen in a mouse model of tumor growth and metastasis. Cell 2015;**160**:1246-60.

Figure Legends

Figure 1. Co-occurring molecular events in stem-cell niche, microsatellite instability and senescence pathways in *BRAF^{V600E}* mutant serrated CRC. Of the 50 patients with *BRAF^{V600E}* CRC from the TCGA CRC cohort (n=527 patients total), we depict the co-alteration (non-synonymous mutation and/or hyper-methylation) of selected genes in these pathways. Number of patients with each alterations is indicated by bar graph on right, % of *BRAF^{V600E}* cases containing the alteration is indicated by numbers on left. Coloured blocks indicate gene is altered in the sample, grey is unaltered.

Figure 2. Introduction of genetic alterations associated with serrated CRC promotes independence from niche factor requirements. A, activation of MAPK pathway in *Braf^{V600E}* organoids visualized by phosphorylation of the ERK1/2 effector protein, 4-hydroxytamoxifen (4-OHT). **B,** Generation of a 'serratoid' series from normal mouse colonic organoids through sequential CRISPR/Cas9 targeting and *in vitro* selection. *Braf^{V600E}*, *Braf^{V600E}Tgfbr2$^{\Delta/\Delta}$ (Braf^{V600E}ΔT)*, *Braf^{V600E} Tgfbr2$^{\Delta/\Delta}$ Rnf43$^{\Delta/\Delta}$/Znrf3$^{\Delta/\Delta}$ p16Ink4a$^{\Delta/\Delta}$ (Braf^{V600E}ΔTRZI)*, *Braf^{V600E} Tgfbr2$^{\Delta/\Delta}$Rnf43$^{\Delta/\Delta}$/Znrf3$^{\Delta/\Delta}$ p16Ink4a$^{\Delta/\Delta}$Mlh1$^{\Delta/\Delta}$ (Braf^{V600E}ΔTRZIM)*. Normal media components required as stem cell niche factors Wnt-3a (W), Rspo-2 (R), Noggin (N), additional selection with TGFβ1 (T) and chemotherapeutic agent, 5-Fluorouracil (5FU). **C,** DNA sequence verification of biallelic insertion/deletion (indel) mutations that result in prematurely truncated proteins.

Figure 3. *Braf^{V600E}* alone is not sufficient for colon tumour formation, but with increasing serrated pathway genetic alterations tumour penetrance and growth rate increases. A, colonoscopic images showing injection and rapid growth of serratoid *Braf^{V600E}ΔTRZI* line. **B,** Tumour penetrance as a percentage of the number of organoid injections that gave rise to a tumour/mouse in 3 months for each line, with 1-3 injections/mouse. **C,** Colonoscopic scoring of largest tumour in each mouse (n=5 mice per group, Becker scale). **D,** Kaplan-Meier plot showing overall survival post-injection with organoid lines *Braf^{V600E}* n=4 mice, *Braf^{V600E}ΔT* n=12 mice, *Braf^{V600E}ΔTRZI* n=11 mice, *Braf^{V600E}ΔTRZIM* n=8 mice, compared to *Braf^{V600E}* using a Bonferroni adjustment for multiple comparisons. ns=not significant, *=p≤0.05, **=p≤0.01, ***=p≤0.001.

Figure 4. Multi-hit 'serratoids' generate invasive adenocarcinoma with features of human serrated CRC. Colonoscopy **(A)** and histology **(B-H)** images of mouse colon orthotopically injected with mutant organoid lines *Braf^{V600E}*, *Braf^{V600E}ΔT*, *Braf^{V600E}ΔTRZI*, *Braf^{V600E}ΔTRZIM*. **B,** H&E stained sections of whole colon. **C,** higher magnification H&E, arrows denote position of muscularis mucosae, * denotes remnant ink from injection. **D,** immunohistochemical staining for mutant Braf^{V600E} protein clearly delineates serratoid derived tumour cells. **E,** representative images of desmoplastic stromal response and **F,** tumour budding (circled). **G,** tumour stromal response stains positive for alpha-smooth muscle actin (aSMA). **H,** mucin lakes present in mucinous adenocarcinoma visualised using Alcian Blue stain. Scale bars are (B) 500um, (C-H) 100um.

Figure 5. Serrated pathway tumours are molecularly distinct from conventional pathway tumours. A, multi-dimensional scaling plot of RNA expression data from normal mouse colon (black), serrated pathway *Braf*^{V600E}*ΔT* (blue), *Braf*^{V600E}*ΔTRZI* (red) and *Braf*^{V600E}*ΔTRZIM* (yellow) and conventional pathway tumours *Kras*^{G12D}*;Apc*$^{\Delta/\Delta}$ (grey), n=4 samples per group. **B,** gene set enrichment analysis (GSEA) for Sphingolipid *de novo* biosynthesis Reactome between *Braf*^{V600E}*ΔTRZI* serrated tumour and normal mouse colon. Enrichment score (ES), normalised enrichment score (NES), false discovery rate (FDR). **C**, Expression of *Sphk1* is increased and *Sgpp1* is decreased in mouse *Braf*^{V600E} serrated CRC compared to normal mouse colon. Fold induction of mRNA expression is normalized to *Gapdh*, with transcript level in normal colon set to 1. Results from at least four animals with triplicate technical replicates are shown, error bars denote standard deviation. Two-tailed t-test used for pair-wise statistical analysis. **D,** Violin plots depicting z-score values for normalized expression of *SPHK1* (top) and *SGPP1* (bottom) transcripts in 622 human TCGA CRC and normal colon samples separated into wild-type *BRAF/KRAS*, *KRAS* mutant and *BRAF*^{V600E} CRC. **E,** Kaplan-Meier plots showing TCGA patient survival probability based on expression level of *SPHK1* (top, *SPHK1* high group n=139 in red, low group n=483 in green) or *SGPP1* (bottom, *SGPP1* low group n=145 in green, high group n=477 in red). *=p≤0.05, **=p≤0.01, ***=p≤0.001, NS= not significant.

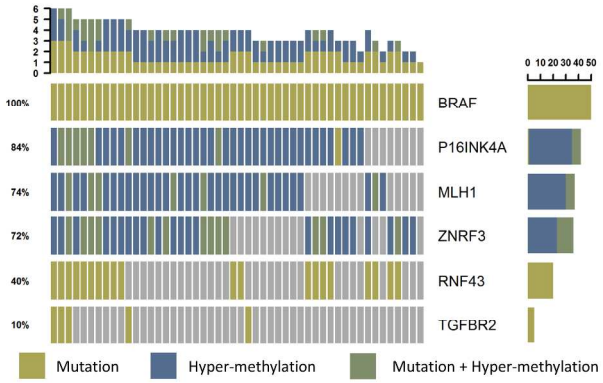

Figure 1.

Figure 1. Co-occurring molecular events in stem-cell niche, microsatellite instability and senescence pathways in BRAFV600E mutant serrated CRC. Of the 50 patients with BRAFV600E CRC from the TCGA CRC cohort (n=527 patients total), we depict the co-alteration (non-synonymous mutation and/or hyper-methylation) of selected genes in these pathways. Number of patients with each alterations is indicated by bar graph on right, % of BRAFV600E cases containing the alteration is indicated by numbers on left. Coloured blocks indicate gene is altered in the sample, grey is unaltered.

254x190mm (300 x 300 DPI)

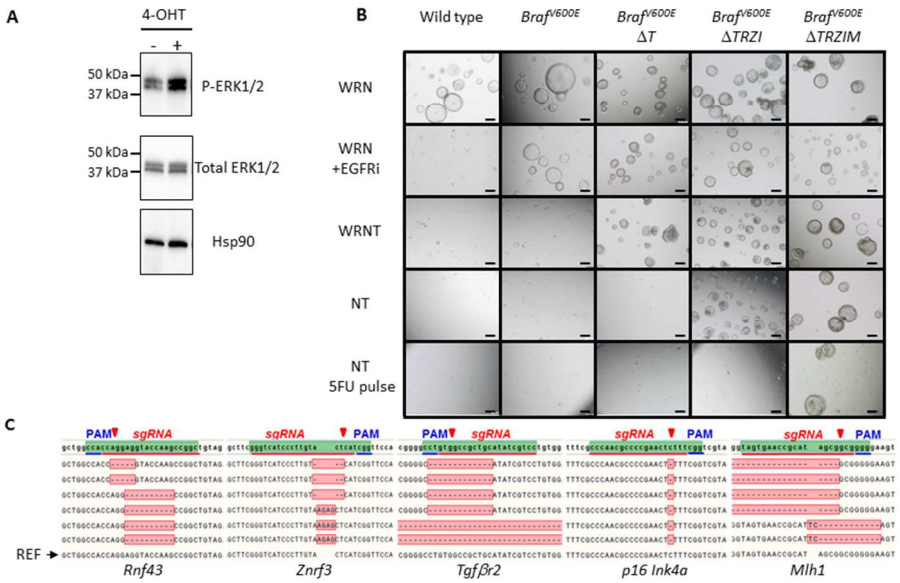

Figure 2.

Figure 2. Introduction of genetic alterations associated with serrated CRC promotes independence from niche factor requirements. A, activation of MAPK pathway in BrafV600E organoids visualized by phosphorylation of the ERK1/2 effector protein, 4-hydroxytamoxifen (4-OHT). B, Generation of a 'serratoid' series from normal mouse colonic organoids through sequential CRISPR/Cas9 targeting and in vitro selection. BrafV600E, BrafV600ETgfbr2Δ/Δ (BrafV600EΔT), BrafV600E Tgfbr2Δ/Δ Rnf43Δ/Δ/Znrf3Δ/Δ p16Ink4aΔ/Δ (BrafV600EΔTRZI), BrafV600E Tgfbr2Δ/Δ Rnf43Δ/Δ /Znrf3Δ/Δ p16Ink4aΔ/Δ Mlh1Δ/Δ (BrafV600EΔTRZIM). Normal media components required as stem cell niche factors Wnt-3a (W), Rspo-2 (R), Noggin (N), additional selection with TGFβ1 (T) and chemotherapeutic agent, 5-Fluorouracil (5FU). C, DNA sequence verification of biallelic insertion/deletion (indel) mutations that result in prematurely truncated proteins.

254x190mm (96 x 96 DPI)

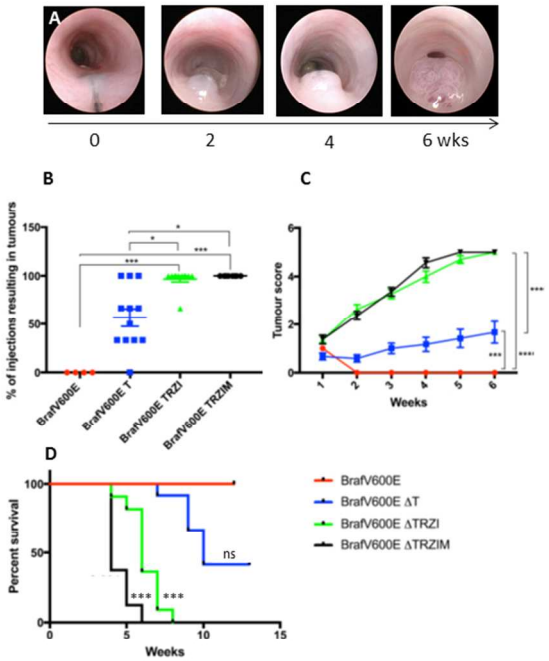

Figure 3.

Figure 3. BrafV600E alone is not sufficient for colon tumour formation, but with increasing serrated pathway genetic alterations tumour penetrance and growth rate increases. A, colonoscopic images showing injection and rapid growth of serratoid BrafV600EΔTRZI line. B, Tumour penetrance as a percentage of the number of organoid injections that gave rise to a tumour/mouse in 3 months for each line, with 1-3 injections/mouse. C, Colonoscopic scoring of largest tumour in each mouse (n=5 mice per group, Becker scale). D, Kaplan-Meier plot showing overall survival post-injection with organoid lines BrafV600E n=4 mice, BrafV600EΔT n=12 mice, BrafV600EΔTRZI n=11 mice, BrafV600EΔTRZIM n=8 mice, compared to BrafV600E using a Bonferroni adjustment for multiple comparisons. ns=not significant, *=p≤0.05, **=p≤0.01, ***=p≤0.001.

254x190mm (96 x 96 DPI)

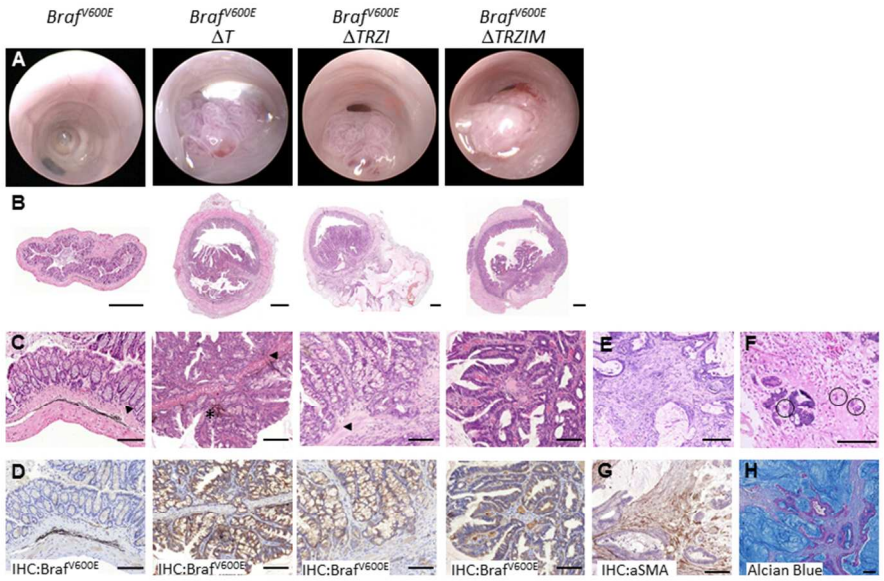

Figure 4.

Figure 4. Multi-hit 'serratoids' generate invasive adenocarcinoma with features of human serrated CRC. Colonoscopy (A) and histology (B-H) images of mouse colon orthotopically injected with mutant organoid lines BrafV600E, BrafV600EΔT, BrafV600EΔTRZI, BrafV600EΔTRZIM. B, H&E stained sections of whole colon. C, higher magnification H&E, arrows denote position of muscularis mucosae, * denotes remnant ink from injection. D, immunohistochemical staining for mutant BrafV600E protein clearly delineates serratoid derived tumour cells. E, representative images of desmoplastic stromal response and F, tumour budding (circled). G, tumour stromal response stains positive for alpha-smooth muscle actin (aSMA). H, mucin lakes present in mucinous adenocarcinoma visualised using Alcian Blue stain. Scale bars are (B) 500um, (C-H) 100um.

254x190mm (96 x 96 DPI)

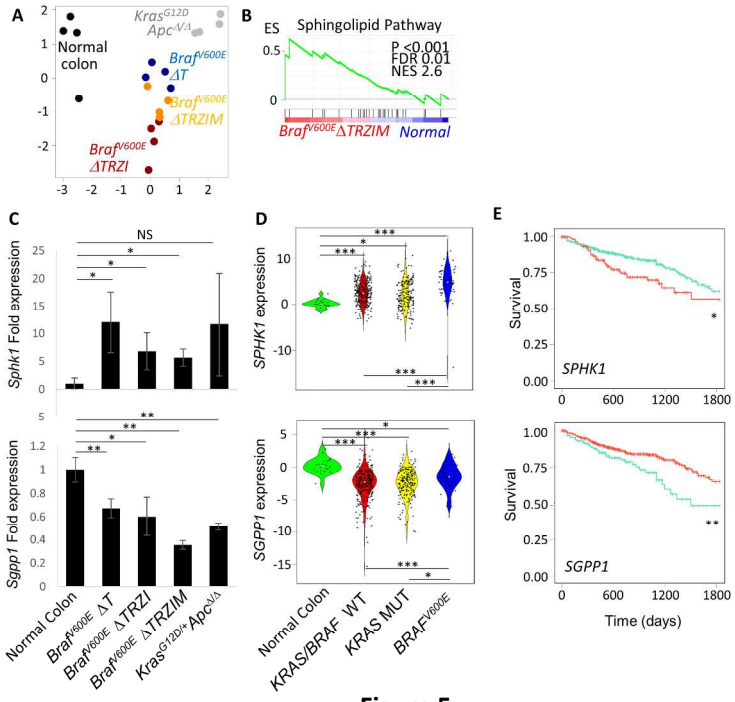

Figure 5.

Figure 5. Serrated pathway tumours are molecularly distinct from conventional pathway tumours. A, multi-dimensional scaling plot of RNA expression data from normal mouse colon (black), serrated pathway BrafV600EΔT (blue), BrafV600EΔTRZI (red) and BrafV600EΔTRZIM (yellow) and conventional pathway tumours KrasG12D;Apc Δ/Δ (grey), n=4 samples per group. B, gene set enrichment analysis (GSEA) for Sphingolipid de novo biosynthesis Reactome between BrafV600EΔTRZI serrated tumour and normal mouse colon. Enrichment score (ES), normalised enrichment score (NES), false discovery rate (FDR). C, Expression of Sphk1 is increased and Sgpp1 is decreased in mouse BrafV600E serrated CRC compared to normal mouse colon. Fold induction of mRNA expression is normalized to Gapdh, with transcript level in normal colon set to 1. Results from at least four animals with triplicate technical replicates are shown, error bars denote standard deviation. Two-tailed t-test used for pair-wise statistical analysis. D, Violin plots depicting z-score values for normalized expression of SPHK1 (top) and SGPP1 (bottom) transcripts in 622 human TCGA CRC and normal colon samples separated into wild-type BRAF/KRAS, KRAS mutant and BRAFV600E CRC. E, Kaplan-Meier plots showing TCGA patient survival probability based on expression level of SPHK1 (top, SPHK1 high group n=139 in red, low group n=483 in green) or SGPP1 (bottom, SGPP1 low group n=145 in green, high group n=477 in red). *=p≤0.05, **=p≤0.01, ***=p≤0.001, NS= not significant.

254x190mm (300 x 300 DPI)

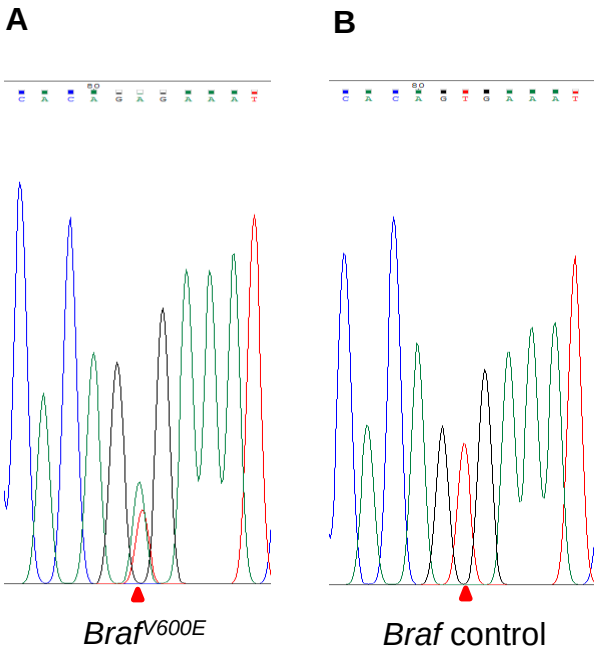

Supplementary Figure 1-Presence of *Braf*^{V600E} mutation in organoids verified by Sanger sequencing. gDNA prepared from 4-hydroxy tamoxifen treated organoids from *Villin*^{CreERT}; *Braf*^{CA} mice (*A*) or vehicle treated controls (B).

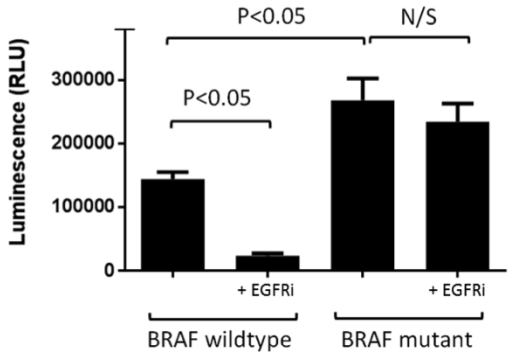

Supplementary Figure 2-Functional Braf^{V600E} in colonic organoids results in increased cellular proliferation and resistance to epidermal growth factor receptor inhibitor (EGFRi) treatment. Quantification of metabolically active cells using Real Time-Glo in *Braf* wild-type or *Braf*^{V600E} mutant mouse colonic organoid cultures after treatment with vehicle or EGFRi. Control cells did not survive in the presence of EGFRi, whilst *Braf*^{V600E} organoids were resistant. Representative experiment conducted in triplicate, error bars denote st.dev.

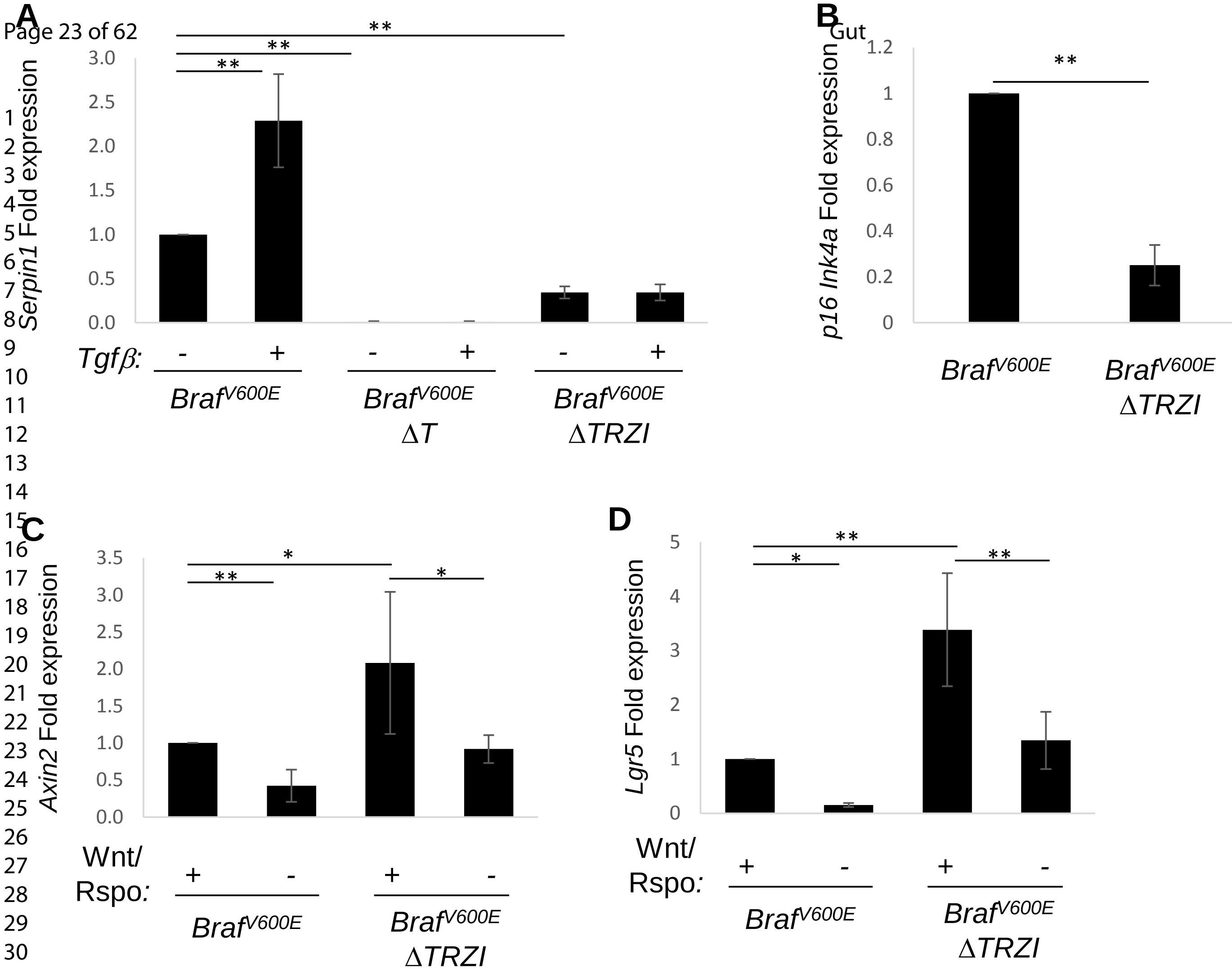

Supplementary Figure 3. **A,** Expression of *Serpin-1*, a Tgfβ response gene, is not induced following treatment with Tgfβ in *Tgfβr2* mutant organoids. **B,** *p16Ink4a* RNA levels are decreased in *p16Ink4a* mutant organoids. **C-D,** Transcript levels of two Wnt-responsive genes, *Axin2* and *Lgr5*, are increased in organoids with mutations in the two negative regulators of the Wnt-pathway, *Rnf43* and *Znrf3*. Fold induction of mRNA expression is normalized to *Gapdh*, with transcript level in *Braf^{V600E}* organoids in complete medium set to 1. Results from at least three independent experiments performed in triplicate are shown, error bars denote standard deviation. Two-tailed t-test was used for pair-wise statistical analysis. *=p≤0.05, **=p≤0.01.

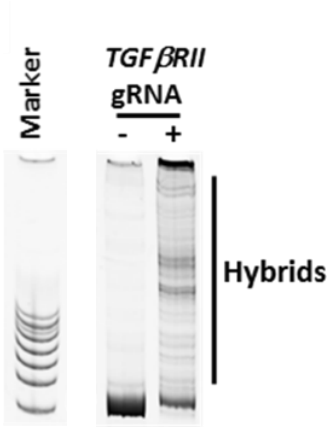

Supplementary Figure 4. Effective targeting of genes associated with serrated CRC using CRISPR/Cas9 gene editing followed by media selection of correctly targeted clones. **A,** Melt/reanneal of PCR amplicons from *Tgfβr2* targeted genomic region in edited clones show the formation of hybrid complexes (slower migrating bands) in the presence of specific gRNAs but not the empty gRNA control by PAGE.

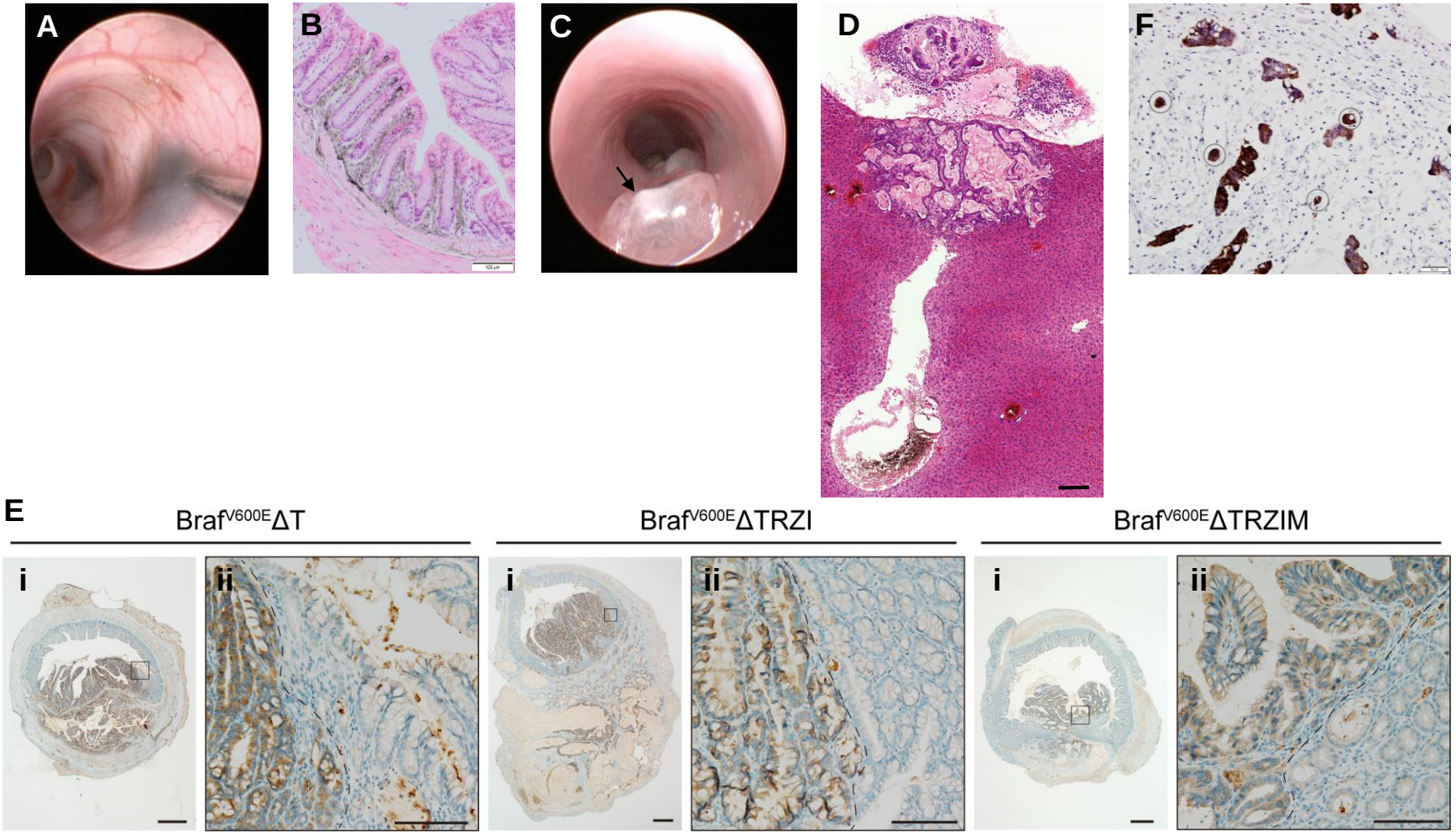

Supplementary Figure 5. Orthotopic injection site in colon wall. **A**, Colonoscopic image with needle and dark ink spots at injection sites and **B**, histological location of injected dye immediately adjacent to the colonic epithelium in the mucosal layer. **C,** Representative colonoscopy image of *Braf^{V600E}ΔTRZI* tumours showing white mucous cap on *Braf^{V600E}ΔTRZI* tumours (arrow). **D,** histology of infrequent liver metastasis (n=1 from 11 mice) in *Braf^{V600E}ΔTRZI* injected animals. **E,** low (i) and high (ii) power images of immunohistochemical staining for mutant BrafV600E protein in serratoid derived tumour cells. These are the same samples as depicted in Figure 4D but here high power image focusses on part of the section with tumour (to left of dashed line in ii) and normal epithelium (to right of dashed line in ii). **F,** tumour budding (circled) from *Braf^{V600E}ΔTRZI* tumours is positive for cytokeratin 20 (CK20) by immunohistochemistry. Scale bars 500um (Ei), 100um (B, D Eii), 50um (F).

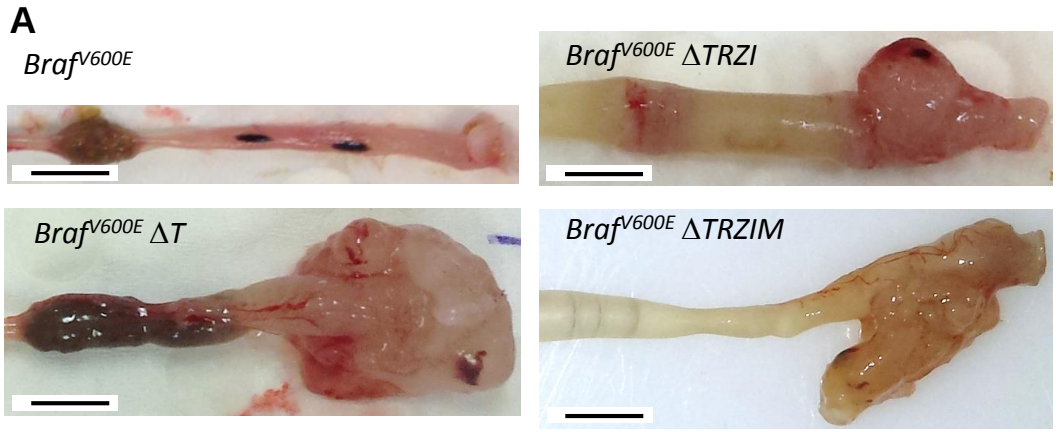

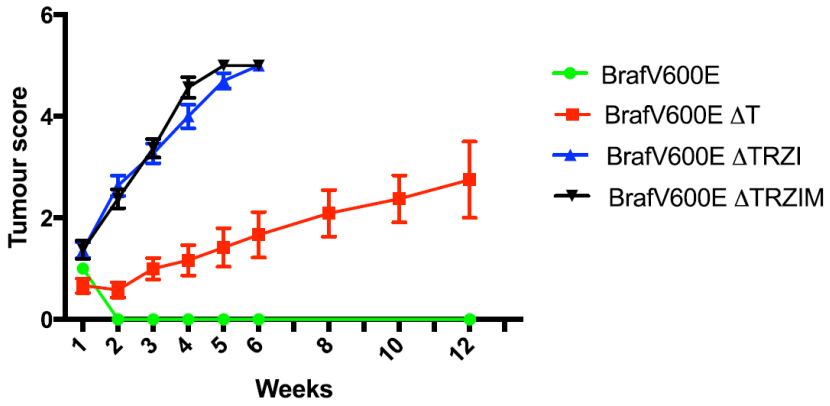

Supplementary Figure 6. A, Necropsy images of dissected distal colon showing ink spots only following *Braf*^{V600E} organoid injections and invasion/extra-colonic growth from more complex organoid lines. Scale bar is 0.5cm. **B,** Colonoscopic scoring of largest tumour in each mouse (n=5 mice per group, Becker scale). Extended time course for tumour scoring to show relatively slow growth of *Braf*^{V600E} *ΔT* tumours out to 12 weeks (Figure 3C depicts the same data but finishes at 6weeks).

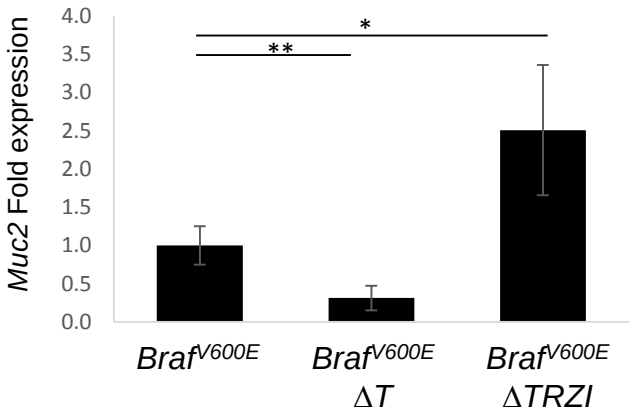

Supplementary Figure 7. Expression *Muc2*, a goblet cell marker and core component of the mucus layer is increased in *Braf*^{V600E}*ΔTRZI* but not *Braf*^{V600E}*ΔT* mutant organoids. Fold induction of mRNA expression is normalized to *Gapdh*, with transcript level in *Braf*^{V600E} organoids in complete medium set to 1. Results from at least three independent experiments performed in triplicate are shown, error bars denote standard deviation. Two-tailed t-test was used for pair-wise statistical analysis. *=p≤0.05, **=p≤0.01.

A

	Gut Microsatellite Markers				
	mBat-26	mBat-67	mBat-37	GA29	TG27
Organoid donor mouse gDNA	wt	wt	wt	wt	wt
BrafV ΔTRZI Organoids	wt	wt	wt	wt	wt
Colon tumours generated by orthotopic injection of *BrafV ΔTRZI* Organoid (n=5)	wt	wt	wt	wt	wt
	wt	wt	wt	wt	wt
	wt	wt	wt	wt	wt
	wt	wt	wt	wt	wt
	wt	wt	wt	wt	wt
BrafV ΔTRZIM Organoid Line 1 (*Mlh1*$^{\Delta/\Delta}$)	1bp Del	3bp Del	1bp Del	wt	wt
BrafV ΔTRZIM Organoid Line 2 (*Mlh1*$^{\Delta/\Delta}$)	ND	ND	1bp Del	wt	2bp Del
BrafV ΔTRZIM Organoid Line 3 (*Mlh1*$^{\Delta/+}$)	ND	ND	1bp Del	wt	wt
Colon tumours generated by orthotopic injection of *BrafV ΔTRZIM* Organoid Line 1 (n=6)	2bp Del	5bp Del + 32bp Del	3bp Del	wt	wt
	1bp Del	4bp Del	wt	wt	wt
	1bp Del	5bp Del	1bp Ins	wt	wt
	1bp Del	4bp Del + 22bp Del	1bp Del	wt	wt
	1bp Del	4bp Del + 22bp Del	1bp Del	wt	wt
	1bp Del	4bp Del + 22bp Del	wt	wt	wt

B

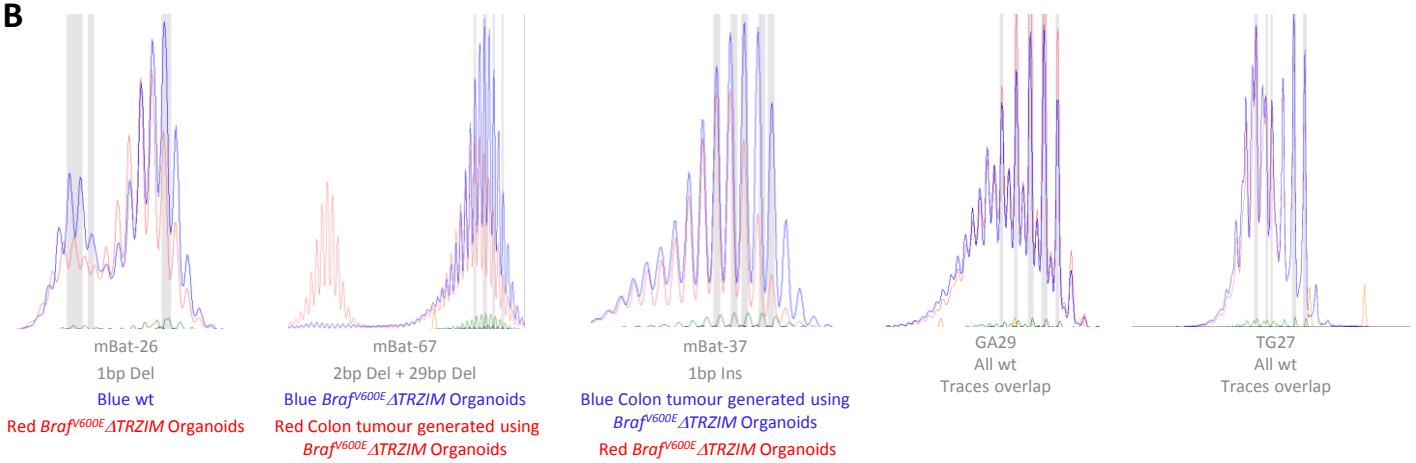

Supplementary Figure 8. Analysis of microsatellite instability using 5 validated mouse microsatellite markers. **A,** repeat tract length for 5 validated mouse microsatellite markers shows variability (MSI) in *Mlh* mutant organoids and tumours. ND not determined. **B,** representative sequence traces of microsatellite marker length.

Supplementary Figure 9. A, colonic organoids derived from *Kras*$^{LSL\text{-}G12D/+}$;*Apc*$^{fl/fl}$ mice, that were treated with Ad5CMV::Cre survived culture in the absence of Wnt3a or Rspo1. **B,** colonoscopic image showing orthotopic growth of *Kras*$^{G12D/+}$;*Apc* $^{\Delta 580l/\Delta 580}$ organoids. **C,** H&E and **D,** Ctnnb1 immunohistochemistry of *Kras*$^{G12D/+}$;*Apc* $^{\Delta 580l/\Delta 580}$ tumours (20x). Genotyping of transgenic alleles confirm **(E)** homozygous recombination of the floxed *Apc* locus and **(F)** heterozygous recombination of the floxed *Kras* locus.

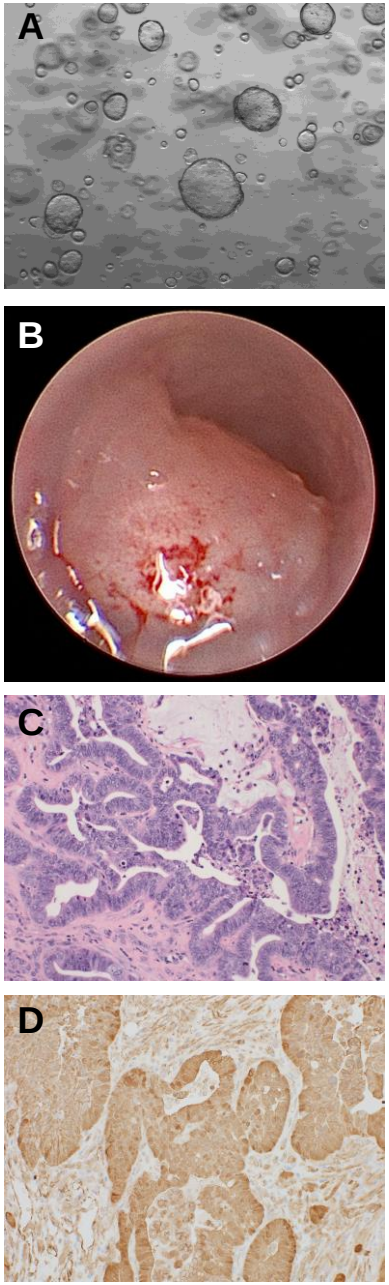

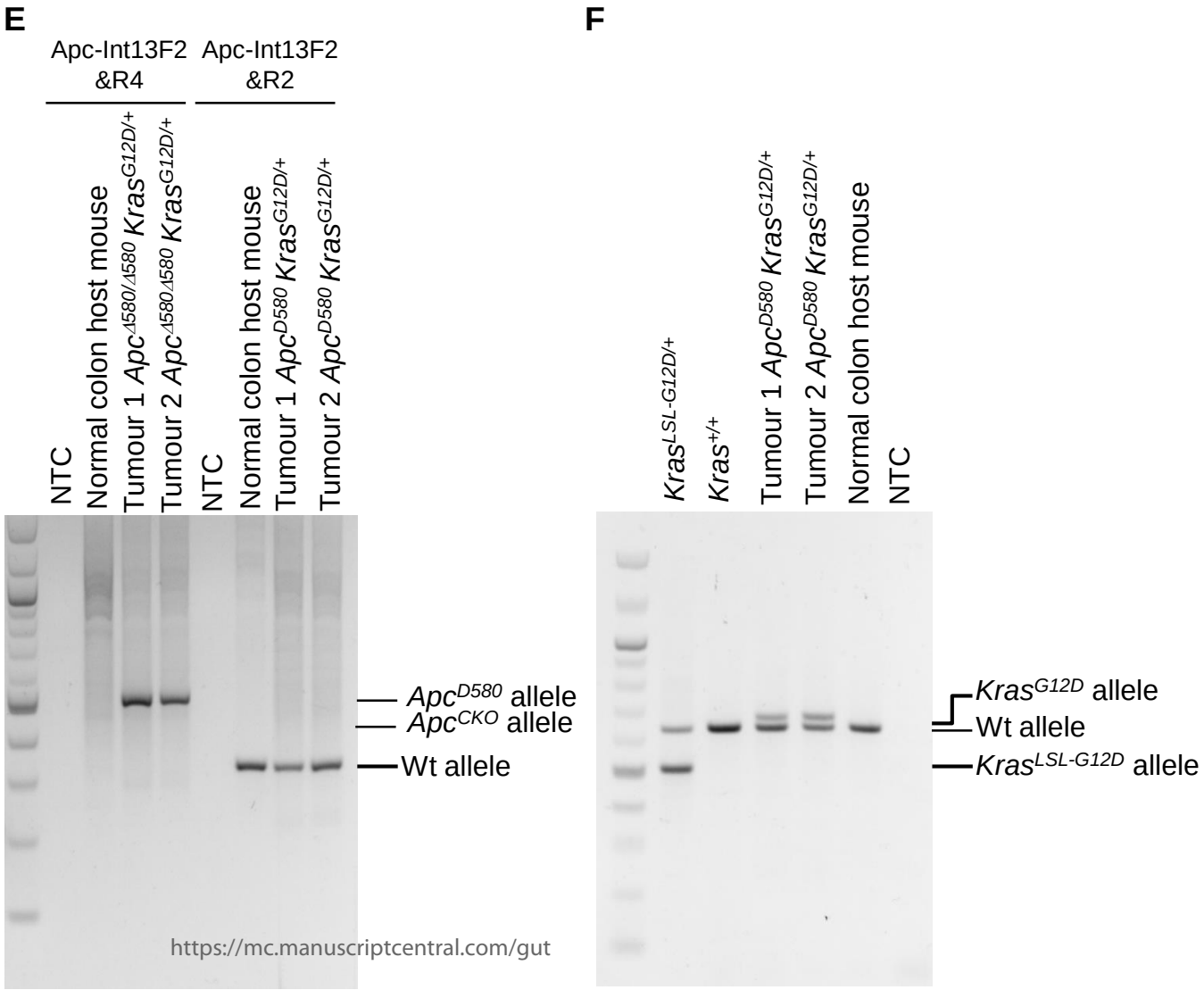

Supplementary Table 1-Sanger sequencing the top bioinformatically predicted *Tgfbr2* and *Bmpr2* gRNA off-target sites reveals no off-target events in mutant organoid lines.

	Location	Sequence	Mismatches	Strand	Type	Comments-sequencing each locus in gDNA isolated from CRISPR/Cas9 gene edited organoid
Tgfbr2 gRNA On-site	9:116174992-116175014	GGACGATATGCAGCGGCCAC AGG	0	+	Exonic	
Tgfbr2_off_site1	18:65431501-65431523	GGAAGATATGAAGGGGCCAC TGG	3	-	Intronic	No change compared to reference mouse genome
Tgfbr2_off_site2	13:74221583-74221605	**GGACCATATGCAGTGGTCAC AGG**	3	+	Intronic	No change compared to reference mouse genome
Tgfbr2_off_site3	12:26345670-26345692	GGCTCACATGCAGCGGCCAC AGG	4	-	Intronic	No change compared to reference mouse genome
Tgfbr2_off_site4	4:74305539-74305561	GGAGCTTATGCAGAGGCCAC AGG	4	-	Intronic	Repeat sequence, Sanger sequencing not possible
Tgfbr2_off_site5	4:124246525-124246547	**GGAAGAGAAGCAGAGGCCAC AGG**	4	+	Intergenic	No change compared to reference mouse genome
Tgfbr2_off_site6	1:87663023-87663045	**GGACGGGAAGCAGAGGCCAC TGG**	4	+	Intronic	No change compared to reference mouse genome
Tgfbr2_off_site7	7:69437642-69437664	GGACCATGTGAAGGGGCCAC TGG	4	-	Intergenic	No change compared to reference mouse genome
Tgfbr2_off_site8	12:118438479-118438501	**GGATTATATGCACAGGCCAC TGG**	4	+	Intergenic	No change compared to reference mouse genome
Tgfbr2_off_site9	8:13155901-13155923	**GGAATATATGCAAAGGCCAC AGG**	4	+	Intergenic	No change compared to reference mouse genome
Tgfbr2_off_site10	6:29249997-29250019	GGAAGATATGAAAAGGCCAC AGG	4	-	Intergenic	No change compared to reference mouse genome

	Location	Sequence	Mismatches	Strand	Type	Comments-sequencing each locus in gDNA isolated from CRISPR/Cas9 gene edited organoid
Mlh1 gRNA On-site	9:111271459-111271481	TAGTGAACCGCATAGCGGCG GGG	0	-	Exonic	
Mlh1_Off_Site1	12:99158597-99158619	CAGTGAACAGCATAGCGGGG AGG	3	-	Intergenic	No change compared to reference mouse genome
Mlh1_Off_Site2	14:53741961-53741983	TAGTAAACAGCAGCGCGGCG AGG	4	+	Intergenic	Identical to reference mouse genome except for SNP:rs579384457. This SNP present in parental mouse gDNA, i.e. not an off-target event.
Mlh1_Off_Site3	15:84631904-84631926	TAGAGAACAGCATGGGGCG GGG	4	-	Intergenic	No change compared to reference mouse genome
Mlh1_Off_Site4	15:36853646-36853668	**TAGTGATCCCCATAGGGCCG GGG**	4	+	Intergenic	No change compared to reference mouse genome
Mlh1_Off_Site5	9:69989986-69990008	**TAGTGCACCCCATAGCCTCG GGG**	4	+	Intronic	No change compared to reference mouse genome
Mlh1_Off_Site6	10:61247708-61247730	**TAGAGAAACGCAGAGCGGGG AGG**	4	+	Intronic	No change compared to reference mouse genome
Mlh1_Off_Site7	5:137788331-137788353	**TACTGAACCCCACAGCGGAG GGG**	4	-	Intronic	No change compared to reference mouse genome
Mlh1_Off_Site8	8:50161834-50161856	TAGTGAACAACAGAGCGGGG GGG	4	-	Intergenic	Repeat sequence, Sanger sequencing not possible
Mlh1_Off_Site9	1:143952103-143952125	TAGAGAACCACATAGTGGTG TGG	4	-	Intergenic	No change compared to reference mouse genome

Supplementary Table 2. Loss of function insertions/deletions (indels) at target sites using CRISPR/Cas9 combined with media selection for correctly targeted organoid clones. Sanger sequencing of each target site allele and resulting change to protein sequence is displayed in the table below. N.B.* we sequenced 7 plasmid clones containing PCR-amplified *p16Ink4a* target genomic sequence and all were identical. This suggests that likely both alleles were altered in an identical manner or a larger deletion has removed the PCR primer sites at the target site for allele 2.

	wt protein	DNA Δ	Change to Protein	DNA Δ	Change to Protein
		Allele 1		**Allele 2**	
Rnf43	784 aa	5bp del	p.R246fs* (premature stop 250aa)	10bp del	p.R246fs* (premature stop 272aa)
Znrf3	913 aa	3bp del	p.T308*del* (912aa)	4bp ins	p.T308*ins** (premature stop 337aa)
Tgfβr2	567 aa	13bp del	p.L9fs* (premature stop 51aa)	339bp del	Removes +1ATG translation start site
p16Ink4a	168 aa	1 bp del	p. S34fs* (premature stop 42aa)	*	
Mlh1	760 aa	31bp del	p.L10fs* (premature stop 24aa)	*2bp ins+12bp del*	p.A19fs* (premature stop 31aa)

	Tumour ID	Type	Serrated Features										Desmoplastic stromal reaction	Infiltrative growth	Tumour budding
			eosinophilic cytoplasm	abundant cytoplasm	basal nuclei	vesicular nuclei	prominent nucleolus	luminal serrations	absence of necrosis	mucin	cell balls and papillary rods	Total score			
$Braf^{V600E}\Delta T$ (n=6)	402	Adenocarcinoma	1	0	0	1	1	0	1	0	0	4	Minimal	Present	Absent
	197	Adenocarcinoma	0	0	1	1	0	0	1	0	0	3	Present	Present	Absent
	199	Adenocarcinoma	0	0	1	0	0	1	1	0	0	3	Minimal	Present	Absent
	457	Adenocarcinoma	0	0	1	1	1	0	1	0	0	4	Minimal	Present	Absent
	401	Adenocarcinoma	1	0	1	1	1	0	1	1	1	7	Present	Present	Absent
	403	Adenocarcinoma	0	0	0	0	0	0	1	0	0	1	Absent	Present	Absent
$Braf^{V600E}\Delta TRZI$ (n=14)	348	High grade tubulovillous adenoma	0	0	0	0	0	0	1	0	0	1	Absent	Absent	Absent
	349	Adenocarcinoma	0	0	0	1	1	0	1	1	0	4	Present	Absent	Absent
	351	Mucinous adenocarcinoma	0	0	0	0	0	0	1	1	1	3	Present	Present	Present (low level)
	352	Adenocarcinoma	0	0	0	1	1	0	1	0	0	3	Absent	Present	Absent
	353	Mucinous adenocarcinoma	0	0	0	0	0	0	1	1	1	3	Present	Present	Present (low level)
	354	Mucinous adenocarcinoma	0	0	0	0	0	0	1	1	1	3	Present	Present	Absent
	112	Mucinous adenocarcinoma	0	0	1	0	0	0	1	1	0	3	Present	Present	Present (low level)
	111	Adenocarcinoma	0	0	1	1	0	0	1	1	0	4	Present	Present	Absent
	109	Adenocarcinoma	0	0	1	0	0	0	1	1	1	4	Present	Present	Absent
	108	Adenocarcinoma	0	0	1	0	0	0	1	1	0	3	Present	Present	Absent
	107	Adenocarcinoma	0	0	1	1	0	0	1	1	0	4	Present	Present	Present (low level)
	106	Adenocarcinoma	0	0	1	0	0	0	1	1	0	3	Present	Present	Present (low level)
	105	Mucinous adenocarcinoma	0	0	0	0	0	0	1	1	1	3	Present	Present	Present (low level)
$Braf^{V600E}\Delta TRZIM$ (n=6)	516	Adenocarcinoma	0	0	0	0	0	0	1	0	0	1	Absent	Absent	Absent
	517	Mucinous adenocarcinoma	0	0	0	0	0	0	1	1	1	3	Present	Present	Absent
	518	Adenocarcinoma	0	0	0	0	0	0	0	0	0	0	Absent	Present	Absent
	519	Mucinous adenocarcinoma	0	0	0	0	0	0	1	1	1	3	Present	Present	Absent
	566	Mucinous adenocarcinoma	0	0	0	0	0	0	1	1	1	3	Present	Present	Present (low level)
	567	Adenocarcinoma	0	0	0	1	1	0	1	0	0	3	Minimal	Absent	Absent

Supplementary Table 3. Pathology scoring of mouse tumours for type (WHO classification 4th Ed, 2010), serrated features common to human serrated adenocarcinoma (WHO classification 4th Ed, 2010), the desmoplastic stromal reaction, infiltrative growth and tumour budding properties.

	ES	NES	NOM.p val	FDR q-val
Top 5 GSEAs *Braf*^{V600E} *ΔT* tumour vs normal colon				
REACTOME_SPHINGOLIPID_DE_NOVO_BIOSYNTHESIS	0.539	2.629	0.00	0.013
REACTOME_SPHINGOLIPID_METABOLISM	0.494	2.276	0.00	0.013
KEGG_LYSOSOME	0.452	2.147	0.00	0.018
KEGG_TOLL_LIKE_RECEPTOR_SIGNALING_PATHWAY	0.581	1.989	0.00	0.015
KEGG_CHEMOKINE_SIGNALING_PATHWAY	0.638	1.948	0.00	0.016
Top 5 GSEAs *Braf*^{V600E} *ΔTRZI* tumour vs normal colon				
REACTOME_SPHINGOLIPID_DE_NOVO_BIOSYNTHESIS	0.45	2.267	0.00	0.028
KEGG_LEISHMANIA_INFECTION	0.743	2.145	0.00	0.023
KEGG_TOLL_LIKE_RECEPTOR_SIGNALING_PATHWAY	0.556	2.061	0.00	0.022
ST_ERK1_ERK2_MAPK_PATHWAY	0.578	2.045	0.00	0.023
REACTOME_DEADENYLATION_OF_MRNA	0.523	1.97	0.00	0.031
Top 5 GSEAs *Braf*^{V600E} *ΔTRZIM* tumour vs normal colon				
REACTOME_SPHINGOLIPID_DE_NOVO_BIOSYNTHESIS	0.502	2.526	0.00	0.013
KEGG_APOPTOSIS	0.389	2.027	0.00	0.038
ST_P38_MAPK_PATHWAY	0.39	1.93	0.00	0.030
KEGG_LEISHMANIA_INFECTION	0.672	1.889	0.00	0.027
KEGG_RIG_I_LIKE_RECEPTOR_SIGNALING_PATHWAY	0.348	1.88	0.00	0.030
Top 5 GSEAs in *Kras*^{G12D}*Apc*$^{\Delta/\Delta}$ tumour vs normal				
REACTOME_EGFR_DOWNREGULATION	0.439	2.058	0.00	0.055
REACTOME_ANTIVIRAL_MECHANISM_BY_IFN_STIMULATED_GENES	0.33	1.662	0.00	1.000
KEGG_CITRATE_CYCLE_TCA_CYCLE	0.607	1.621	0.00	0.723
KEGG_PYRUVATE_METABOLISM	0.597	1.619	0.00	0.683
REACTOME_GLUCONEOGENESIS	0.595	1.604	0.00	0.644

Supplementary Table 4. Top 5 gene sets enriched for each pair-wise comparison of normal mouse colon with tumour samples. Nominal p values (NOM.p val) all <0.001. Enrichment score (ES), false discovery rate (FDR), normalized enrichment score (NES).

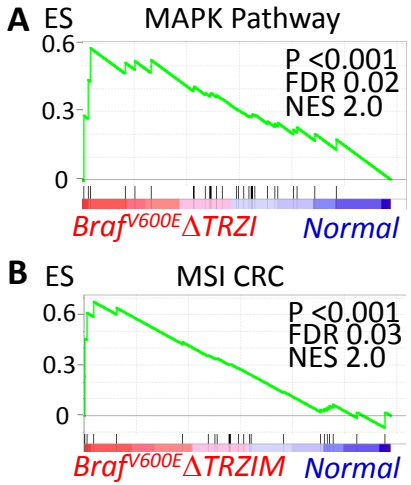

Supplementary Figure 10. GSEA identified differential expression of **(A)** ERK1/2 MAPK pathway transcripts in the *Braf*^{V600E}*ΔTRZI* tumours and **(B)** transcripts up-regulated in a human MSI-CRC gene set (Watanabe *et al*., Cancer Res 2006;66:9804-8) in the *Braf*^{V600E}*ΔTRZIM* tumours compared to normal colon. Enrichment score (ES), false discovery rate (FDR), normalized enrichment score (NES).

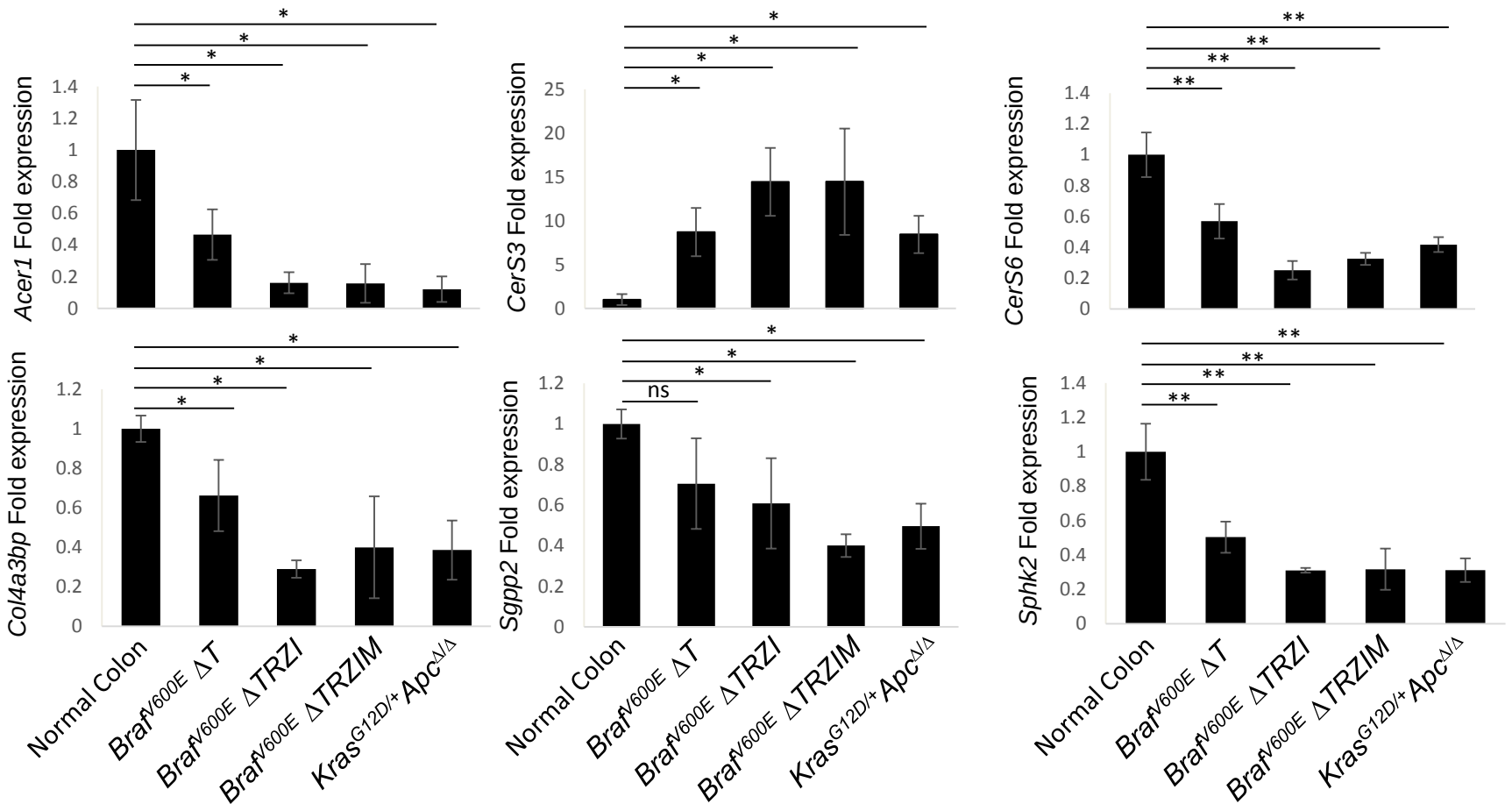

Supplementary Figure 11. Differential expression of spingolipid metabolism transcripts in normal mouse colon and tumours generated from *Braf*^{V600E} organoid series and *Kras*$^{G12D/+}$*Apc*$^{\Delta/\Delta}$organoids. qPCR validation of RNAseq leading edge genes from GSEA. Expression of *CerS3* is increased and *Acer1, CerS6, Col4a3bp, Sgpp2, Sphk2 are* decreased in tumours compared to normal colon. Fold induction of mRNA expression is normalized to *Gapdh*, with transcript level in normal colon set to 1. Results from at least four animals with triplicate technical replicates are shown, error bars denote standard deviation. Two-tailed t-test was used for pair-wise statistical analysis. ns=not significant, *=p≤0.05, **=p≤0.01.

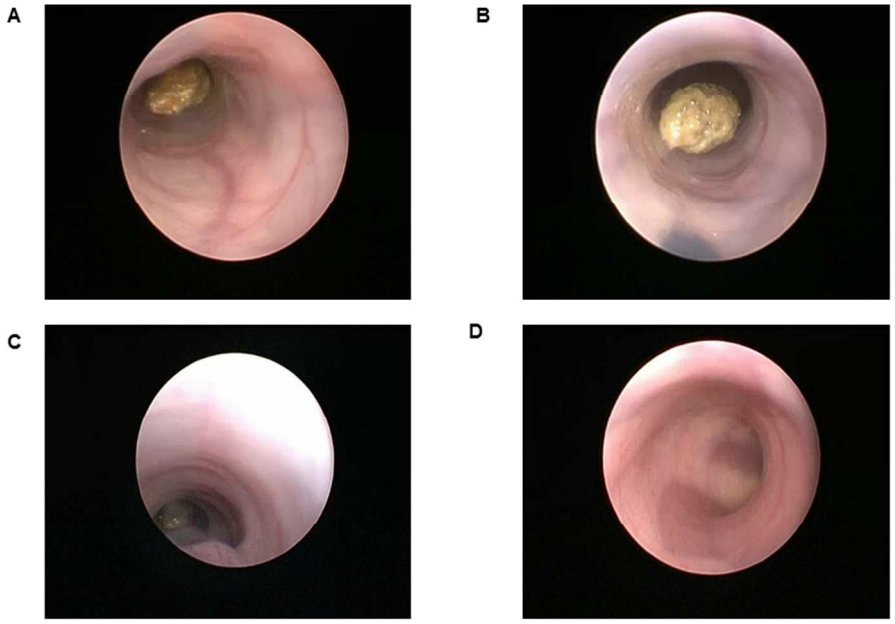

Supp Videos. Multi-hit 'serratoids' generate invasive adenocarcinoma with serrated features. Colonoscopy videos of NSG mouse colon orthotopically injected with mutant organoid lines **(A)** *Braf*^{V600E} 8 weeks post-injection, **(B)** *Braf*^{V600E} *ΔTgfbr2* 4 weeks post-injection, **(C)** *Braf*^{V600E} *ΔTgfbr2 ΔRnf43/Znrf3 Δp16Ink4a* 3 weeks post-injection, **(D)** *Braf*^{V600E} *ΔTgfbr2 ΔRnf43/Znrf3 Δp16Ink4a ΔMlh1* 3 weeks post-injection.

254x190mm (96 x 96 DPI)

Supplementary methods

TCGA data analysis. The Cancer Genome Atlas (TCGA) colonic adenocarcinoma and rectal adenocarcinoma (TCGA-COAD and TCGA-READ respectively) annotated mutation and methylation files were extracted from the GDC portal (https://portal.gdc.cancer.gov/) for 527 cases only, as the remaining cases did not have complete data for mutation and methylation. We determined that there were 50 $BRAF^{V600E}$ CRC cases within this cohort and used $BRAF^{V600E}$ to mark the serrated CRC subtype. We do not examine *KRAS* mutant serrated CRC herein, as *KRAS* mutation also marks the conventional pathway to CRC. We then used the analysis pipeline described below to examine alteration (both DNA mutation and hypermethylation) to candidate genes involved in regulation of the stem cell niche, senescence and DNA mismatch repair including; the Wnt-pathway, Bone Morphogenic Protein (BMP)/transforming growth factor-beta (TGFβ) pathways, *P16 INK4A*, *MLH1*. TCGA methylation data generated using two different platforms, the Infinium Human Methylation 27K and 450K, were combined. No batch effects were observed. The median beta-value across multiple microarray probes corresponding to the same gene was used to summarise methylation for each gene, with Beta-value for hyper-methylation cut off set to 0.47. All data processing was undertaken using software R, version 3.4.1 Patched. Waterfall plots (Figure 1) were generated with R package oncoPrint() function in ComplexHeatmap R package version 1.12.0 [1]. To examine whether Sphingolipid pathway genes were differentially regulated in the TCGA $BRAF^{V600E}$ CRC cohort and examine the effect on patient survival we analysed RNA expression and patient survival by downloading 622 cases with clinical and RNA expression data using R Bioconductor TCGAbiolinks package, version 2.7.5. Maximal survival time analysed was 5 years. RNA expression values were transformed using the 'voom' method limma package, version 3.30.13. Normalised, transformed expression values were used to classify patients into high and low expressor groups for each gene of interest using the surv_cutpoint() function in survminer R, the minimal proportion of observations was set at 20% for each gene [2]. The prognosis of each group was examined using Kaplan-Meier survival estimators with the survminer R package, version 0.4.1, with survival outcome compared by log-rank tests.

Genome engineering & Organoid culture (cont). Organoids were dissociated to single cells and small clumps of cells with TrypLE express, washed and transfected in the presence of basal medium without antibiotics and supplemented with 1uM Jagged-1 (Anaspec) using LF2000 and plasmid DNA in a 96 well plate for 3 hours at 37°C. Empty px458-GFP plasmid was used to visualise transfection efficiency and used as a kill test control for selection medium conditions. Cells were washed and plated onto 50% matrigel in non-selective culture medium containing 1uM Jagged-1. The following day, media was gently aspirated and top layer of 50% matrigel added. Plate was spun 20 minutes at 200xg at room temperature followed by 30 minute incubation at 37 degrees C before addition of non-selective culture medium containing 1uM Jagged-1. 72 hours after transfection, media was changed to selection medium, with media changes subsequently 2-3 times weekly.

Single organoids were handpicked and expanded for DNA sequence analysis. For novel gRNAs, genomic DNA was isolated from pooled, polyclonal organoids and subjected to PCR amplification of target genomic region, followed by PAGE analysis of duplex formation to measure indel formation. Genomic DNA from single organoid lines was also isolated and target genomic regions amplified by PCR. PCR products were cloned into a p-JET1.2 cloning

vector according to the manufacturer's instructions (ThermoFisher). Plasmid DNA from at least 6 clones was analysed by Sanger sequencing to determine biallelic target gene alteration.

We found optimal recovery and expansion of organoids from single cells as required for the transfection protocol using a matrigel "sandwich" and used this method for all cultures described herein [3]. To facilitate visualisation of the entire 48-well in a flat plane we modify the "sandwich" method to include the addition of 60ul 50:50 ADMEM:Matrigel mixture to a 48-well, centrifuge this bottom matrigel layer for 40minutes at 200xg at room temp, followed by a 30 minute incubation at 37 degC to solidify matrigel before plating organoids in growth medium on top. The following day we remove the media and any non-attached organoids, cover with 40ul 50:50 ADMEM:Matrigel mixture and centrifuge 100xg for 20 minutes. After a 30 minute incubation at 37degC, organoids in matrigel are covered with 200-250ul growth medium. The basal culture medium for mouse colon organoids was Advanced Dulbecco's modified Eagle medium/F12 (Life Technologies) supplemented with 1x gentamicin/antimycotic/antibiotic (Life Technologies), 10mM HEPES, 2mM GlutaMAX, 1xB27 (Life Technologies), 1xN2 (Life Technologies). The following niche factors were used: 50ng/ml mouse recombinant EGF (Peprotech), 100 ng/ml mouse recombinant noggin (Peprotech), 20% R-spondin-2 conditioned medium, 50% Wnt-3A conditioned medium. To select mutant organoids the following reagents were used: 1uM 4-OHT for 24h (Sigma-Aldrich), 10ng/ml human recombinant TGF-β1 (Peprotech), 1uM EGFR inhibitor (EGFRi, Calbiochem #324840), 20uM 5-FU (Sigma-Aldrich). Following initial isolation and immediately after each split, organoids were cultured in 10uM Y-27632 (In Vitro Technologies), 3uM iPSC (Calbiochem Cat #420220), 3uM GSK-3 inhibitor (XVI, Calbiochem, # 361559) for the first 3 days. Prior to transfection, organoids were cultured with 10mM Nicotinamide (Sigma-Aldrich) and 10uM GSK-3 inhibitor for 2 passages [4].

Kras$^{G12D/+}$; *Apc*$^{\Delta 580l/\Delta 580}$ (AK) colonic organoids were generated by treating organoids from Kras$^{LSL\text{-}G12D/+}$;*Apc*$^{CKO/CKO}$ mice with Ad5CMV::Cre, followed by selection in medium without Wnt ligands [5].

Orthotopic Injection (cont). A customised needle (Hamilton Inc. part number 7803-05, removable needle, 33 gauge, 12 inches long, point 4, 12 degree bevel) was used. Colonoscopy was performed using a Karl Storz Image 1 Camera System comprised of: Image1 HDTV HUB CCU; Cold Light Fountain LED Nova 150 light source; Full HD Image1 3 Chip H3-Z Camera Head; Hopkins Telescope, 1.9mm, 0 degrees. A sealed luer lock was placed on the working channel of the telescope sheath to ensure minimal air leakage (Coherent Scientific, part number 14034-40). In each mouse up to 3 injections of 20µl were performed. Injection sites were monitored by weekly colonoscopy and the videos were viewed offline using QuickTime Player for analysis. Tumour growth of the largest tumour visualised was scored as previously described using the Becker scale [6]. A Clinical Record Score was used to determine humane endpoint, scores were obtained by one point being given for the presence of each of the following observations: weight loss >15%; hunched/ruffled coat; inability to pass stool; dehydrated; absence of movement; or facial grimace. Once a score of 3 was reached the mice were euthanased. Statistical analysis performed using Prism.

Western blot analysis. To reduce endogenous MAPK signalling organoids were cultured without EGF for 4 days and with 1uM EGFRi for one day prior to treatment with 1uM 4-OHT for 16h. Cells were harvested using cold PBS containing 1x Halt™ Protease and Phosphatase Inhibitor Cocktail (PPI, Thermo Scientific), pelleted and lysed using RIPA buffer (150mM sodium chloride, 1% NP40, 0.5% sodium deoxycholate, 0.1% SDS, 50mM Tris, pH8.0) containing 1x PPI. Protein was quantitated using the DC™ Protein Assay Kit II (Bio-Rad) and analysed using 4-20% (Bio-Rad) SDS-PAGE. Standard western blot analyses were performed using the following primary antibodies: anti- Phospho-p44/42 MAPK (Erk1/2) (#4370, Cell Signaling Technology, 1:2000), total p44/42 MAPK (Erk1/2, #137F5, Cell Signaling Technology, 1:2000), anti-Hsp90 loading control (sc-7947, Santa Cruz Biotechnology, 1:1000). Primary antibody binding was detected using HRP-conjugated secondary anti-Rabbit antibody (Novex, #A24537, 1:10,000) and visualised with ECL Western Blotting Detection Reagents (Amersham, RPN2209) and Gel Doc™ XR+ Gel Documentation System (Bio-Rad).

Immunohistochemistry and histology. Tissues were fixed in 10% formalin, paraffin embedded and sectioned. Consecutive sections were prepared using a rotary microtome. H&E and alcian blue stains were preformed according to standard procedures. The $Braf^{V600E}$ staining was performed on a Ventana Benchmark Ultra, using a prediluted Ventana mouse primary antibody. Antigen retrieval was for 64 min using Ventana retrieval solution CC1. The primary antibody was incubated for 32 min at 36 degrees C. The Ventana Optiview DAB detection system was used with Ventana Haematoxylin II as the nuclear counterstain. The alpha-smooth muscle actin (aSMA) staining was completed using a rabbit polyclonal aSMA antibody (1:500, Abcam ab5694) and Keratin 20 using a rabbit polyclonal (1:200, Sigma SAB4502249). Antigen retrieval was performed in Vector Antigen Unmasking solution (Vector Laboratories, H-3300) and carried out in a Biocare Medical pressurised decloaker (Metagene). A goat anti-rabbit HRP secondary antibody (1:400, Life Technologies A24537) followed by DAB (BioLegend 926901) was used to visualise signal. Histological evaluation of mouse tumours was undertaken by a pathologist with expertise in human serrated pathway lesions. In line with current WHO standards mucinous adenocarcinoma was not graded (low versus high), and mucinous adenocarcinoma was defined as >50% mucinous differentiation [7]. Tumour budding was evaluated using H&E stained tumour sections in a hotspot area of $0.785mm^2$ by counting the number of buds as described for diagnostic practice [8]. 0 = Absent; 1-4 = low level; intermediate 5-9 and 10 or more is high level.

Nucleic acid analysis. Total RNA and gDNA was extracted from organoids, tumours and normal control colon tissue using AllPrep DNA/RNA Mini or RNeasy Mini Kit (QIAGEN) or UltraClean® Tissue & Cells DNA Isolation Kit (Mo Bio Laboratories). For qRT-PCR, 300-1000 ng RNA was reverse transcribed to cDNA using Superscript IV according to the manufacturer's instructions (Thermo Scientific). cDNA was diluted 1:5 and level of transcripts of interest evaluated using Primer:probe assays (IDT) with KAPA PROBE FAST qPCR Master Mix (KAPABiosystems) master mix and run on a QuantStudio 7 Flex Real-Time PCR System (Thermo Scientific). For RNAseq analysis, 1ug of total RNA was used for sequencing library preparation using a BIOO stranded Poly-A kit (PerkinElmer) according to the manufacturer's instructions and sequenced on Illumina HiSeq to generate 1 x 100bp single-end reads.

RNAseq data processing. Images generated by HiSeq™ 2500 were converted into nucleotide sequences by a base calling pipeline and stored in fastq.gz format, and examined QC plots with FastQC version 0.11.3. Raw reads with low quality were removed using Trim Galore prior to analysing the data. The criteria of removing low quality reads were set as: quality Phred score less than 28, reads contains adaptor sequences. FastQC was performed again, all low quality reads were removed. All the subsequent analyses were based on trimmed reads, which were then mapped to reference mouse genome mm10 GRCm38, using STAR 2.4.2a modified. No more than 1 base mismatch were allowed. Only uniquely mapped reads were retained. quantMode was enabled to generate gene level quantification. The counts files were then merged into a table for downstream differential expression analysis. All data preprocessing were completed in shell HPC command line environment.

Differential expression analysis. Differentially expressed genes (DEG) were analysed using the glmFit() glmLRT() function in R Bioconductor edgeR Package version 3.16.5 [9]. A negative binomial generalized log-linear model was employed, with Benjamini-Hochberg correction using false discovery rate (FDR) of *P* values. Hierarchical clustering was performed on DEGs only, using Euclidean distance and complete linkage clustering option with Heatmap() function in ComplexHeatmap R package version 1.12.0 [1]. MDS plots were generated using the plotMDS() function in Limma R package version 3.30.13 [10]. Differentially expressed genes were defined as FDR < 0.05, and absolute value of Log_2 (fold change) > 2.

Gene set enrichment analysis (GSEA). GSEA methodology was developed using guidelines for RNAseq datasets [11] . Transcript counts generated from STAR aligner were sub-grouped into files with pairwise comparison groups of normal colon to tumour. The PreprocessReadCounts (V1 Beta) module of GenePattern was used to normalise and transform counts. Briefly, lowly expressed genes were removed from the analysis if they had <1 read/million in four of the samples, as four is the smallest group of biological replicates [12]. The remaining data was then normalised using Trimmed Mean of M-values [13]. Mean-variance transformation to approximate a normal distribution was performed subsequently using voom [10]. Gene set enrichment analyses were performed using online module GSEA (v18).

Microsatellite instability. MSI status was assessed using a panel of five markers (*m-Bat-26, mBat-67, m-Bat-37, GA29, TG27*-see Supplementary Methods Table 1 for sequence) [14, 15, 16]. These included 3 mononucleotide and 2 dinucleotide repeats. Fragment sizes were assayed using PCR coupled with fluorescent detection on an ABI3100 Capillary Sequencer. Differences in fragment sizes were assessed using the GeneMarker software.

Supplementary methods table 1-Microsatellite marker primer information

Marker	Type	Annealing Tm	Forward Primer	Reverse Primer	Reference
mBat-26	Mononucleotide	59	TCACCATCCATTGCACAGTT	CTGCGAGAAGGTACTCACCC	Bacher et al, 2005
mBat-37	Mononucleotide	59	TCTGCCCAAACGTGCTTAAT	CCTGCCTGGGCTAAAATAGA	Bacher et al, 2005
mBat-67	Mononucleotide	59	CCGACTGCTCTTCCGAAGGTC	TTGCCCATTTATCATCTAGTTCAT	Bacher et al, 2005
TG27	Dinucleotide	60	GGATCACTCGATGTACGGCTACTC	CCAGGCAGGCAAAGCATTTAT	Kabbarah et al,

					2003
GA29	Dinucleotide	59	CAGGAGGTCAAGGTCATCCTAAG	CCACCATGGTAGGAGCTTGCTA	Kabbarah et al, 2003

Supplementary methods table 2- gRNA sequence

Target gene	gRNA sequence
Rnf43	CCACCAGGAGGTACCAAGCCGGC
Znrf3	GGGTCATCCCTTGTACTCATCGG
Tgfbr2	CCTGTGGCCGCTGCATATCGTCC
p16 Ink4a	CCCAACGCCCCGAACTCTTTCGG
Mlh1	TAGTGAACCGCATAGCGGCGGGG

Supplementary Methods References

1 Gu Z, Eils R, Schlesner M. Complex heatmaps reveal patterns and correlations in multidimensional genomic data. Bioinformatics 2016;**32**:2847-9.

2 Hothorn T, Lausen B. On the exact distribution of maximally selected rank statistics. Computational Statistics & Data Analysis 2003;**43**:121-37.

3 Onuma K, Ochiai M, Orihashi K, Takahashi M, Imai T, Nakagama H*, et al.* Genetic reconstitution of tumorigenesis in primary intestinal cells. Proc Natl Acad Sci U S A 2013;**110**:11127-32.

4 Schwank G, Andersson-Rolf A, Koo BK, Sasaki N, Clevers H. Generation of BAC transgenic epithelial organoids. PLoS One 2013;**8**:e76871.

5 Roper J, Tammela T, Cetinbas NM, Akkad A, Roghanian A, Rickelt S*, et al.* In vivo genome editing and organoid transplantation models of colorectal cancer and metastasis. Nat Biotechnol 2017;**35**:569-76.

6 Becker C, Fantini MC, Wirtz S, Nikolaev A, Kiesslich R, Lehr HA*, et al.* In vivo imaging of colitis and colon cancer development in mice using high resolution chromoendoscopy. Gut 2005;**54**:950-4.

7 Bosman FT, Carneiro, F., Hruban, R.H., Theise, N.D. WHO Classification of Tumours of the Digestive System, 2010.

8 Lugli A, Kirsch R, Ajioka Y, Bosman F, Cathomas G, Dawson H*, et al.* Recommendations for reporting tumor budding in colorectal cancer based on the International Tumor Budding Consensus Conference (ITBCC) 2016. Modern pathology : an official journal of the United States and Canadian Academy of Pathology, Inc 2017;**30**:1299-311.

9 McCarthy DJ, Chen Y, Smyth GK. Differential expression analysis of multifactor RNA-Seq experiments with respect to biological variation. Nucleic Acids Res 2012;**40**:4288-97.

10 Smyth GK. limma: Linear Models for Microarray Data. In: Gentleman R, Carey VJ, Huber W, Irizarry RA, Dudoit S, eds. Bioinformatics and Computational Biology Solutions Using R and Bioconductor. New York, NY: Springer New York, 2005:397-420.

11 Rahmatallah Y, Emmert-Streib F, Glazko G. Gene set analysis approaches for RNA-seq data: performance evaluation and application guideline. Brief Bioinform 2016;**17**:393-407.
12 Anders S, McCarthy DJ, Chen Y, Okoniewski M, Smyth GK, Huber W, *et al.* Count-based differential expression analysis of RNA sequencing data using R and Bioconductor. Nat Protoc 2013;**8**:1765-86.
13 Robinson MD, Oshlack A. A scaling normalization method for differential expression analysis of RNA-seq data. Genome Biol 2010;**11**:R25.
14 Bacher JW, Abdel Megid WM, Kent-First MG, Halberg RB. Use of mononucleotide repeat markers for detection of microsatellite instability in mouse tumors. Mol Carcinog 2005;**44**:285-92.
15 Kabbarah O, Mallon MA, Pfeifer JD, Edelmann W, Kucherlapati R, Goodfellow PJ. A panel of repeat markers for detection of microsatellite instability in murine tumors. Mol Carcinog 2003;**38**:155-9.
16 Bond CEL, C.; Kawamata, F.; McKeone,D.M.; Fernando, W.; Jamieson, S.; Pearson, S.; Kane, A.; Woods, S.L.; Lannagan, T.R.M.; Somashekar, R.; Lee, Y.; Dumenil, T.; Spring, K.J.; Borowsky, J.; Fennell, L.; Bettington, M.; Lee, J.; Worthley, D.L.; Leggett, B.A.; Whitehall, V.L.J. Oncogenic BRAF Mutation Induces DNA Methylation Changes in a Murine Model for Human Serrated Colorectal Neoplasia. Epigenetics 2017;**In Press**.

Title: Genetic editing of colonic organoids provides a molecularly distinct and orthotopic preclinical model of serrated carcinogenesis.

Dual corresponding author details:
Dr. Susan Woods, PhD.
Postal address- GICB Lab, Level 5 South
South Australian Health & Medical Research Institute (SAHMRI)
North Terrace
Adelaide SA 5000
AUSTRALIA
p: (08) 8128 4386 m: 0488 737408 e: susan.woods@adelaide.edu.au

Dr. Daniel Worthley, MBBS(Hons), PhD, MPH, FRACP.
Postal address- GICB Lab, Level 5 South
South Australian Health & Medical Research Institute (SAHMRI)
North Terrace
Adelaide SA 5000
AUSTRALIA
p: (08) 8128 4386 m: 0400 363208 e: Dan.worthley@sahmri.com

Co-author details:
Tamsin RM Lannagan[1], Young K Lee[1], Tongtong Wang[1], Jatin Roper[2,3], Mark L Bettington[4,5], Lochlan Fennell[5], Laura Vrbanac[1], Lisa Jonavicius[6], Roshini Somashekar[1], Krystyna Gieniec[1], Miao Yang[1], Jia Q Ng[1], Nobumi Suzuki[1], Mari Ichinose[1], Josephine A Wright[1], Hiroki Kobayashi[1], Tracy L Putoczki[7], Siddhartha Mukherjee[8], Yoku Hayakawa[9],Simon Leedham[10], Helen E Abud[11], Ömer H. Yilmaz[2,12], Julie Marker[13], Sonja Klebe[6], Pratyaksha Wirapati[14], Sabine Tejpar[15], Barbara A Leggett[5,16,17], Vicki LJ Whitehall[5,16,18], Daniel L Worthley[1]*, Susan L Woods[1]*.

Affiliations as listed page 2 of manuscript.

Word count: (excluding title page, affiliations, abstract, references, figures and tables.)
3883

Abbreviations: colorectal cancer (CRC), mitogen activated kinase (MAPK), CpG Island Methylator Phenotype (CIMP), chromosomal instability (CIN), *Adenomatous polyposis coli* (*APC),* Epidermal growth factor (EGF), bone morphogenic protein (BMP), The Cancer Genome Atlas (TCGA), microsatellite instability (MSI), transforming growth factor-β (TGFβ), *MutL homolog 1* (*MLH1),* 4-hydroxytamoxifen (4-OHT), epidermal growth factor receptor (EGFR), clustered regularly interspaced short palindromic repeats (CRISPR), wild type (WT), Quantitative real-time PCR (qRT-PCR), guideRNAs (gRNAs), MSI-High (MSI-H), NOD.Cg-*Prkdc*^{scid}*Il2rg*$^{tm1Wjl/Szj}$ (NSG), multidimensional scaling (MDS), gene set enrichment analysis (GSEA), sphingolipid (SP), sphingosine kinase 1 (SPHK1), sphingosine-1-phosphate phosphatase 1 (SGPP1), sphingosine 1-phosphate (S1P), *Braf*^{V600E}*Tgfbr2*$^{Δ/Δ}$ *(Braf*^{V600E}*ΔT)*, *Braf*^{V600E} *Tgfbr2*$^{Δ/Δ}$ *Rnf43*$^{Δ/Δ}$*/Znrf3*$^{Δ/Δ}$ *p16Ink4a*$^{Δ/Δ}$ *(Braf*^{V600E}*ΔTRZI)*, *Braf*^{V600E} *Tgfbr2*$^{Δ/Δ}$*Rnf43*$^{Δ/Δ}$*/Znrf3*$^{Δ/Δ}$ *p16Ink4a*$^{Δ/Δ}$*Mlh1*$^{Δ/Δ}$ *(Braf*^{V600E}*ΔTRZIM),* Wnt-3a (W), Rspo-2 (R), Noggin (N), TGFβ1 (T), 5-Fluorouracil (5FU), Enrichment score (ES), normalised enrichment score (NES), false discovery rate (FDR).

Title: Genetic editing of colonic organoids provides a molecularly distinct and orthotopic preclinical model of serrated carcinogenesis.

Tamsin RM Lannagan[1], Young K Lee[1], Tongtong Wang[1], Jatin Roper[2,3], Mark L Bettington[4,5], Lochlan Fennell[5], Laura Vrbanac[1], Lisa Jonavicius[6], Roshini Somashekar[1], Krystyna Gieniec[1], Miao Yang[1], Jia Q Ng[1], Nobumi Suzuki[1], Mari Ichinose[1], Josephine A Wright[1], Hiroki Kobayashi[1], Tracy L Putoczki[7], Siddhartha Mukherjee[8], Yoku Hayakawa[9],Simon Leedham[10], Helen E Abud[11], Ömer H. Yilmaz[2,12], Julie Marker[13], Sonja Klebe[6], Pratyaksha Wirapati[14], Sabine Tejpar[15], Barbara A Leggett[5,16,17], Vicki LJ Whitehall[5,16,18], Daniel L Worthley[1]*, Susan L Woods[1]*.

[1]School of Medicine, University of Adelaide and South Australian Health and Medical Research Institute, Adelaide, SA Australia
[2] The David H. Koch Institute for Integrative Cancer Research at MIT, Cambridge, MA
[3]Division of Gastroenterology, Tufts Medical Center, Boston, MA, United States
[4]Envoi Specialist Pathologists, Brisbane, QLD Australia
[5]QIMR Berghofer Medical Research Institute, Brisbane, QLD Australia
[6]Department of Anatomical Pathology, Flinders Medical Centre, Bedford Park, SA Australia
[7]Department of Medical Biology, University of Melbourne and the Walter and Eliza Hall Institute of Medical Research, Melbourne, VIC Australia
[8]Department of Medicine, Columbia University Medical Center, New York, NY, USA.
[9]Dept of Gastroenterology, University of Tokyo, Japan
[10]Gastrointestinal Stem Cell Biology Laboratory, Wellcome Trust Centre for Human Genetics University of Oxford, Oxford, & Translational Gastroenterology Unit, Experimental Medicine Division, Nuffield Department of Clinical Medicine, John Radcliffe Hospital, Oxford, Headington, UK
[11]Cancer Program, Monash Biomedicine Discovery Institute and the Department of Anatomy and Developmental Biology, Monash University, Clayton, VIC Australia
[12]Department of Pathology, Massachusetts General Hospital, Boston, MA United States
[13]Cancer Voices SA, SA Australia
[14]Swiss Institute of Bioinformatics, Bioinformatics Core Facility, Lausanne, Switzerland.
[15]Digestive Oncology Unit, Department of Oncology, University Hospitals Leuven, Leuven, Belgium.
[16]School of Medicine, University of Queensland, QLD Australia
[17]Royal Brisbane and Womens Hospital, Brisbane, QLD Australia
[18]Pathology Queensland, Brisbane, QLD

*=correspondence to either:
Dr. Daniel Worthley, South Australian Health & Medical Research Institute, Adelaide SA Australia. Dan.Worthley@sahmri.com
Dr. Susan Woods, South Australian Health & Medical Research Institute, Adelaide SA Australia. Susan.Woods@adelaide.edu.au

ABSTRACT:

Objective: Serrated colorectal cancer (CRC) accounts for approximately 25% of cases, and includes tumours that are amongst the most treatment resistant and with worst outcomes. This CRC subtype is associated with activating mutations in the mitogen activated kinase (MAPK) pathway gene, *BRAF*, and epigenetic modifications termed the CpG Island Methylator Phenotype (CIMP), leading to epigenetic silencing of key tumour suppressor genes. It is still

not clear which (epi-)genetic changes are most important in neoplastic progression and we begin to address this knowledge gap herein.

Design: We utilise organoid culture combined with CRISPR/Cas9 genome engineering, to sequentially introduce genetic alterations associated with serrated CRC and which regulate the stem cell niche, senescence and DNA mismatch repair.

Results: Targeted biallelic gene alterations were verified by DNA sequencing. Organoid growth in the absence of niche factors was assessed, as well as analysis of downstream molecular pathway activity. Orthotopic engraftment of complex organoid lines, but not $Braf^{V600E}$ alone, quickly generated adenocarcinoma *in vivo* with serrated features consistent with human disease. Loss of the essential DNA mismatch repair enzyme, Mlh1, led to microsatellite instability. Sphingolipid metabolism genes are differentially regulated in both our mouse models of serrated CRC and human CRC, with key members of this pathway having prognostic significance in the human setting.

Conclusion: We generate rapid, complex models of serrated CRC to determine the contribution of specific genetic alterations to carcinogenesis. Analysis of our models alongside patient data has led to the identification of a potential susceptibility for this tumour type.

SUMMARY BOX:

What is already known about this subject:

- 25% of colorectal cancers (CRC) form via an alternate molecular pathway typified by activating mutation in the BRAF kinase and accrual of epigenetic modifications at specific promoter locations.
- The molecular evolution of these serrated CRCs and how this relates to natural history is poorly understood and may hold the key to better treatment and prevention options for this form of CRC.

What are the new findings:

- Here we use next generation sequence information from human serrated CRC, combined with organoid culture, gene editing and orthotopic transplantation techniques to rapidly generate complex, preclinical models of serrated CRC.

How might it impact on clinical practice in the foreseeable future?

- These preclinical models will allow therapeutic evaluation in known, previously untested genetic landscapes.
- Transcriptomic analysis of our models, combined with patient data, have suggested potential vulnerabilities for this tumour type that we will test in the future.

INTRO:

Sporadic colorectal cancer (CRC) develops via two main genetic pathways. The conventional pathway described by Fearon & Vogelstein [1] has characteristic chromosomal instability (CIN) with stepwise loss of key tumour suppressors (eg. *Adenomatous polyposis coli*, *APC*)

and activation of oncogenes (eg. *KRASG12D* mutation). In the last two decades, an alternate molecular pathway has been identified that accounts for 25% of CRC [2]. This subtype of CRC is named for the serrated, or saw-toothed, morphology of the precursor lesion, including sessile serrated polyps, and comprises a molecularly distinct, somewhat heterogeneous tumour type that forms without CIN. It can be best differentiated from conventional CRC by two characteristic molecular markers; the presence of the $BRAF^{V600E}$ mutation that activates the mitogen-activated protein kinase (MAPK) pathway and the coincident, coordinated epigenetic modification of specific target promoters termed the CpG Island Methylator Phenotype (CIMP) [3]. $BRAF^{V600E}$/$CIMP^{+}$ tumours account for 8-20% of all CRC [2, 4]. These are preferentially located in the proximal colon, frequently present with higher grade and contain a group of cancers with the worst prognosis of all CRC [2, 5]. Furthermore, of relevance to the gastrointestinal cancer preventionist, these serrated lesions are less well detected by current CRC screening programs and are overrepresented in colonoscopic interval cancers [6, 7]. The molecular basis for these subtype characteristics are not well understood, but may hold the key to preventing and treating serrated CRC.

The culture of normal and tumour derived organoids pioneered by Hans Clevers and his group [8, 9] allows the indefinite, *in vitro* propagation of primary gut epithelia and neoplastic specimens. Cells are grown in self-organising aggregates with representative epithelial architecture, suspended within a basement membrane-gel matrix and supported by stem cell niche signalling factors. For the colon these factors, Wnt/R-spondin, Epidermal growth factor (EGF), and Noggin activate the Wnt and MAPK pathways and inhibit the bone morphogenic protein (BMP) pathway, respectively. This culture system supports the stem cell population, as well as more differentiated cell types, allowing long-term primary culture containing many of the representative epithelial cell types of the original tissue.

The next-generation sequencing revolution has armed us with more information than ever before about the (epi-)genetic changes associated with serrated CRC. Mining this static data is relatively simple, yet understanding the contribution of genetic events to carcinogenesis is a real challenge. To this end, we have combined recent advances in stem cell biology [10] with genome editing techniques [11], to produce a system in which multiple genetic alterations can be assessed for their contribution to serrated CRC. This is analogous to the approach taken to model the conventional pathway to CRC [12, 13] and is inspired by the observation that many recurrent CRC mutations lie within genes involved in key signalling pathways that are essential for maintenance of the intestinal stem cell niche [14]. Our work provides new insights into the importance of common (epi-)genetic alterations found in human serrated CRC and highlights a potential vulnerability of this cancer type.

RESULTS:

To identify recurrent serrated CRC associated alterations in stem cell niche signalling and senescence pathways, we analysed The Cancer Genome Atlas (TCGA) (epi-)genomic data for 633 CRC cases [15]. $BRAF^{V600E}$ mutation is estimated to mark 50-67% of serrated CRCs [2] and, in the absence of microsatellite instability (MSI), is associated with poor outcome for late stage disease [2, 16]. As only 30% of serrated CRCs retain serrated crypt morphology [2], we use the $BRAF^{V600E}$ molecular marker rather than histological appearance to extract serrated CRC cases from the TCGA set. In the 50 TCGA CRC cases that contain $BRAF^{V600E}$ (depicted in **Figure 1**), we then used a candidate gene approach to look for frequently co-

altered genes that play important roles in regulating the stem cell niche or senescence. *p16 INK4A* encodes a tumour suppressor protein critical for oncogene induced senescence. Loss of *p16 INK4a* expression is associated with the conversion of serrated polyps to high-grade dysplasia/CRC and cooperates with $Braf^{V600E}$ in a mouse model of serrated CRC [17, 18, 19]. Consistent with previous reports, we detected *p16 INK4A* hypermethylation or mutation in 46% of TCGA CRC cases overall and in 84% of $BRAF^{V600E}$ CRC (**Figure 1**) [20, 21, 22]. The Wnt pathway intricately regulates intestinal stem cell proliferation and differentiation. The classic Wnt-pathway regulator, *APC*, is the most commonly mutated gene in CRC [15]. However for $BRAF^{V600E}$ CRC, we identified two negative regulators, *ZNRF3* and *RNF43*, as the most commonly altered Wnt pathway genes (**Figure 1**) [23]. Interestingly, in mice, cooperative inactivation of both *Rnf43* and *Znrf3* are required for polyp formation [24] and we detect alteration of both genes in 32% of $BRAF^{V600E}$ CRC. This is consistent with reports of differential Wnt pathway disruption in precursor lesions of the serrated pathway to CRC compared to the conventional pathway [25, 26]. The mutation rate of *RNF43* is likely under-represented in the TCGA dataset due to incomplete calling of frame-shift mutations because of their similarity to technical DNA polymerase slippage errors [27]. The transforming growth factor-β (TGFβ) pathway is frequently aberrantly regulated in CRC, often through mutation of *TGFβ receptor 2* (*TGFβR2*) [15]. *TGFβR2* mutation occurred in 10% of the $BRAF^{V600E}$ CRC cases we examined (**Figure 1**), again reflecting under calling of the polyadenine repeat tract mutations in the TCGA dataset as use of older sequencing modalities identified *TGFBR2* as mutated in 90% of MSI CRC [28]. Lastly, we wanted to model MSI CRC and so examined the key mismatch repair gene, *MutL homolog 1* (*MLH1)*. In line with a meta-analysis of *MLH1* methylation frequency in CRC, we detected *MLH1* hypermethylation in 20% of TCGA CRC cases [29]. This increased to 74% alteration in $BRAF^{V600E}$ CRC (**Figure 1**).

Carcinogenesis is a story of liberation and, as we genetically engineer successive stages of serrated CRC, we select organoids through their unique biology, microenvironmental requirements and treatment sensitivities. Firstly, the $BRAF^{V600E}$ mutation is an early genetic change in serrated polyps [30]. To first incorporate this mutation, we established colon organoid cultures from $BRAF^{CA}/Villin^{CreERT}$mice (**Figure 2**). *In vitro* treatment with 4-hydroxytamoxifen (4-OHT) induced highly efficient recombination to $Braf^{V600E}$ (**Supplementary Figure 1**) and activation of ERK1/2 phosphorylation (**Figure 2A**). This *in vitro* system mimics the chemoresistance to epidermal growth factor receptor (EGFR) inhibitors observed for MAPK mutant CRC in the clinic [31]. Treatment with EGFR inhibitor results in a significant growth inhibition of wild-type organoids in culture but not $Braf^{V600E}$ organoids (**Figure 2B**, **Supplementary Figure 2**).

Genome editing using microbial Cas9 nucleases from the clustered regularly interspaced short palindromic repeats (CRISPR) adaptive immune system has revolutionised the field of genome editing [11]. We have modelled serrated CRC using this genome editing technique. Thus, following mutation of *Braf* we sequentially incorporated 4 further genetic alterations using CRISPR/Cas9 [11] (**Figure 2**). Similar to previous work [12, 13], the addition of Tgfβ to culture medium selected for organoids with functional loss of the Tgfβ pathway, in this case Tgfβr2 ($Braf^{V600E}$*;* $Tgfbr2^{\Delta/\Delta}$, abbreviated to $Braf^{V600E}\Delta T$) (**Figure 2B**). Indeed, wild type (WT), $Braf^{V600E}$ and control transfected cultures do not survive in the presence of Tgfβ [32] (**Figure 2B**). Quantitative real-time PCR (qRT-PCR) analysis of the Tgfβ response gene,

Serpin1, showed that Tgfβ can activate this pathway in *Braf*^{V600E} organoids as shown by an increase in *Serpin1* mRNA levels. However, organoids containing loss of function of *Tgfβr2* have low basal expression of *Serpin1* and are not Tgfβ responsive (**Supplementary Figure 3**). Next, removal of Wnt-ligands, Wnt3a and Rspo2, kills WT, *Braf*^{V600E}, *Braf*^{V600E}Δ*T* and control transfected cultures (**Figure 2B)**. However, transfection of plasmids encoding Cas9 and guideRNAs (gRNAs) targeting the negative Wnt regulators, *Rnf43* and *Znrf3*, allowed outgrowth of organoids with cystic morphology (**Figure 2B,** growth of organoids in Wnt-ligand deficient NT medium). Loss of the p16Ink4a tumour suppressor was not directly selected for using changed media conditions, but this gene was targeted simultaneously with *Rnf43* and *Znrf3* and its loss likely provided a growth advantage to *Braf*^{V600E} mutant cells [17]. This resulted in *Braf*^{V600E}*;Tgfbr2*$^{\Delta/\Delta}$*;Rnf43*$^{\Delta/\Delta}$*/Znrf3*$^{\Delta/\Delta}$*;p16 Ink4a*$^{\Delta/\Delta}$ (*Braf*^{V600E}Δ*TRZI)* organoids. qRT-PCR analysis of the Wnt-pathway response genes, *Axin2* and *Lgr5*, showed that activation of this pathway in the *Braf*^{V600E}Δ*TRZI* organoids in the absence of Wnt ligands is similar to the level in control *Braf*^{V600E} organoids cultured in the presence of Wnt ligands, i.e. the pathway is super-activated by targeting *Rnf43* and *Znrf3* (**Supplementary Figure 3**). qRT-PCR analysis also indicates a reduction in p16Ink4a mRNA levels in *Braf*^{V600E}Δ*TRZI* compared to *Braf*^{V600E} organoids (**Supplementary Figure 3**).

Lastly, to select for loss of *Mlh1* we exploited the clinical finding that MSI-High (MSI-H) cancers are reported to show relative resistance to backbone chemotherapeutic 5-fluorouracil (5-FU) [33]. We used media containing 5-FU to promote DNA mismatches [34]. Mlh1 is an essential component of the DNA mismatch machinery [35] and so we hypothesised that inactivation of *Mlh1* would lead to increased survival of cells despite DNA damage-arrest signals, consistent with the poor response of MSI CRC to 5-FU based adjuvant chemotherapy [33]. Organoids that had been transfected with a plasmid encoding Cas9 and a gRNA targeting *Mlh1* (*Braf*^{V600E}Δ*TRZIM)* were better able to withstand a pulse of 5FU treatment than control transfected *Braf*^{V600E}Δ*TRZI* (**Figure 2B**). The activity of previously unpublished gRNAs (*Tgfβr2* and *Mlh1* gRNAs) was evaluated in polyclonal organoids before proceeding to handpicking single clones and expansion of lines (**Supplementary Figure 4**). We also used bioinformatic prediction of the possible off-target sites for each of these gRNAs and verified that they were not changed in our organoid lines by Sanger sequencing (**Supplementary Table 1**). Bi-allelic, loss of function insertions and deletions (indels) in target genes were verified using DNA sequencing (**Figure 2C, Supplementary Table 2**).

To assess the effect of this series of genetic alterations on colorectal tumourigenesis, we transplanted organoids into NOD.Cg-*Prkdc*^{scid}*Il2rg*$^{tm1Wjl/Szj}$ (NSG) mice and used *in vivo* murine colonoscopy to directly visualize and score pathologic changes (**Figure 3A, Supplementary Videos**). Using a modified needle attachment, we injected organoids into the orthotopic site, the mucosal layer of the colon wall (**Figure 3A, Supplementary Figure 5A, 5B**) [36]. Injection of *Braf*^{V600E} mutant organoids failed to induce tumour formation over a 3 month time course as assessed by colonoscopic surveillance, at necropsy and by pathological evaluation (**Figure 3B, 4B, Supplementary Figure 6**). Introduction of Tgfβ pathway perturbation in *Braf*^{V600E}Δ*T* organoids results in 57% of organoid injections forming tumours within 3 months (**Figure 3B**). However, significantly more *Braf*^{V600E}Δ*TRZI* and *Braf*^{V600E}Δ*TRZIM* injected organoids formed tumours, 98% and 100% respectively (**Figure 3B**, $p<0.05$). Similar to human sessile serrated polyps, 94% (n=11 mice) of *Braf*^{V600E}Δ*TRZI*

and 100% (n=8 mice) of *Braf*^{V600E}Δ*TRZIM* tumours developed a noticeable mucus cap visible from two weeks post-injection via colonoscopic surveillance [37] (**Supplementary Figure 5C**). This is in contrast to only 9% (n=12 mice) of the *Braf*^{V600E}Δ*T* tumours with a mucus cap. The more genetically complex organoids (*Braf*^{V600E}Δ*TRZI* and *Braf*^{V600E}Δ*TRZIM*) grew significantly more quickly than *Braf*^{V600E}Δ*T* tumours (**Figure 3C, Supplementary Figure 6,** p<0.001) and overall survival was also significantly decreased, with mean time from injection to humane endpoint of the experiment at 6 weeks for *Braf*^{V600E}Δ*TRZI* and 4 weeks for *Braf*^{V600E}Δ*TRZIM* (**Figure 3D**, p<0.001).

Histologically, tumours generated using *Braf*^{V600E}Δ*T*, *Braf*^{V600E}Δ*TRZI* and *Braf*^{V600E}Δ*TRZIM* organoids are invasive, adenocarcinomas with features of human serrated CRC (**Figure 4, Supplementary Table 3**) [2, 38]. We observed infrequent liver metastasis (9% or 1 out of 11) mice), with no macro-metastasis to other sites (lung, peritoneum) after injection with *Braf*^{V600E}Δ*TRZI* (**Supplementary Figure 5D**). Organoid-derived cells were readily visualised by morphology and using immunohistochemical detection of Braf^{V600E} (**Figure 4D, Supplementary Figure 5E**). The tumours display a substantial desmoplastic stromal reaction (**Figure 4E**), particularly with *Braf*^{V600E}Δ*TRZI* compared to the less genetically complex *Braf*^{V600E}Δ*T* (85% vs. 33% p<0.05, **Supplementary Table 3**). Thus the genetics of the tumour in this model was important in the co-evolution of the stroma. This stromal reaction is composed of smooth muscle actin expressing cancer activated fibroblasts amongst other cell types (**Figure 4G**). The more complex *Braf*^{V600E}Δ*TRZI* and *Braf*^{V600E}Δ*TRZIM,* but not *Braf*^{V600E}Δ*T* tumours, featured tumour budding (**Figure 4F, Supplementary Figure 5F**) and approximately half were categorised as mucinous adenocarcinoma [38], indicating a change to the amount of mucin produced by tumours with more complex genetic alterations, (42-50% vs. 0% p<0.01, **Supplementary Table 3**). This could also be visualised using Alcian Blue mucin staining (**Figure 4G**). *Muc2* mRNA, encoding a core component of mucus, was increased in the *Braf*^{V600E}Δ*TRZI* but not the *Braf*^{V600E} or *Braf*^{V600E}Δ*T* organoids (p<0.05, **Supplementary Figure 7**).

To investigate the consequences of mutating the essential DNA damage response gene, *Mlh1*, we analysed microsatellite marker length in our organoid series. *Braf*^{V600E}Δ*TRZIM,* but not *Braf*^{V600E}Δ*TRZI* organoids have altered microsatellite length (MSI) when compared to the donor mouse from which organoids were derived, in 4 mononucleotide markers previously validated for use in mouse [39, 40]. These cells accrued further MSI *in vivo*, with *Braf*^{V600E}Δ*TRZIM*, but not *Braf*^{V600E}Δ*TRZI* tumours containing additional microsatellite tract length variability (**Supplementary Figure 8**).

Discrete transcript profiles of serrated and conventional pathway tumours

In addition to our series of serrated pathway tumours, we also generated tumours driven by alteration of commonly mutated conventional CRC pathway genes, *Apc* and *Kras*^{G12D}. Similar to previous reports [36], colonic organoids expressing adeno-virally delivered Cre, derived from *Kras*$^{LSL\text{-}G12D/+}$;*Apc*$^{fl/fl}$ mice survived culture in the absence of Wnt3a or Rspo2 (**Supplementary Figure 9**). Adenocarcinomas arising from orthotopic injection of *Kras*$^{G12D/+}$;*Apc*$^{fl/fl}$ organoids, were verified as *Kras*$^{G12D/+}$;*Apc*$^{\Delta 580l/\Delta 580}$ (*Kras*^{G12D};*Apc*$^{\Delta/\Delta}$) genotype and displayed nuclear β-catenin localisation (**Supplementary Figure 9**). We isolated RNA from our series of serrated and conventional pathway tumours and compared

mRNAseq expression profiles between these different tumours and normal colonic mucosa from tumour bearing animals (n=4 biological replicates per group). The multidimensional scaling (MDS) plot generated from our RNAseq data showed that, as expected, the normal colon samples had quite different transcript profiles to the tumour samples (**Figure 5A**). In comparison, the *Braf*^{V600E}, serrated subtype tumours all clustered closely together and separated from the *Kras*^{G12D}*;Apc*$^{\Delta/\Delta}$ tumours (**Figure 5A**). Consistent with alterations to the MAPK pathway in our *Braf*^{V600E} organoid series, gene set enrichment analysis (GSEA) identified differential expression of MAPK-pathway transcripts as enriched in the *Braf*^{V600E} tumours compared to normal colon (**Supplementary Figure 10A**). Validating our attempt to model MSI CRC, the tumours derived from *Braf*^{V600E}Δ*TRZIM* organoids were also significantly enriched for differential expression of a human MSI CRC-associated gene set (**Supplementary Figure 10B**) [41].

The top enriched gene set based on normalised enrichment score in our analyses across all *Braf*^{V600E}, but not *Kras*^{G12D}*;Apc*$^{\Delta/\Delta}$, tumours when compared to normal colon was the sphingolipid (SP) *de novo* biosynthesis pathway (**Figure 5B, Supplementary Table 4**). We validated the differential expression of SP pathway transcripts from the leading edge of the GSEA by real-time qPCR in *Braf*^{V600E} and conventional pathway tumours (**Figure 5C, Supplementary Figure 11)**. Two key enzymes regulating S1P levels in this pathway are sphingosine kinase 1 (SPHK1) and the counter-acting sphingosine-1-phosphate phosphatase 1 (SGPP1) [42]. Consistent with previous reports in human CRC [43, 44], we observed increased expression of *Sphk1* transcripts in our series of *Braf*^{V600E} tumours compared to normal mouse colon and a converse decrease in *Sgpp1* transcripts (**Figure 5C)**. This suggested at the transcriptomic level that the pathway may be primed for increased production of the pro-survival molecule sphingosine 1-phosphate (S1P) in our model of serrated CRC [42]. We next wished to determine if this shift at the transcript level was also observed in human CRC samples. *SPHK1* was significantly upregulated in 622 TCGA CRC samples compared to matched normal controls, with greatest expression levels in *BRAF*^{V600E} tumours (**Figure 5D**). Conversely, *SGPP1* expression was significantly decreased in all CRC samples compared to matched normal controls. Increased expression of *SPHK1* and decreased expression of *SGPP1* were both separately associated with poor survival in the TCGA cohort (**Figure 5E**).

DISCUSSION:

Here we have focused on the serrated pathway to CRC that accounts for up to 25% of all CRC, and for microsatellite stable cases has very poor outcome [2]. We have developed a panel of CRISPR/Cas9 genome engineered organoids that model DNA alterations found in *BRAF* mutant serrated CRC. In this way we are producing novel, preclinical models of colorectal adenocarcinoma with features of serrated CRC, and most notably desmoplastic stromal responses, infiltrative growth, tumour budding and mucinous differentiation [2, 45, 46] (**see Figure 4, Supplementary Table 3 & Figure 5**). Mucous caps characterise human serrated polyps at colonoscopy. When we look at an early time point in tumour development in our serrated CRC mouse models with complex genetics (*Braf*^{V600E}Δ*TRZI* and *Braf*^{V600E}Δ*TRZIM*) we also observe mucous caps. Previous studies using CRISPR/Cas9 to model the conventional molecular pathway to CRC using human intestinal organoids were

either unable to generate invasive CRC [12], or required 4 gene alterations for invasive tumour growth [13]. We find here that alterations to just two genes, *Braf* and *Tgfbr2*, results in transmurally invasive adenocarcinoma. Further altering the oncogene-induced senescence factor, *p16 Ink4a*, and the Wnt pathway leads to increased tumour initiation and decreased survival time (**Figure 3 & 4**). These more genetically complex tumours had increased stromal response, tumour budding and mucinous differentiation. We also model MSI "hypermutator" CRC by inducing loss-of-function mutations in the DNA mismatch repair gene, *Mlh1*. Similar to recent work describing a 6-fold higher DNA mutation rate in CRISPR/Cas9 engineered $MLH1^{\Delta/\Delta}$ human colon organoid lines [47], we have successfully generated the MSI phenotype as judged by instability in microsatellite repeat tract length (**Supplementary Figure 8**).

We utilise the recently adapted small animal colonoscopy technique [36, 48] to enable rapid, orthotopic injection of engineered organoids to the mucosal layer of the colon wall and tumour monitoring thereafter (**Supplementary Figure 5 & videos**). This is especially salient given the observed differences in metastatic potential for engineered conventional pathway CRC organoids delivered either subcutaneously or using a rectal prolapse model, where only tumours growing at the orthotopic colon site produced liver metastases [49]. A second report using similar conventional pathway mutant organoids injected using a colonoscope resulted in metastasis in 30% of mice [36]. We observe liver metastasis in the serrated CRC models presented here, albeit infrequently, and no lung or peritoneal spread of the disease. This may be due to the model not containing strong metastasis promoting alterations or alternately, in the future, luminal preservation through colonoscopic biopsy may allow a more complete evaluation of disease progression.

These models will advance this field by providing a rapid, inexpensive and pathologically faithful approach to studying the biology of serrated CRC. Other models, whilst valuable in their own right, are slow, require complicated *in vivo* breeding and have a prescribed number and sequence of genetic alterations [18, 19, 50, 51, 52, 53]. Our models can be readily adapted to investigate the many leads generated by next generation sequencing of human serrated CRC and will be particularly valuable for testing potential therapeutics in the setting of complex, but known, genetic landscapes. Transcriptome analysis of our genome engineered models of serrated and conventional CRC have identified putative changes to sphingolipid metabolism in these tumours. The differential expression of transcripts encoding two key enzymes in this pathway are mirrored in human CRC and are associated with worse prognosis. Future work will investigate the therapeutic efficacy of targeting the sphingolipid biosynthesis pathway for $BRAF^{V600E}$ CRC.

METHODS

Mouse experiments. This study was approved by the MIT Institutional Animal Care and Use Committee, QIMR Berghofer and SAHMRI Animal Ethics committees (P1208, SAM174, SAM205). Mice heterozygous for both the conditionally active $Braf^{CA}$ and $Villin\text{-}Cre^{ERT2}$ alleles to induce the mutation analogous to human $BRAF^{V600E}$ specifically in the intestine were generated as described [52]. Similarly, mice containing the $Kras^{LSL\text{-}G12D/+}$ [54] and $Apc^{CKO/CKO}$ [55] alleles were interbred to produce double transgenic offspring that were used to generate $Kras^{G12D/+}$; $Apc^{\Delta 580l/\Delta 580}$ colonic organoids [36].

Orthotopic Injection. NOD.Cg-*Prkdc*^{scid}*Il2rg*^{tm1Wjl}/SzJ (NSG) mice (male and female, 6-12 weeks old) were obtained from the SAHMRI Bioresources facility and housed under pathogen-free conditions. Organoids were isolated from matrigel and dissociated to single cells and small clusters using TrypLE. The cell clusters (equivalent to ~150 organoids) were washed three times with cold PBS containing 10uM Y-27632 and then resuspended in 20ul 10% GFR matrigel 1:1000 india ink, 10uM Y-27632 in PBS and injected into the mucosa of the distal colon of anaesthetised NSG mice. Colonoscopy-guided orthotopic injection into the colon wall was undertaken as previously described [36] with modifications described in Supplementary methods.

Genome engineering. gRNAs specific for each target gene were either published sequences targeting *Rnf43, Znrf3* or *p16 Ink4a* [56, 57] or designed *de novo* using the CRISPR design Tool to target the first exon immediately downstream of the translation start codon [11] (see Supplementary Methods table 2). gRNA oligos were cloned into px-459, which expresses both the Cas9 nuclease and single gRNAs [11]. Organoid transfection and culture details are included in the Supplementary methods section.

Nucleic acid analyses, bioinformatics, western blotting and immunohistochemistry. Please see the Supplementary Methods section.

ACKNOWLEDGMENTS:

The Rspo-2 expression plasmid was a kind gift from Prof. Anthony Burgess (Walter & Eliza Hall Institute of Medical Research, Australia), L-Wnt3a cells were a kind gift of Prof. Hans Clevers (Hubrecht Institute, The Netherlands). Dr. Mark Van der Hoek and staff at the David R. Gunn Genomics Facility at SAHMRI, John Toubia, Andreas Schreiber, Joel Geoghegan and staff at the Adelaide Australian Cancer Research Foundation Genomics Facility for useful discussions.

This work was supported by Cure Cancer Australia/Cancer Australia (APP1102534), the Cancer Council SA Beat Cancer Project on behalf of its donors and the State Government of South Australia through the Department of Health SA, by Pathology Queensland, by the Australian National Health and Medical Research Council (NHMRC) through (APP1081852, APP1140236), by the National Institutes of Health (NIH) (K08 CA198002, R00 AG045144, R01 CA211184), the Department of Defense (CA120198), the V Foundation V Scholar Award, the Sidney Kimmel Scholar Award, the Pew-Stewart Trust Scholar Award, the Koch Institute Frontier Research Program through the Kathy and Curt Marble Cancer Research Fund, the American Federation of Aging Research, as well as by the Koch Institute Support Grant P30-CA14051 from the National Cancer Institute. DLW is supported by a NHMRC Career Development Fellowship, VLW by a Gastroenterological Society of Australia Senior Research Fellowship.

REFERENCES

1 Fearon ER, Vogelstein B. A genetic model for colorectal tumorigenesis. Cell 1990;**61**:759-67.

2 Bettington M, Walker N, Clouston A, Brown I, Leggett B, Whitehall V. The serrated pathway to colorectal carcinoma: current concepts and challenges. Histopathology 2013;**62**:367-86.
3 Weisenberger DJ, Siegmund KD, Campan M, Young J, Long TI, Faasse MA*, et al.* CpG island methylator phenotype underlies sporadic microsatellite instability and is tightly associated with BRAF mutation in colorectal cancer. Nature genetics 2006;**38**:787-93.
4 Tejpar S, Bertagnolli M, Bosman F, Lenz HJ, Garraway L, Waldman F*, et al.* Prognostic and predictive biomarkers in resected colon cancer: current status and future perspectives for integrating genomics into biomarker discovery. Oncologist 2010;**15**:390-404.
5 Pai RK, Jayachandran P, Koong AC, Chang DT, Kwok S, Ma L*, et al.* BRAF-mutated, microsatellite-stable adenocarcinoma of the proximal colon: an aggressive adenocarcinoma with poor survival, mucinous differentiation, and adverse morphologic features. Am J Surg Pathol 2012;**36**:744-52.
6 Rex DK, Ahnen DJ, Baron JA, Batts KP, Burke CA, Burt RW*, et al.* Serrated lesions of the colorectum: review and recommendations from an expert panel. Am J Gastroenterol 2012;**107**:1315-29.
7 Anderson JC, Robertson DJ. Serrated Polyp Detection by the Fecal Immunochemical Test: An Imperfect FIT. Clinical gastroenterology and hepatology : the official clinical practice journal of the American Gastroenterological Association 2017;**15**:880-2.
8 Sato T, Stange DE, Ferrante M, Vries RG, Van Es JH, Van den Brink S*, et al.* Long-term expansion of epithelial organoids from human colon, adenoma, adenocarcinoma, and Barrett's epithelium. Gastroenterology 2011;**141**:1762-72.
9 Barker N. Adult intestinal stem cells: critical drivers of epithelial homeostasis and regeneration. Nature reviews Molecular cell biology 2014;**15**:19-33.
10 Clevers H. Modeling Development and Disease with Organoids. Cell 2016;**165**:1586-97.
11 Ran FA, Hsu PD, Wright J, Agarwala V, Scott DA, Zhang F. Genome engineering using the CRISPR-Cas9 system. Nat Protoc 2013;**8**:2281-308.
12 Matano M, Date S, Shimokawa M, Takano A, Fujii M, Ohta Y*, et al.* Modeling colorectal cancer using CRISPR-Cas9-mediated engineering of human intestinal organoids. Nat Med 2015;**21**:256-62.
13 Drost J, van Jaarsveld RH, Ponsioen B, Zimberlin C, van Boxtel R, Buijs A*, et al.* Sequential cancer mutations in cultured human intestinal stem cells. Nature 2015;**521**:43-7.
14 Fujii M, Shimokawa M, Date S, Takano A, Matano M, Nanki K*, et al.* A Colorectal Tumor Organoid Library Demonstrates Progressive Loss of Niche Factor Requirements during Tumorigenesis. Cell Stem Cell 2016;**18**:827-38.
15 Cancer Genome Atlas N. Comprehensive molecular characterization of human colon and rectal cancer. Nature 2012;**487**:330-7.
16 Cohen R, Cervera P, Svrcek M, Pellat A, Dreyer C, de Gramont A*, et al.* BRAF-Mutated Colorectal Cancer: What Is the Optimal Strategy for Treatment? Curr Treat Options Oncol 2017;**18**:9.
17 Kriegl L, Neumann J, Vieth M, Greten FR, Reu S, Jung A*, et al.* Up and downregulation of p16(Ink4a) expression in BRAF-mutated polyps/adenomas indicates a senescence barrier in the serrated route to colon cancer. Modern pathology : an official journal of the United States and Canadian Academy of Pathology, Inc 2011;**24**:1015-22.
18 Bennecke M, Kriegl L, Bajbouj M, Retzlaff K, Robine S, Jung A*, et al.* Ink4a/Arf and oncogene-induced senescence prevent tumor progression during alternative colorectal tumorigenesis. Cancer Cell 2010;**18**:135-46.
19 Rad R, Cadinanos J, Rad L, Varela I, Strong A, Kriegl L*, et al.* A genetic progression model of Braf(V600E)-induced intestinal tumorigenesis reveals targets for therapeutic intervention. Cancer Cell 2013;**24**:15-29.
20 Krtolica K, Krajnovic M, Usaj-Knezevic S, Babic D, Jovanovic D, Dimitrijevic B. Comethylation of p16 and MGMT genes in colorectal carcinoma: correlation with clinicopathological features and prognostic value. World J Gastroenterol 2007;**13**:1187-94.

21 Ma X, Wang YW, Zhang MQ, Gazdar AF. DNA methylation data analysis and its application to cancer research. Epigenomics 2013;**5**:301-16.
22 Herman JG, Merlo A, Mao L, Lapidus RG, Issa JP, Davidson NE*, et al.* Inactivation of the CDKN2/p16/MTS1 gene is frequently associated with aberrant DNA methylation in all common human cancers. Cancer Res 1995;**55**:4525-30.
23 Bond CE, McKeone DM, Kalimutho M, Bettington ML, Pearson SA, Dumenil TD*, et al.* RNF43 and ZNRF3 are commonly altered in serrated pathway colorectal tumorigenesis. Oncotarget 2016;**7**:70589-600.
24 Koo BK, Spit M, Jordens I, Low TY, Stange DE, van de Wetering M*, et al.* Tumour suppressor RNF43 is a stem-cell E3 ligase that induces endocytosis of Wnt receptors. Nature 2012;**488**:665-9.
25 Murakami T, Mitomi H, Saito T, Takahashi M, Sakamoto N, Fukui N*, et al.* Distinct WNT/beta-catenin signaling activation in the serrated neoplasia pathway and the adenoma-carcinoma sequence of the colorectum. Modern pathology : an official journal of the United States and Canadian Academy of Pathology, Inc 2015;**28**:146-58.
26 Borowsky J, Dumenil T, Bettington M, Pearson SA, Bond C, Fennell L*, et al.* The role of APC in WNT pathway activation in serrated neoplasia. Modern pathology : an official journal of the United States and Canadian Academy of Pathology, Inc 2017.
27 Giannakis M, Hodis E, Jasmine Mu X, Yamauchi M, Rosenbluh J, Cibulskis K*, et al.* RNF43 is frequently mutated in colorectal and endometrial cancers. Nature genetics 2014;**46**:1264-6.
28 Parsons R, Myeroff LL, Liu B, Willson JK, Markowitz SD, Kinzler KW*, et al.* Microsatellite instability and mutations of the transforming growth factor beta type II receptor gene in colorectal cancer. Cancer research 1995;**55**:5548.
29 Li X, Yao X, Wang Y, Hu F, Wang F, Jiang L*, et al.* MLH1 promoter methylation frequency in colorectal cancer patients and related clinicopathological and molecular features. PLoS One 2013;**8**:e59064.
30 IJspeert J, Vermeulen L, Meijer GA, Dekker E. Serrated neoplasia-role in colorectal carcinogenesis and clinical implications. Nat Rev Gastroenterol Hepatol 2015;**12**:401-9.
31 Di Nicolantonio F, Martini M, Molinari F, Sartore-Bianchi A, Arena S, Saletti P*, et al.* Wild-type BRAF is required for response to panitumumab or cetuximab in metastatic colorectal cancer. Journal of clinical oncology : official journal of the American Society of Clinical Oncology 2008;**26**:5705-12.
32 Fessler E, Drost J, van Hooff SR, Linnekamp JF, Wang X, Jansen M*, et al.* TGFbeta signaling directs serrated adenomas to the mesenchymal colorectal cancer subtype. EMBO Mol Med 2016;**8**:745-60.
33 Ribic CM, Sargent DJ, Moore MJ, Thibodeau SN, French AJ, Goldberg RM*, et al.* Tumor Microsatellite-Instability Status as a Predictor of Benefit from Fluorouracil-Based Adjuvant Chemotherapy for Colon Cancer. New England Journal of Medicine 2003;**349**:247-57.
34 Longley DB, Harkin DP, Johnston PG. 5-fluorouracil: mechanisms of action and clinical strategies. Nat Rev Cancer 2003;**3**:330-8.
35 Li GM. Mechanisms and functions of DNA mismatch repair. Cell Res 2008;**18**:85-98.
36 Roper J, Tammela T, Cetinbas NM, Akkad A, Roghanian A, Rickelt S*, et al.* In vivo genome editing and organoid transplantation models of colorectal cancer and metastasis. Nat Biotechnol 2017;**35**:569-76.
37 Saito S, Tajiri H, Ikegami M. Serrated polyps of the colon and rectum: Endoscopic features including image enhanced endoscopy. World J Gastrointest Endosc 2015;**7**:860-71.
38 Bosman FT, Carneiro, F., Hruban, R.H., Theise, N.D. WHO Classification of Tumours of the Digestive System, 2010.
39 Bacher JW, Abdel Megid WM, Kent-First MG, Halberg RB. Use of mononucleotide repeat markers for detection of microsatellite instability in mouse tumors. Mol Carcinog 2005;**44**:285-92.
40 Kabbarah O, Mallon MA, Pfeifer JD, Edelmann W, Kucherlapati R, Goodfellow PJ. A panel of repeat markers for detection of microsatellite instability in murine tumors. Mol Carcinog 2003;**38**:155-9.

41 Watanabe T, Kobunai T, Toda E, Yamamoto Y, Kanazawa T, Kazama Y*, et al.* Distal colorectal cancers with microsatellite instability (MSI) display distinct gene expression profiles that are different from proximal MSI cancers. Cancer Res 2006;**66**:9804-8.
42 Pitson SM. Regulation of sphingosine kinase and sphingolipid signaling. Trends Biochem Sci 2011;**36**:97-107.
43 Kawamori T, Osta W, Johnson KR, Pettus BJ, Bielawski J, Tanaka T*, et al.* Sphingosine kinase 1 is up-regulated in colon carcinogenesis. FASEB J 2006;**20**:386-8.
44 Oskouian B, Saba J. Sphingosine-1-phosphate metabolism and intestinal tumorigenesis: lipid signaling strikes again. Cell Cycle 2007;**6**:522-7.
45 Chen D, Huang JF, Liu K, Zhang LQ, Yang Z, Chuai ZR*, et al.* BRAFV600E mutation and its association with clinicopathological features of colorectal cancer: a systematic review and meta-analysis. PLoS One 2014;**9**:e90607.
46 Garcia-Solano J, Conesa-Zamora P, Trujillo-Santos J, Makinen MJ, Perez-Guillermo M. Tumour budding and other prognostic pathological features at invasive margins in serrated colorectal adenocarcinoma: a comparative study with conventional carcinoma. Histopathology 2011;**59**:1046-56.
47 Drost J, van Boxtel R, Blokzijl F, Mizutani T, Sasaki N, Sasselli V*, et al.* Use of CRISPR-modified human stem cell organoids to study the origin of mutational signatures in cancer. Science 2017;**358**:234-8.
48 Zigmond E, Halpern Z, Elinav E, Brazowski E, Jung S, Varol C. Utilization of murine colonoscopy for orthotopic implantation of colorectal cancer. PLoS One 2011;**6**:e28858.
49 de Sousa e Melo F, Kurtova AV, Harnoss JM, Kljavin N, Hoeck JD, Hung J*, et al.* A distinct role for Lgr5(+) stem cells in primary and metastatic colon cancer. Nature 2017;**543**:676-80.
50 Carragher LA, Snell KR, Giblett SM, Aldridge VS, Patel B, Cook SJ*, et al.* V600EBraf induces gastrointestinal crypt senescence and promotes tumour progression through enhanced CpG methylation of p16INK4a. EMBO molecular medicine 2010;**2**:458-71.
51 Davies EJ, Marsh Durban V, Meniel V, Williams GT, Clarke AR. PTEN loss and KRAS activation leads to the formation of serrated adenomas and metastatic carcinoma in the mouse intestine. The Journal of pathology 2014;**233**:27-38.
52 Bond CE, Liu C, Kawamata F, McKeone DM, Fernando W, Jamieson S*, et al.* Oncogenic BRAF mutation induces DNA methylation changes in a murine model for human serrated colorectal neoplasia. Epigenetics 2017:01-20.
53 Coffee EM, Faber AC, Roper J, Sinnamon MJ, Goel G, Keung L*, et al.* Concomitant BRAF and PI3K/mTOR blockade is required for effective treatment of BRAF(V600E) colorectal cancer. Clinical cancer research : an official journal of the American Association for Cancer Research 2013;**19**:2688-98.
54 Jackson EL, Willis N, Mercer K, Bronson RT, Crowley D, Montoya R*, et al.* Analysis of lung tumor initiation and progression using conditional expression of oncogenic K-ras. Genes Dev 2001;**15**:3243-8.
55 Kuraguchi M, Wang XP, Bronson RT, Rothenberg R, Ohene-Baah NY, Lund JJ*, et al.* Adenomatous polyposis coli (APC) is required for normal development of skin and thymus. PLoS Genet 2006;**2**:e146.
56 Schwank G, Koo BK, Sasselli V, Dekkers JF, Heo I, Demircan T*, et al.* Functional repair of CFTR by CRISPR/Cas9 in intestinal stem cell organoids of cystic fibrosis patients. Cell Stem Cell 2013;**13**:653-8.
57 Chen S, Sanjana NE, Zheng K, Shalem O, Lee K, Shi X*, et al.* Genome-wide CRISPR screen in a mouse model of tumor growth and metastasis. Cell 2015;**160**:1246-60.

Figure Legends

Figure 1. Co-occurring molecular events in stem-cell niche, microsatellite instability and senescence pathways in *BRAF^{V600E}* mutant serrated CRC. Of the 50 patients with *BRAF^{V600E}* CRC from the TCGA CRC cohort (n=527 patients total), we depict the co-alteration (non-synonymous mutation and/or hyper-methylation) of selected genes in these pathways. Number of patients with each alterations is indicated by bar graph on right, % of *BRAF^{V600E}* cases containing the alteration is indicated by numbers on left. Coloured blocks indicate gene is altered in the sample, grey is unaltered.

Figure 2. Introduction of genetic alterations associated with serrated CRC promotes independence from niche factor requirements. A, activation of MAPK pathway in *Braf^{V600E}* organoids visualized by phosphorylation of the ERK1/2 effector protein, 4-hydroxytamoxifen (4-OHT). **B,** Generation of a 'serratoid' series from normal mouse colonic organoids through sequential CRISPR/Cas9 targeting and *in vitro* selection. *Braf^{V600E}*, *Braf^{V600E}Tgfbr2$^{\Delta/\Delta}$ (Braf^{V600E}ΔT)*, *Braf^{V600E} Tgfbr2$^{\Delta/\Delta}$ Rnf43$^{\Delta/\Delta}$/Znrf3$^{\Delta/\Delta}$ p16Ink4a$^{\Delta/\Delta}$ (Braf^{V600E}ΔTRZI)*, *Braf^{V600E} Tgfbr2$^{\Delta/\Delta}$Rnf43$^{\Delta/\Delta}$/Znrf3$^{\Delta/\Delta}$ p16Ink4a$^{\Delta/\Delta}$Mlh1$^{\Delta/\Delta}$ (Braf^{V600E}ΔTRZIM)*. Normal media components required as stem cell niche factors Wnt-3a (W), Rspo-2 (R), Noggin (N), additional selection with TGFβ1 (T) and chemotherapeutic agent, 5-Fluorouracil (5FU). **C,** DNA sequence verification of biallelic insertion/deletion (indel) mutations that result in prematurely truncated proteins.

Figure 3. *Braf^{V600E}* alone is not sufficient for colon tumour formation, but with increasing serrated pathway genetic alterations tumour penetrance and growth rate increases. A, colonoscopic images showing injection and rapid growth of serratoid *Braf^{V600E}ΔTRZI* line. **B,** Tumour penetrance as a percentage of the number of organoid injections that gave rise to a tumour/mouse in 3 months for each line, with 1-3 injections/mouse. **C,** Colonoscopic scoring of largest tumour in each mouse (n=5 mice per group, Becker scale). **D,** Kaplan-Meier plot showing overall survival post-injection with organoid lines *Braf^{V600E}* n=4 mice, *Braf^{V600E}ΔT* n=12 mice, *Braf^{V600E}ΔTRZI* n=11 mice, *Braf^{V600E}ΔTRZIM* n=8 mice, compared to *Braf^{V600E}* using a Bonferroni adjustment for multiple comparisons. ns=not significant, *=p≤0.05, **=p≤0.01, ***=p≤0.001.

Figure 4. Multi-hit 'serratoids' generate invasive adenocarcinoma with features of human serrated CRC. Colonoscopy **(A)** and histology **(B-H)** images of mouse colon orthotopically injected with mutant organoid lines *Braf^{V600E}*, *Braf^{V600E}ΔT*, *Braf^{V600E}ΔTRZI*, *Braf^{V600E}ΔTRZIM*. **B,** H&E stained sections of whole colon. **C,** higher magnification H&E, arrows denote position of muscularis mucosae, * denotes remnant ink from injection. **D,** immunohistochemical staining for mutant Braf^{V600E} protein clearly delineates serratoid derived tumour cells. **E,** representative images of desmoplastic stromal response and **F,** tumour budding (circled). **G,** tumour stromal response stains positive for alpha-smooth muscle actin (aSMA). **H,** mucin lakes present in mucinous adenocarcinoma visualised using Alcian Blue stain. Scale bars are (B) 500um, (C-H) 100um.

Figure 5. Serrated pathway tumours are molecularly distinct from conventional pathway tumours. A, multi-dimensional scaling plot of RNA expression data from normal mouse colon (black), serrated pathway *Braf*^{V600E}*ΔT* (blue), *Braf*^{V600E}*ΔTRZI* (red) and *Braf*^{V600E}*ΔTRZIM* (yellow) and conventional pathway tumours *Kras*^{G12D}*;Apc*$^{\Delta/\Delta}$ (grey), n=4 samples per group. **B,** gene set enrichment analysis (GSEA) for Sphingolipid *de novo* biosynthesis Reactome between *Braf*^{V600E}*ΔTRZI* serrated tumour and normal mouse colon. Enrichment score (ES), normalised enrichment score (NES), false discovery rate (FDR). **C**, Expression of *Sphk1* is increased and *Sgpp1* is decreased in mouse *Braf*^{V600E} serrated CRC compared to normal mouse colon. Fold induction of mRNA expression is normalized to *Gapdh*, with transcript level in normal colon set to 1. Results from at least four animals with triplicate technical replicates are shown, error bars denote standard deviation. Two-tailed t-test used for pair-wise statistical analysis. **D,** Violin plots depicting z-score values for normalized expression of *SPHK1* (top) and *SGPP1* (bottom) transcripts in 622 human TCGA CRC and normal colon samples separated into wild-type *BRAF/KRAS*, *KRAS* mutant and *BRAF*^{V600E} CRC. **E,** Kaplan-Meier plots showing TCGA patient survival probability based on expression level of *SPHK1* (top, *SPHK1* high group n=139 in red, low group n=483 in green) or *SGPP1* (bottom, *SGPP1* low group n=145 in green, high group n=477 in red). *=p≤0.05, **=p≤0.01, ***=p≤0.001, ns= not significant.

Supplementary methods

TCGA data analysis. The Cancer Genome Atlas (TCGA) colonic adenocarcinoma and rectal adenocarcinoma (TCGA-COAD and TCGA-READ respectively) annotated mutation and methylation files were extracted from the GDC portal (https://portal.gdc.cancer.gov/) for 527 cases only, as the remaining cases did not have complete data for mutation and methylation. We determined that there were 50 $BRAF^{V600E}$ CRC cases within this cohort and used $BRAF^{V600E}$ to mark the serrated CRC subtype. We do not examine *KRAS* mutant serrated CRC herein, as *KRAS* mutation also marks the conventional pathway to CRC. We then used the analysis pipeline described below to examine alteration (both DNA mutation and hypermethylation) to candidate genes involved in regulation of the stem cell niche, senescence and DNA mismatch repair including; the Wnt-pathway, Bone Morphogenic Protein (BMP)/transforming growth factor-beta (TGFβ) pathways, *P16 INK4A*, *MLH1*. TCGA methylation data generated using two different platforms, the Infinium Human Methylation 27K and 450K, were combined. No batch effects were observed. The median beta-value across multiple microarray probes corresponding to the same gene was used to summarise methylation for each gene, with Beta-value for hyper-methylation cut off set to 0.47. All data processing was undertaken using software R, version 3.4.1 Patched. Waterfall plots (Figure 1) were generated with R package oncoPrint() function in ComplexHeatmap R package version 1.12.0 [1]. To examine whether Sphingolipid pathway genes were differentially regulated in the TCGA $BRAF^{V600E}$ CRC cohort and examine the effect on patient survival we analysed RNA expression and patient survival by downloading 622 cases with clinical and RNA expression data using R Bioconductor TCGAbiolinks package, version 2.7.5. Maximal survival time analysed was 5 years. RNA expression values were transformed using the 'voom' method limma package, version 3.30.13. Normalised, transformed expression values were used to classify patients into high and low expressor groups for each gene of interest using the surv_cutpoint() function in survminer R, the minimal proportion of observations was set at 20% for each gene [2]. The prognosis of each group was examined using Kaplan-Meier survival estimators with the survminer R package, version 0.4.1, with survival outcome compared by log-rank tests.

Genome engineering & Organoid culture (cont). Organoids were dissociated to single cells and small clumps of cells with TrypLE express, washed and transfected in the presence of basal medium without antibiotics and supplemented with 1uM Jagged-1 (Anaspec) using LF2000 and plasmid DNA in a 96 well plate for 3 hours at 37°C. Empty px458-GFP plasmid was used to visualise transfection efficiency and used as a kill test control for selection medium conditions. Cells were washed and plated onto 50% matrigel in non-selective culture medium containing 1uM Jagged-1. The following day, media was gently aspirated and top layer of 50% matrigel added. Plate was spun 20 minutes at 200xg at room temperature followed by 30 minute incubation at 37 degrees C before addition of non-selective culture medium containing 1uM Jagged-1. 72 hours after transfection, media was changed to selection medium, with media changes subsequently 2-3 times weekly.

Single organoids were handpicked and expanded for DNA sequence analysis. For novel gRNAs, genomic DNA was isolated from pooled, polyclonal organoids and subjected to PCR amplification of target genomic region, followed by PAGE analysis of duplex formation to measure indel formation. Genomic DNA from single organoid lines was also isolated and target genomic regions amplified by PCR. PCR products were cloned into a p-JET1.2 cloning

vector according to the manufacturer's instructions (ThermoFisher). Plasmid DNA from at least 6 clones was analysed by Sanger sequencing to determine biallelic target gene alteration.

We found optimal recovery and expansion of organoids from single cells as required for the transfection protocol using a matrigel "sandwich" and used this method for all cultures described herein [3]. To facilitate visualisation of the entire 48-well in a flat plane we modify the "sandwich" method to include the addition of 60ul 50:50 ADMEM:Matrigel mixture to a 48-well, centrifuge this bottom matrigel layer for 40minutes at 200xg at room temp, followed by a 30 minute incubation at 37 degC to solidify matrigel before plating organoids in growth medium on top. The following day we remove the media and any non-attached organoids, cover with 40ul 50:50 ADMEM:Matrigel mixture and centrifuge 100xg for 20 minutes. After a 30 minute incubation at 37degC, organoids in matrigel are covered with 200-250ul growth medium. The basal culture medium for mouse colon organoids was Advanced Dulbecco's modified Eagle medium/F12 (Life Technologies) supplemented with 1x gentamicin/antimycotic/antibiotic (Life Technologies), 10mM HEPES, 2mM GlutaMAX, 1xB27 (Life Technologies), 1xN2 (Life Technologies). The following niche factors were used: 50ng/ml mouse recombinant EGF (Peprotech), 100 ng/ml mouse recombinant noggin (Peprotech), 20% R-spondin-2 conditioned medium, 50% Wnt-3A conditioned medium. To select mutant organoids the following reagents were used: 1uM 4-OHT for 24h (Sigma-Aldrich), 10ng/ml human recombinant TGF-β1 (Peprotech), 1uM EGFR inhibitor (EGFRi, Calbiochem #324840), 20uM 5-FU (Sigma-Aldrich). Following initial isolation and immediately after each split, organoids were cultured in 10uM Y-27632 (In Vitro Technologies), 3uM iPSC (Calbiochem Cat #420220), 3uM GSK-3 inhibitor (XVI, Calbiochem, # 361559) for the first 3 days. Prior to transfection, organoids were cultured with 10mM Nicotinamide (Sigma-Aldrich) and 10uM GSK-3 inhibitor for 2 passages [4].

Kras$^{G12D/+}$; *Apc*$^{\Delta 580l/\Delta 580}$ (AK) colonic organoids were generated by treating organoids from Kras$^{LSL\text{-}G12D/+}$;*Apc*$^{CKO/CKO}$ mice with Ad5CMV::Cre, followed by selection in medium without Wnt ligands [5].

Orthotopic Injection (cont). A customised needle (Hamilton Inc. part number 7803-05, removable needle, 33 gauge, 12 inches long, point 4, 12 degree bevel) was used. Colonoscopy was performed using a Karl Storz Image 1 Camera System comprised of: Image1 HDTV HUB CCU; Cold Light Fountain LED Nova 150 light source; Full HD Image1 3 Chip H3-Z Camera Head; Hopkins Telescope, 1.9mm, 0 degrees. A sealed luer lock was placed on the working channel of the telescope sheath to ensure minimal air leakage (Coherent Scientific, part number 14034-40). In each mouse up to 3 injections of 20µl were performed. Injection sites were monitored by weekly colonoscopy and the videos were viewed offline using QuickTime Player for analysis. Tumour growth of the largest tumour visualised was scored as previously described using the Becker Scale [6]. A Clinical Record Score was used to determine humane endpoint, scores were obtained by one point being given for the presence of each of the following observations: weight loss >15%; hunched/ruffled coat; inability to pass stool; dehydrated; absence of movement; or facial grimace. Once a score of 3 was reached the mice were euthanased. Statistical analysis performed using Prism.

Western blot analysis. To reduce endogenous MAPK signalling organoids were cultured without EGF for 4 days and with 1uM EGFRi for one day prior to treatment with 1uM 4-OHT for 16h. Cells were harvested using cold PBS containing 1x Halt™ Protease and Phosphatase Inhibitor Cocktail (PPI, Thermo Scientific), pelleted and lysed using RIPA buffer (150mM sodium chloride, 1% NP40, 0.5% sodium deoxycholate, 0.1% SDS, 50mM Tris, pH8.0) containing 1x PPI. Protein was quantitated using the DC™ Protein Assay Kit II (Bio-Rad) and analysed using 4-20% (Bio-Rad) SDS-PAGE. Standard western blot analyses were performed using the following primary antibodies: anti- Phospho-p44/42 MAPK (Erk1/2) (#4370, Cell Signaling Technology, 1:2000), total p44/42 MAPK (Erk1/2, #137F5, Cell Signaling Technology, 1:2000), anti-Hsp90 loading control (sc-7947, Santa Cruz Biotechnology, 1:1000). Primary antibody binding was detected using HRP-conjugated secondary anti-Rabbit antibody (Novex, #A24537, 1:10,000) and visualised with ECL Western Blotting Detection Reagents (Amersham, RPN2209) and Gel Doc™ XR+ Gel Documentation System (Bio-Rad).

Immunohistochemistry and histology. Tissues were fixed in 10% formalin, paraffin embedded and sectioned. Consecutive sections were prepared using a rotary microtome. H&E and alcian blue stains were preformed according to standard procedures. The $Braf^{V600E}$ staining was performed on a Ventana Benchmark Ultra, using a prediluted Ventana mouse primary antibody. Antigen retrieval was for 64 min using Ventana retrieval solution CC1. The primary antibody was incubated for 32 min at 36 degrees C. The Ventana Optiview DAB detection system was used with Ventana Haematoxylin II as the nuclear counterstain. The alpha-smooth muscle actin (aSMA) staining was completed using a rabbit polyclonal aSMA antibody (1:500, Abcam ab5694) and Keratin 20 using a rabbit polyclonal (1:200, Sigma SAB4502249). Antigen retrieval was performed in Vector Antigen Unmasking solution (Vector Laboratories, H-3300) and carried out in a Biocare Medical pressurised decloaker (Metagene). A goat anti-rabbit HRP secondary antibody (1:400, Life Technologies A24537) followed by DAB (BioLegend 926901) was used to visualise signal. Histological evaluation of mouse tumours was undertaken by a pathologist with expertise in human serrated pathway lesions. In line with current WHO standards mucinous adenocarcinoma was not graded (low versus high), and mucinous adenocarcinoma was defined as >50% mucinous differentiation [7]. Tumour budding was evaluated using H&E stained tumour sections in a hotspot area of $0.785mm^2$ by counting the number of buds as described for diagnostic practice [8]. 0 = Absent; 1-4 = low level; intermediate 5-9 and 10 or more is high level.

Nucleic acid analysis. Total RNA and gDNA was extracted from organoids, tumours and normal control colon tissue using AllPrep DNA/RNA Mini or RNeasy Mini Kit (QIAGEN) or UltraClean® Tissue & Cells DNA Isolation Kit (Mo Bio Laboratories). For qRT-PCR, 300-1000 ng RNA was reverse transcribed to cDNA using Superscript IV according to the manufacturer's instructions (Thermo Scientific). cDNA was diluted 1:5 and level of transcripts of interest evaluated using Primer:probe assays (IDT) with KAPA PROBE FAST qPCR Master Mix (KAPABiosystems) master mix and run on a QuantStudio 7 Flex Real-Time PCR System (Thermo Scientific). For RNAseq analysis, 1ug of total RNA was used for sequencing library preparation using a BIOO stranded Poly-A kit (PerkinElmer) according to the manufacturer's instructions and sequenced on Illumina HiSeq to generate 1 x 100bp single-end reads.

RNAseq data processing. Images generated by HiSeq™ 2500 were converted into nucleotide sequences by a base calling pipeline and stored in fastq.gz format, and examined QC plots with FastQC version 0.11.3. Raw reads with low quality were removed using Trim Galore prior to analysing the data. The criteria of removing low quality reads were set as: quality Phred score less than 28, reads contains adaptor sequences. FastQC was performed again, all low quality reads were removed. All the subsequent analyses were based on trimmed reads, which were then mapped to reference mouse genome mm10 GRCm38, using STAR 2.4.2a modified. No more than 1 base mismatch were allowed. Only uniquely mapped reads were retained. quantMode was enabled to generate gene level quantification. The counts files were then merged into a table for downstream differential expression analysis. All data preprocessing were completed in shell HPC command line environment.

Differential expression analysis. Differentially expressed genes (DEG) were analysed using the glmFit() glmLRT() function in R Bioconductor edgeR Package version 3.16.5 [9]. A negative binomial generalized log-linear model was employed, with Benjamini-Hochberg correction using false discovery rate (FDR) of *P* values. Hierarchical clustering was performed on DEGs only, using Euclidean distance and complete linkage clustering option with Heatmap() function in ComplexHeatmap R package version 1.12.0 [1]. MDS plots were generated using the plotMDS() function in Limma R package version 3.30.13 [10]. Differentially expressed genes were defined as FDR < 0.05, and absolute value of Log_2 (fold change) > 2.

Gene set enrichment analysis (GSEA). GSEA methodology was developed using guidelines for RNAseq datasets [11] . Transcript counts generated from STAR aligner were sub-grouped into files with pairwise comparison groups of normal colon to tumour. The PreprocessReadCounts (V1 Beta) module of GenePattern was used to normalise and transform counts. Briefly, lowly expressed genes were removed from the analysis if they had <1 read/million in four of the samples, as four is the smallest group of biological replicates [12]. The remaining data was then normalised using Trimmed Mean of M-values [13]. Mean-variance transformation to approximate a normal distribution was performed subsequently using voom [10]. Gene set enrichment analyses were performed using online module GSEA (v18).

Microsatellite instability. MSI status was assessed using a panel of five markers (*m-Bat-26, mBat-67, m-Bat-37, GA29, TG27*-see Supplementary Methods Table 1 for sequence) [14, 15, 16]. These included 3 mononucleotide and 2 dinucleotide repeats. Fragment sizes were assayed using PCR coupled with fluorescent detection on an ABI3100 Capillary Sequencer. Differences in fragment sizes were assessed using the GeneMarker software.

Supplementary methods table 1-Microsatellite marker primer information

Marker	Type	Annealing Tm	Forward Primer	Reverse Primer	Reference
mBat-26	Mononucleotide	59	TCACCATCCATTGCACAGTT	CTGCGAGAAGGTACTCACCC	Bacher et al, 2005
mBat-37	Mononucleotide	59	TCTGCCCAAACGTGCTTAAT	CCTGCCTGGGCTAAAATAGA	Bacher et al, 2005
mBat-67	Mononucleotide	59	CCGACTGCTCTTCCGAAGGTC	TTGCCCATTTATCATCTAGTTCAT	Bacher et al, 2005
TG27	Dinucleotide	60	GGATCACTCGATGTACGGCTACTC	CCAGGCAGGCAAAGCATTTAT	Kabbarah et al,

					2003
GA29	Dinucleotide	59	CAGGAGGTCAAGGTCATCCTAAG	CCACCATGGTAGGAGCTTGCTA	Kabbarah et al, 2003

Supplementary methods table 2- gRNA sequence

Target gene	gRNA sequence
Rnf43	CCACCAGGAGGTACCAAGCCGGC
Znrf3	GGGTCATCCCTTGTACTCATCGG
Tgfbr2	CCTGTGGCCGCTGCATATCGTCC
p16 Ink4a	CCCAACGCCCCGAACTCTTTCGG
Mlh1	TAGTGAACCGCATAGCGGCGGGG

Supplementary Methods References

1 Gu Z, Eils R, Schlesner M. Complex heatmaps reveal patterns and correlations in multidimensional genomic data. Bioinformatics 2016;**32**:2847-9.
2 Hothorn T, Lausen B. On the exact distribution of maximally selected rank statistics. Computational Statistics & Data Analysis 2003;**43**:121-37.
3 Onuma K, Ochiai M, Orihashi K, Takahashi M, Imai T, Nakagama H*, et al.* Genetic reconstitution of tumorigenesis in primary intestinal cells. Proc Natl Acad Sci U S A 2013;**110**:11127-32.
4 Schwank G, Andersson-Rolf A, Koo BK, Sasaki N, Clevers H. Generation of BAC transgenic epithelial organoids. PLoS One 2013;**8**:e76871.
5 Roper J, Tammela T, Cetinbas NM, Akkad A, Roghanian A, Rickelt S*, et al.* In vivo genome editing and organoid transplantation models of colorectal cancer and metastasis. Nat Biotechnol 2017;**35**:569-76.
6 Becker C, Fantini MC, Wirtz S, Nikolaev A, Kiesslich R, Lehr HA*, et al.* In vivo imaging of colitis and colon cancer development in mice using high resolution chromoendoscopy. Gut 2005;**54**:950-4.
7 Bosman FT, Carneiro, F., Hruban, R.H., Theise, N.D. WHO Classification of Tumours of the Digestive System, 2010.
8 Lugli A, Kirsch R, Ajioka Y, Bosman F, Cathomas G, Dawson H*, et al.* Recommendations for reporting tumor budding in colorectal cancer based on the International Tumor Budding Consensus Conference (ITBCC) 2016. Modern pathology : an official journal of the United States and Canadian Academy of Pathology, Inc 2017;**30**:1299-311.
9 McCarthy DJ, Chen Y, Smyth GK. Differential expression analysis of multifactor RNA-Seq experiments with respect to biological variation. Nucleic Acids Res 2012;**40**:4288-97.
10 Smyth GK. limma: Linear Models for Microarray Data. In: Gentleman R, Carey VJ, Huber W, Irizarry RA, Dudoit S, eds. Bioinformatics and Computational Biology Solutions Using R and Bioconductor. New York, NY: Springer New York, 2005:397-420.

11 Rahmatallah Y, Emmert-Streib F, Glazko G. Gene set analysis approaches for RNA-seq data: performance evaluation and application guideline. Brief Bioinform 2016;**17**:393-407.
12 Anders S, McCarthy DJ, Chen Y, Okoniewski M, Smyth GK, Huber W, *et al.* Count-based differential expression analysis of RNA sequencing data using R and Bioconductor. Nat Protoc 2013;**8**:1765-86.
13 Robinson MD, Oshlack A. A scaling normalization method for differential expression analysis of RNA-seq data. Genome Biol 2010;**11**:R25.
14 Bacher JW, Abdel Megid WM, Kent-First MG, Halberg RB. Use of mononucleotide repeat markers for detection of microsatellite instability in mouse tumors. Mol Carcinog 2005;**44**:285-92.
15 Kabbarah O, Mallon MA, Pfeifer JD, Edelmann W, Kucherlapati R, Goodfellow PJ. A panel of repeat markers for detection of microsatellite instability in murine tumors. Mol Carcinog 2003;**38**:155-9.
16 Bond CEL, C.; Kawamata, F.; McKeone,D.M.; Fernando, W.; Jamieson, S.; Pearson, S.; Kane, A.; Woods, S.L.; Lannagan, T.R.M.; Somashekar, R.; Lee, Y.; Dumenil, T.; Spring, K.J.; Borowsky, J.; Fennell, L.; Bettington, M.; Lee, J.; Worthley, D.L.; Leggett, B.A.; Whitehall, V.L.J. Oncogenic BRAF Mutation Induces DNA Methylation Changes in a Murine Model for Human Serrated Colorectal Neoplasia. Epigenetics 2017;**In Press**.